1-1-2005

Investigation of sub-carrier multiplexed fiber optic link supporting WLAN and WCDMA

Roland MC Yuen
Ryerson University

Investigation of Sub-Carrier Multiplexed Fiber Optic Link Supporting WLAN and WCDMA

by

Roland M. C. Yuen

B.Eng., Ryerson University, Canada, 2003

A thesis
presented to Ryerson University
in partial fulfillment of the
requirement for the degree of
Master of Applied Science
in the Program of
Electrical and Computer Engineering.

Toronto, Ontario, Canada, 2005

Author's Declaration

I hereby declare that I am the sole author of this thesis.

I authorize Ryerson University to lend this thesis to other institutions or individuals for the purpose of scholarly research.

I further authorize Ryerson University to reproduce this thesis by photocopying or by other means, in total or in part, at the request of other institutions or individuals for the purpose of scholarly research.

Abstract

Investigation of Sub-Carrier Multiplexed Fiber Optic Link Supporting WLAN and WCDMA, 2005
Roland M. C. Yuen
Master of Applied Science
Program of Electrical and Computer Engineering
Ryerson University

In this thesis, an optical fiber based radio access architecture that simultaneously provides services of the wireless local area network (WLAN) and the third generation (3G) mobile communication system is investigated. The subcarrier multiplexed (SCM) technique of the fiber optic system is considered. The SCM architecture does not require frequency conversion and plays an important role enabling the WLAN to complement the cellular mobile communication systems so that the user can have both services as needed. In the SCM architecture, the two mediums that signals propagate are the air interface and the radio over fiber (ROF) link. In the air interface, the signal experience path loss and multipath fading that have effect on the system performance. The ROF link introduces nonlinear distortions and optical noise. The uplink and downlink analysis are performed in this thesis considering all the impairments from the air interface and the ROF link. Thereafter, numerical results are generated for both the uplink and downlink to illustrate the performance of the SCM architecture. The analysis identifies the interdependent relationship of the WLAN and the WCDMA system. The numerical results graphically illustrate such interdependent relationship. In the downlink, a 5 km ROF link operating at optimal power can support a WCDMA system with 1 km radius of coverage that has 26 dB of signal to distortion and noise ratio (SDNR); and a WLAN system with 400 m radius of coverage that has 27 dB of SDNR. The throughput of IEEE 802.11 WLAN depends on the medium access control. Hence, the medium access control is investigated and the throughput expression is modified to adapt to the SCM architecture where, signals travel extra distance in a fiber.

Acknowledgements

I would like to express my sincere acknowledgement to my supervisor Dr. X. N. Fernando. This work is only possible with his mature supervision and insightful guidance especially his patience with me. He is extremely knowledgeable in his field as well as many other related fields. His knowledge helped me widen my experience in my academic study. His help has even improved my writing skills.

Financial matters are very important issues for a graduate student. So my thanks go out to Dr. Fernando who provided sufficient financial support throughout my study. The WINCORE lab also provided me with a unique environment to carry out my research.

Last, I would like to thank my family and especially to my grandma who gave me the drive to complete my work.

Table of Contents

List of Tables

List of Figures

List of Symbols

Some Conventions	Description
$\mathrm{E}[x]$, $\overline{x}$	Expectation of variable x
σ_x^2, $\langle x^2 \rangle$	Variance of variable x
σ_x^i	ith order expectation of variable x

Greek Symbols	Description
γ	Path loss exponent
δ	Duration of propagation
$\delta(\cdot)$	Impulse function
ϵ	Duration of an empty slot
η	Standard deviation of channel loss
η_f	Fiber attenuation per distance
θ	Phase shift of a signal
κ	Time between each clipping event
λ	Wavelength of a transmitted signal
μ	Cumulative RMS optical modulation index
ϖ	Normalization of the time between each clipping event (κ)
ρ	Ratio of the square of the laser bias current to two times the RF power input to the laser
τ	Time delay of a signal
τ_β	Time delay of a WLAN signal
τ_i	Time delay of the ith WCDMA signal
$\Phi_{\mathrm{up,wl}}$	Noise spectrum of air for uplink
ϕ_β	Phase shift of a WLAN signal
ϕ_i	Phase shift of the ith WCDMA signal
$\Re$	Responsivity of a photodetector

ω	Radian frequency
ω_α	Carrier frequency of the WCDMA system
ω_β	Carrier frequency of the WLAN system
ω_c	Radian carrier frequency

English Symbols	**Description**
A_i	Signal amplitude of the ith WCDMA signal
a	Signal amplitude
a_2	Second order nonlinearity parameter
a_3	Third order nonlinearity parameter
B	Bandwidth of a signal
B_β	Signal amplitude of a WLAN signal
B_{wcdma}	Bandwidth of the WCDMA system
B_{wlan}	Bandwidth of the WLAN system
$\mathbf{C}$	Code word of HR/DSSS/CCK scheme
c	Speed of light (3×10^8 m/s)
$c_\beta(t)$	Coded waveform for the WLAN system
$c_i(t)$	Coded waveform for the WCDMA system
$\text{cSDNR}_{down,wcdma}$	Cumulative SDNR of a downlink WCDMA signal
$\text{cSDNR}_{down,wlan}$	Cumulative SDNR of a downlink WLAN signal
D	Packet delay
D_{wcdma}	Desired WCDMA signal from the photocurrent
D_{wlan}	Desired WLAN signal from the photocurrent
d	Fiber length
$d_\beta(t)$	Data sequence of the WLAN signal
$d_i(t)$	Data sequence of the ith WCDMA signal
d_k	Differential code sequence
E_{sym}	Energy of a data symbol
$\text{erfc}(\cdot)$	Complementary error function
F	Noise figure of an amplifier
f	Frequency in Hertz
$\mathbf{G}$	Generator matrix
G_m	Modulation gain of a laser
$G_{\text{up,wcdma}}$	Gain of an amplifier for the WCDMA system in the uplink

$G_{\text{up,wlan}}$	Gain of an amplifier for the WLAN system in the uplink
$g(t)$	Zero-mean Gaussian process
H	Duration of a physical layer header and a medium access control layer header
$h_b(\cdot)$	Baseband equivalent of a multipath fading channel
h_i	Coded sequence
I_{B}	Laser bias current
I_{D}	Average photocurrent
$\text{I}_{\text{o}}(\cdot)$	Modified Bessel function of the first kind and zero-order
i_{D}	Photocurrent
$i_{\text{D,wcdma}}$	Photocurrent that limited to the WCDMA band
$i_{\text{D,wlan}}$	Photocurrent that limited to the WLAN band
K	Absolute temperature
k_{B}	Boltzmann's constant
L	Number of resolvable signal paths
L_{op}	Total RF power loss in the ROF link
L_{wl}	RF power loss in the air interface
l	Packet size
l_c	Optical power loss of a connector
M_i	Distorted signals in the WLAN band
m	Optical modulation index
$m_{\text{wcdma},i}$	Optical modulation index of the ith WCDMA signal
m_{wlan}	Optical modulation index of a WLAN signal
n	Number of active users in the WCDMA system
n_c	Number of optical connectors
n_{cl}	Clipping process of the SCM architecture
$n_{\text{cl,wcdma}}$	Clipping process of the WCDMA system
$n_{\text{cl,wlan}}$	Clipping process of the WLAN system
n_f	Fiber core index of refraction
n_{op}	Optical noise of the ROF link
$n_{\text{op,wcdma}}$	Optical noise in the WCDMA band
$n_{\text{op,wlan}}$	Optical noise in the WLAN band

$n_{\text{up,air}}$	Combined noise of the WCDMA and WLAN systems in the air interface (uplink)
$n_{\text{up,wcdma}}$	Noise process of the air interface in the WCDMA band (uplink)
$n_{\text{up,wl}}$	Noise process of the air interface in the uplink
$n_{\text{up,wlan}}$	Noise process of the air interface in the WLAN band (uplink)
P	Duration of a packet payload
$P(t)$	Instantaneous optical power
P_c	Probability of collision in transmission
P_{er}	Probability of an error in the received packet
P_o	Mean optical power detected at the photodetector
P_r	Received signal power
P_s	Conditional probability that the current transmission is successful
$P_{s,i}$	Symbol power of the ith WCDMA signal
$P_{s,\text{wlan}}$	Symbol power of a WLAN signal
P_t	Transmitted signal power
P_{tr}	Probability of at least one transmission occurs in a randomly chose slot time
q	Electron charge
R_{90}	90% confidence coverage radius
R_{L}	Receiver resistance
RIN	Parameter of the relative intensity noise
r	Distance between a MS and the base station
$\text{rect}(\cdot)$	Rectangular function
$\text{rect}(t)$	Rectangular pulse
S	Saturated throughput efficiency
S_{sh}	Shadowing effect parameter
$S(\omega)$	Power spectrum of clipping process
$\text{SDINR}_{up,wcdma}$	Cumulative SDINR of an uplink WCDMA signal
$\text{SDNR}_{down,wcdma}$	SDNR of a downlink WCDMA signal
$\text{SDNR}_{down,wlan}$	SDNR of a downlink WLAN signal
$\text{SDNR}_{up,wlan}$	Cumulative SDNR of an uplink WLAN signal
$\text{SINR}_{\text{up,wcdma}}$	SINR of an uplink WCDMA signal
$\text{SNR}_{air,wcdma}$	SNR of a downlink WCDMA signal through the air interface

$\mathrm{SNR}_{air,wlan}$	SNR of a downlink WLAN signal through the air interface
$\mathrm{SNR}_{\mathrm{up,wlan}}$	SNR of an uplink WLAN signal
s, $s(t)$	Continuous signal
s_{RAP}	Signals at the RAP (uplink)
s_{BPSK}	BPSK signal
$s_{DSSS-BPSK}$	DSSS-BPSK signal
$s_{DSSS-QPSK}$	DSSS-QPSK signal
s_{laser}	RF signal that modulates a laser
s_{QPSK}	QPSK signal
s_{wcdma}	WCDMA signal
s_{wlan}	WLAN signal
$slot$	Length of a slot time in bit
T	Optical modulation index ratio
$T_{\mathrm{ACKTimeout}}$	Duration of acknowledgement timeout
T_{ACK}	Duration of positive acknowledgment
T_c	Duration of a station that senses busy due to a collision
T_{chip}	Chip period
T_{DIFS}	Duration of a distributed interframe space
T_{er}	Duration of a station that senses busy due to an error in the received packet
T_s	Duration of a station that senses busy due to a successful transmission
T_{SIFS}	Duration of a short interframe space
T_{sym}	Symbol period
t	Continuous time
v	Expected rate of clipping occurrence condition on the input signal
X	Slot times required for a successful transmission
x	Normalized frequency for the clipping event
$y(x)$	Normalized spectrum of the clipping distortion
Z_i	Distorted signals from the photocurrent in the WCDMA band
Z_{in}	Impedance of a laser
Z_{out}	Impedance of an optical receiver

List of Abbreviations

Abbreviations	Description
3G	Third-generation
BPSK	Binary phase shift keying
CCK	Complementary code keying
CSMA/CA	Carrier sense multiple access with collision avoidance
CW	Contention window
DC	Direct current
DBPSK	Differential binary phase shift keying
DCF	Distributed coordination function
DIFS	Distributed interframe space
DQPSK	Differential quadrature phase shift keying
DS	Direct sequence
DSSS	Direct sequence spread spectrum
DSSS-BPSK	DSSS-binary phase shift keying
DSSS-QPSK	DSSS-quadrature phase shift keying
FDD	Frequency division duplex
FDM	Frequency division multiplexed
HR/DSSS	high rate direct sequence spread spectrum
IMT-2000	International Mobile Telecommunications at 2000 MHz
ISI	Inter symbol interference
LAN	Local area network
LOS	Line of sight
Mbps	Mega bits per second
Mchip/s	Mega chip per second
MS	Mobile station
Msymbol/s	Mega symbol per second
PBCC	Packet binary convolutional coding
PDF	Probability distribution function

PSD	Power spectrum density
QPSK	Quadrature phase shift keying
RAP	Radio access point
RF	Radio Frequency
RIN	Relative intensity noise
RMS	Root means square
ROF	Radio over fiber
SCM	Sub-carrier multiplexed
SDINR	Signal to distortion interference and noise ratio
SDNR	Signal to distortion and noise ratio
SIFS	Short interframe space
SINR	Signal to interference and noise ratio
SNR	Signal to noise ratio
TDD	Time division duplex
UMTS	Universal Mobile Telecommunications System
WCDMA	Wideband code division multiple access
WLAN	Wireless local area network

Chapter 1

Motivation and Background

1.1 Forth Generation Quest

Since the late 1990's, many have explored the potential of wireless broadband communication system to provide high bit rate and mobility. Correia and Prasad [1] provide an overview of wireless broadband systems. They had foreseen that wireless broadband systems will provide bit rate as high as 155 Mbps using the 60 GHz band. They discussed potential wireless applications such as high-definition TV, high-definition videophone, local area network (LAN) interconnection, mobile office, and interactive TV which can only be realized with high data rate systems. They examined different aspects of wave propagation in the wireless environment including average power decay and delay spread. They also discussed challenges in modeling the wave propagation. The challenges encourage further research and development in the wireless broadband system. The applications that require the 155 Mbps bandwidth will soon arrive with advancement in the wireless broadband system. Currently, the IEEE standard 802.11g can provide date rate of 54 Mbps which is one third of what is foreseen. The market is responding strongly to this development and demands for even higher data rate.

In the path towards forth-generation cellular network, wireless local area network (WLAN) will play an important role in the transition. The WLAN hotspots can be used to inter-network with the third-generation (3G) cellular network. The obvious advantages for users are network connectivity everywhere and high date rate at strategic locations. The advantages have been addressed in [2] by Doufexi et al. They quantified the capacity enhancement and benefits of such internetworking. In their simulation results, they have shown that 15 WLAN access points that were used to cover an area of 1 km by 1 km can provide a peak data rate of 42 Mbps. For extra capacity in the 3G cellular system, the simulation has shown that over 1000 extra customers can be supported with the same deployment described above. The increase in capacity is especially beneficial at dense urban areas where hotspots can be used to relieve cellular congestion. Hotspots also support multitude of services in addition to voice. The WLAN trend is high data rate coverage for a small area. In order to support a large area of coverage many hotspots are required. The large scale deployment of WLAN is both technical and economical challenge. In [3], Varshney has discussed that mutual interference can cause degradation in quality of service when there are large number of WLAN hotspots. This is true because there are only three non-overlapping channels in IEEE 802.11b. Therefore, some kind of coordination is required for interference cancellation in large-scale deployment.

1.2 Optical Fiber Based Radio Access

The optical fiber based radio access can integrate both the 3G wideband code division multiple access (WCDMA) system and the IEEE 802.11 WLAN system (see Figure 1.1). One way is to use the sub-carrier multiplexed (SCM) technique to carry signals of both systems through fiber-optic cables between

a central base station and a radio access point (RAP). The cables that support this communication are called the radio over fiber (ROF) link. The RAP operates like an extended antenna from the base station. It transmits and receives the signals of mobile stations (MSs). For the WCDMA system, an MS can be a cellular phone; for the WLAN system, the MS can be a laptop with IEEE 802.11 interface. If a portable unit has both cellular and WLAN interfaces, it can connect to the networks using either one of these standards. This means seamless integration between these two services.

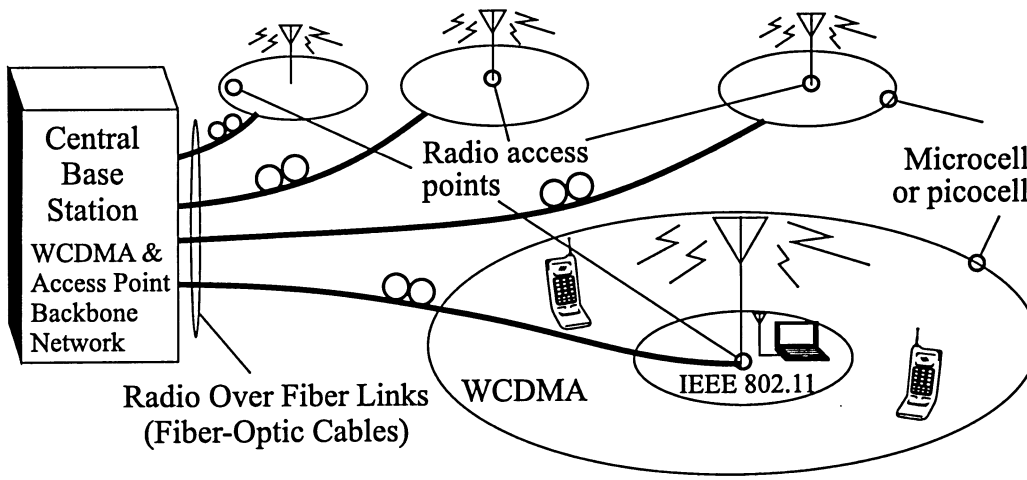

Figure 1.1: Microcellular architecture with employment of ROF links

The integration of the two systems is an excellent solution to the demand for high data rate applications and reasonable mobility. The employment of the ROF link in the SCM architecture allows reduction in cell size that increases the frequency reuse, thus improves the spectral efficiency. The RAP with relatively simple functions is not only inexpensive, but its compact size can also save estate cost. A centralized network can be constructed using ROF links to connect multiple RAPs to a single central base station. This is also illustrated in Figure 1.1. The advantages of this network are: i) flexible radio spectrum management, ii) flexible data flow control, iii) sharing the

cost of the central base station deployment and operation, and iv) ability to handover across systems. The central base station is able to monitor activities in all the cells. That allows radio spectrum, data flow and handover can be easily managed avoiding negotiation with other base stations. Co-channel interference can be reduced because the radio spectrum of adjacent cells are managed by a centralized system.

There has been significant work done in the wireless access using the ROF link by many authors. Tonguz et al. [4] has investigated the personal communications access networks using SCM ROF link. They have derived the carrier to noise ratio of the link that includes the optical noise and the nonlinear distortion in the link. Moreover, they have also investigated the cell coverage of the link. Fernando and Anpalagan [5] also studied the ROF link for fiber based wireless access, and they have derived the cumulative signal to noise ratio (SNR) for the downlink case. Signals go through the ROF link, then through the air interface in the downlink case. They also studied the relationship between the cumulative SNR and the SNR after the optical link. Walker et al. [6] presented the criteria of optimizing the carrier to noise ratio of the SCM optical network. The criterion is the optimal choice of an optical modulation index that is used to modulate a laser. This optical modulation index is dependent on the number of channels and the nonlinearity of the entire optical link. The relative intensity noise in the ROF link is further improved by Fernando in [7] and this improved expression gives a more accurate model for the ROF link. In the paper by Kim and Chung [8], they had investigated several passive optical networks that support micro-cellular communication systems that employ narrow band code division multiple access. One of the passive optical networks that they investigated employs the SCM technique, and they derived the carrier to noise and distortion ratio for the network. Fan et al. [9] investigated the employment of ROF link in micro-cellular personal

communication system. They have included the fading and the co-channel interference of the air interface to improve their model. They had also compared the performance between the uplink and the downlink.

1.3 Major Contributions of the Thesis

The major contribution of this thesis is the uplink and downlink analysis of a SCM based optical fiber based wireless access architecture that is designed to simultaneously support the WLAN (IEEE 802.11b) and WCDMA systems. The analysis includes mathematical derivations and numerical results that quantify the performance of the architecture.

The uplink involves with the signals first propagated through the air interface and then the ROF link. The downlink involves with signals first propagated through the ROF link then the air interface. The air interface introduces linear impairments such as multipath fading, while the ROF link introduces nonlinear impairments such as intermodulation product distortion. The analysis accounts for the cumulative effects of all the impairments. Also we analyze the system with respect to relative power differences between the WLAN and WCDMA systems and define a cumulative modulation depth that is the weighted average of individual modulation depths of these systems.

1.4 Thesis Outline

Chapter 2 provides the background of the WLAN and 3G mobile communication systems. This chapter is the basis for the discussion on simultaneously supporting the two systems. For the WLAN system, the IEEE 802.11 standards are considered, while WCDMA is considered for the 3G mobile communication system. For the IEEE 802.11, the medium access control and

the physical layer specifications for the 2.4 GHz band are discussed. A brief overview of the WCDMA system is provided. There are many factors from the two systems that cumulatively or independently affect the performance of the proposed fiber based radio access SCM architecture.

The fiber-wireless architecture involves both the wireless channel and the optical channels. Chapter 3 provides a reference to the mechanisms in the two channels. In the wireless channel, path loss, multipath fading, and shadowing are the different issues related to the signal propagation in the air. The cause and effect of each of these issues are investigated. The optical channel which is the ROF link has several mechanisms that affect the performance of communication. The mechanisms can be categorized as (1) nonlinear and (2) noise mechanisms. The nonlinear mechanism includes the intermodulation products and clipping distortion. The relative intensity noise, shot noise and thermal noise are the noise mechanisms. The power loss due to the optical-to-electrical and electrical-to-optical conversions, fiber attenuation; and its affect on the signal to noise performance is also discussed.

Chapter 4 presents the fiber based radio access architecture that jointly supports the WLAN and WCDMA systems using SCM technique. According to SCM technique, the pass band WLAN and WCDMA signals are simply added using a RF power combiner and then transmitted through a fiber-optic cable known as the ROF link. The uplink and downlink analysis of the SCM architecture is presented with mathematical derivations to quantify the system performance. The analysis is completed with the numerical results that are presented in chapter 5. The results are graphically plotted for clear understanding. The results also lead to the discussion in chapter 5. This thesis is then concluded with a discussion on future work.

Chapter 2

IEEE 802.11 Wireless Local Area Network and Third Generation Mobile Communication System

To simultaneously support services of the IEEE 802.11 WLAN and WCDMA 3G mobile communication systems, it is important to first understand various issues associated with the two systems because the performance of the fiber based wireless access architecture can be affected by these issues. In this Chapter an overview of IEEE 802.11 WLAN and 3G cellular communication systems are provided.

2.1 IEEE 802.11 Wireless LAN System

The throughput which is a medium access control layer issue can be affected by the infrastructure of the fiber base WLAN. This is illustrated in section 4.3. Therefore, the medium access controls as well as the physical layer specifications of the IEEE 802.11 are investigated in the following sections. For the physical specifications, the two IEEE 802.11 standards that employ the

2.4 GHz band are studied.

2.1.1 Medium Access Control of IEEE 802.11

The IEEE 802.11 standard employs a distributed coordination function (DCF) for the medium access control. The DCF is based on carrier sense multiple access with collision avoidance (CSMA/CA) that provides asynchronous access to the medium with exponential back off. The DCF basic access method is described below and if readers who want more details should refer to clause 9 of [10]. When a packet is ready to be transmitted, the station listens for an idle channel for duration that equals a distributed interframe space (DIFS). If the channel is busy during that duration, the station will wait until the channel becomes idle again for a DIFS time. After the DIFS time, the station holds off transmission for a number of slot times; this is the back off period. The slot time is defined as the duration for a station to detect a transmission from any other station. The number of slot times is uniformly chosen from (0, CW−1) where CW is the current contention window. During the initial back off period the current contention window is at its minimum. It will double for every unsuccessful transmission until the specified maximum is reached. A back off counter keeps track of the remaining slot times that the station holds off transmission during the back off period. The back off counter continues to count down whenever the channel is idle. Otherwise, the counter will stop decrement until the channel becomes idle for duration of a DIFS. When the counter reaches zero, the station will transmit the packet.

When the receiving station receives a packet, it will transmit a positive acknowledgement after a short interframe space (SIFS) time. The received station can transmit the acknowledgement without collision because the immediate waiting time, SIFS, allows fast access to the medium. A SIFS time

together with the channel propagation time is shorter than a DIFS time. A successful transmission is when the acknowledgement is received within the acknowledgement timeout period. An unsuccessful transmission is when the transmitted station does not receive the acknowledgement or it received a packet from other stations. Then, the transmitting station needs to retransmit. The two interframe spaces, DIFS and SIFS, mentioned above are the time intervals between each frame. They are independent of the bit rate of the station. The duration of interframe spaces are determined by the characteristics of the physical layer. A different modulation implies a different physical layer. For a different physical layer, there is a different set of value for the duration of the interframe spaces. The durations are specified in IEEE 802.11 standard [10] except for DIFS. However, DIFS can be determined from a timing relation defined in section 9.2.10 of [10]. The timing relations for a slot time and à DIFS time are given as follows:

$$\begin{aligned} \text{aSlotTime} = {} & \text{aCCATime} + \text{aRxTxTurnaroundTime} \\ & + \text{aAirPropagationTime} + \text{aMACProcessingDelay} \end{aligned} \tag{2.1}$$

$$T_{\text{DIFS}} = T_{\text{SIFS}} + 2 \times \text{aSlotTime} \tag{2.2}$$

where, aCCATime is the duration to perform the clear channel assessment function, aRxTxTurnaroundTime is the turnaround time for reception or transmission, aAirPropagationTime is the air propagation time, and aMACProcessingDelay is the MAC layer processing delay. The values for aCCATime, aRxTxTurnaroundTime, aAirPropagationTime, aMACProcessingDelay, T_{SIFS}, and aSlotTime are listed in the tables 57a and 59 of [10]. The saturated throughput model has been derived in [11], then Chatzimisios et al. [12] improved it to a more accurate model that includes bit error rate of the channel and limited packet retransmission. The saturated throughput refers to a system condition where n contenting

stations always have a packet ready to transmit. The saturated throughput efficiency, S, is given as:

$$\begin{aligned} S &= \frac{P_{tr}P_s l}{\mathrm{E}[slot]} \\ &= \frac{P_{tr}P_s l}{(1-P_{tr})\epsilon + P_{tr}P_s T_s + P_{tr}P_c T_c + P_{tr}P_{er}T_{er}} \end{aligned} \tag{2.3}$$

where, P_{tr} is the probability that at least one transmission occurs in a randomly chosen slot time, P_s is the conditional probability that this transmission is successful, and l is the packet size. The E[$slot$] is the average length of a slot time in bit that includes: i) the average duration of an empty slot, $(1-P_{tr})\epsilon$, where ϵ is the duration of an empty slot; the average time that a station senses ii) a successful transmission, $P_{tr}P_s T_s$, iii) a collision, $P_{tr}P_c T_c$, and iv) a transmission error, $P_{tr}P_{er}T_{er}$. The probability P_c and P_{er} are the probability of collision in transmission and error in the received packet respectively. The time, T_s, T_c and T_{er}, are durations that a station senses busy due to successful transmission, collision, and error in the received packet respectively. In [12], the authors did not define T_s, T_c and T_{er}. However, the authors referred T_s and T_c to [11] where the time is defined. The time T_s and T_c are given as follows:

$$T_s = T_{\mathrm{DIFS}} + \mathrm{H} + \mathrm{P} + 2\delta + T_{\mathrm{SIFS}} + T_{\mathrm{ACK}} \tag{2.4}$$

$$T_c = T_{\mathrm{DIFS}} + \mathrm{H} + \mathrm{P} + \delta \tag{2.5}$$

where, T_{DIFS}, T_{SIFS} and δ are the time for a DIFS, a SIFS, and a propagation delay respectively, H is the duration of the physical layer header and the medium access control layer header, P is the duration of the packet payload, and T_{ACK} is the duration of a positive acknowledgment. The remaining undefined time T_{er} can be derived according to a transmission error scenario. When

error is found in the received packet, no acknowledgement will be transmitted. After the acknowledgement timeout period, the packet will be retransmitted. Therefore, the time T_{er} can be given as:

$$T_{er} = T_{\text{DIFS}} + \text{H} + \text{P} + T_{\text{ACKTimeout}} \tag{2.6}$$

where, $T_{\text{ACKTimeout}}$ is the acknowledgement timeout.

Chatzimisios et al. [12] presents the average packet delay E[D] as:

$$\text{E}[D] = \text{E}[X]\text{E}[slot] \tag{2.7}$$

where, E[X] is the average number of slot times required for a successful transmission.

2.1.2 Physical Layer Specifications of IEEE 802.11 for 2.4 GHz Band

At 2.4 GHz band using the direct sequence spread spectrum (DSSS) technique, the IEEE standards 802.11 and 802.11b have defined four modulation schemes to provide date rates of 1 Mbps, 2 Mbps, 5.5 Mbps, and 11 Mbps. The modulation schemes are DSSS-binary phase shift keying (DSSS-BPSK), DSSS-quadrature phase shift keying (DSSS-QPSK), complementary code keying (CCK), and packet binary convolutional coding (PBCC). DSSS-BPSK and DSSS-QPSK are used to provide 1 Mbps and 2 Mbps respectively. Both CCK and PBCC can provide data rate of 5.5 Mbps and 11 Mbps. In terms of the bandwidth, all the modulation schemes occupy about 22 MHz of bandwidth. A non-overlapping channel is said to be 30 MHz apart. The available spectrum in the 2.4 GHz band can only allocate three non-overlapping channels.

2.1.2.1 Direct Sequence Spread Spectrum–IEEE 802.11

DSSS spreading scheme was included even in the early development of IEEE 802.11 specifications. According to clause 15 of [10], this modulation scheme provides a data rate of 1 Mbps or 2 Mbps. The data is spread with an 11 MHz PN code to obtain a transmission bandwidth of 22 MHz. This DSSS system provides a processing gain of at least 10 dB. The minimum transmission power is 1 mW and for transmission power greater than 100 mW power control must be implemented. Furthermore, the max power of the system should comply with the max power of 1 W for the ISM band. The power control should have no more than four power levels. To provide the 1 Mbps data rate, a differential binary phase shift keying (DBPSK) scheme is employed for baseband modulation. The 2 Mbps data rate is provided using a differential quadrature phase shift keying (DQPSK) scheme for baseband modulation. Differential coding is a memory coding that the actual information of a bit is dependent on both previous and current bits. According to IEEE 802.11 standard, the binary phase shift keying (BPSK) signal has a differential phase shift d_k of 0 degree for logic zero, and a differential phase shift of 180 degree d_k for logic one. The BPSK signal can be expressed as follows,

$$s_{\text{BPSK}} = \sum_{k=-\infty}^{\infty} (1 - 2\,d_k)\sqrt{\frac{2\,E_{sym}}{T_{sym}}}\cos(\omega_c t) \qquad 0 \leq t \leq T_{sym} \qquad (2.8)$$

where, E_{sym} is the energy of a symbol, T_{sym} is the symbol period and ω_c is the carrier frequency. The four phases of QPSK, $0, \frac{\pi}{2}, \pi, \frac{3\pi}{2}$, are encoded with differential codes $d_k\,d_{k+1}$ of $00, 01, 11,$ and 10 respectively. The QPSK signal

can be expressed as follows,

$$s_{\text{QPSK}} = \sum_{k=-\infty}^{\infty} \sqrt{\frac{2\,E_{sym}}{T_{sym}}} \Big[(1-2\,d_k)\cos(\omega_c t) + (1-2d_{k+1})\sin(\omega_c t)\Big] \qquad 0 \le t \le T_{sym} \tag{2.9}$$

In DSSS system, baseband modulation is spread with a 11-chip Barker sequence which is given as $0, 1, 0, 0, 1, 0, 0, 0, 1, 1, 1$. The DSSS-BPSK signal can be written as follows,

$$s_{DSSS-BPSK} = \sqrt{\frac{2\,E_{sym}}{T_{sym}}} \sum_{k=-\infty}^{\infty} \sum_{i=0}^{10} (1-2\,h_i)\,(1-2\,d_k) \cdot \text{rect}(t-iT_{chip}) \cos\Big(\omega_c(t-iT_{chip})\Big) \qquad 0 \le t \le T_{sym} \tag{2.10}$$

Similarly, the DSSS-QPSK signal can be written as follows,

$$s_{DSSS-QPSK} = \sqrt{\frac{2\,E_{sym}}{T_{sym}}} \sum_{k=-\infty}^{\infty} \sum_{i=0}^{10} (1-2\,h_i)\,\text{rect}(t-iT_{chip}) \Big[(1-2\,d_k)\cos\left(\omega_c(t-iT_{chip})\right) + (1-2\,d_{k+1})\sin\left(\omega_c(t-iT_{chip})\right)\Big] \qquad 0 \le t \le T_{sym} \tag{2.11}$$

where, h_i is the coded sequence, d_k is the differential coded message, $\text{rect}(t - iT_{chip})$ is the rectangular pulse with duration of one chip period T_{chip}.

2.1.2.2 High Rate Direct Sequence Spread Spectrum– IEEE 802.11b

The high rate direct sequence spread spectrum (HR/DSSS) is defined in clause 18 of IEEE standard 802.11b [13]. This clause extends the bit rate to provide 5.5 Mbps and 11 Mbps for the DSSS system. The HR/DSSS system also

provides bit rate of 1 Mbps and 2 Mbps as described in the clause 15 of IEEE 802.11 [10]. In order to provide the high date rates (5.5 Mbps and 11 Mbps) without the increase in transmission bandwidth, two modulation schemes are defined: 8-Chip complementary code keying (HR/DSSS/CCK) and packet binary convolutional coding (HR/DSSS/PBCC).

8-Chip Complementary Code Keying The HR/DSSS system has a chipping rate of 11 MHz which occupies about 22 MHz of bandwidth. The HR/DSSS/CCK scheme spreads the baseband signal with a complex chip sequence generated from a complementary code with eight chips in length. The code word of HR/DSSS/CCK is given as follows:

$$\mathbf{C} = \left[e^{j(\phi_1+\phi_2+\phi_3+\phi_4)}, e^{j(\phi_1+\phi_3+\phi_4)}, e^{j(\phi_1+\phi_2+\phi_4)}, e^{j(\phi_1+\phi_4)}, e^{j(\phi_1+\phi_2+\phi_3)}, e^{j(\phi_1+\phi_3)}, e^{j(\phi_1+\phi_2)}, e^{j(\phi_1)} \right] \tag{2.12}$$

The four phases ϕ_1, ϕ_2, ϕ_3, and ϕ_4 relate to the data according to rules defined in the standard [13]. Applying different rules, different sets of complementary code words can be derived which represent data symbols. To achieve the bit rate of 5.5 Mbps, four bits of information is coded in each symbol that spreads with the complementary code words generated according to the rule in the standard. There are 16 distinct complementary code words derived from expression (2.12). By coding four bits of data in a symbol, it leads to a symbol rate of 1.375 Msymbol/s. When double the data rate to 11 Mbps, the amount of information coded into a symbol is also doubled. Therefore, each symbol is coded with eight bits of data. Applying the rule in the standard, a set of 64 distinct complementary code words can be generated from expression (2.12).

Packet Binary Convolutional Coding The HR/DSSS/PBCC scheme has the potential to enhance the system performance when the technology for

the implementation becomes cost effective. The binary convolutional coding scheme uses 64-state binary convolutional code and a 256-bit pseudo-random cover sequence. The output of the binary convolutional encoder gives a pair of bits that is to feed the I and Q channels.

The binary convolutional coding is first encoded to the incoming data that generates two encoded bits for every bit of data. A pseudo-random cover sequence is used to map the encoded data to BPSK and QPSK for 5.5 Mbps and 11 Mbps respectively. The 64-state binary convolutional code has a generator matrix given as below:

$$\mathbf{G} = \left[D^6 + D^4 + D^3 + D + 1, D^6 + D^5 + D^4 + D^3 + D^2 + 1\right] \qquad (2.13)$$

For data of 5.5 Mbps, the encoded bits are mapped to BPSK according to the current value of the cover sequence. For example, when the value of the cover sequence is 1, then the coded data would map to π for '0' and $3\pi/2$ for '1'. The coding and modulation give a half bit of data per symbol. For 5.5 Mbps of throughput, the cover sequences need to generate at 11 Mchip/s. In the case of 11 Mbps, its encoded bits are mapped to QPSK. The mapping to QPSK is according to cover sequence which can be obtained from the standard [13]. Using QPSK the two data bits is mapped to one QPSK symbol, which makes the data to transmit at one bit per symbol. The rate of 11 Mchip/s for the cover sequence results a data rate of 11 Mbps.

2.2 UMTS: Wideband Code Division Multiple Access

The Universal Mobile Telecommunications System (UMTS) is the 3G mobile communication system that is the successor to the Second Generation mobile

standard such as GSM and IS-95. Within the UMTS there are many mobile standards, but in this thesis the standard of interest is WCDMA scheme. The WCDMA standard is part of the International Mobile Telecommunications at 2000 MHz (IMT-2000) family. The characteristics of IMT-2000 system are [14]: i) high data rate of 144 kbps everywhere to 2 Mbps indoor, ii) symmetrical and asymmetrical data transfer, iii) channel switching and packet switching transfer, and iv) high spectrum efficiency.

The WCDMA is a 3G European system [15]. In the WCDMA system, direct sequence system is used for multiple access control (DS-CDMA). The WCDMA signal is spread at 3.84 Mchip/s for operating in frequency division duplex (FDD) mode and it is spread at 1.024 Mchip/s for operating in time division duplex (TDD) mode. The signal occupied a bandwidth of 5 MHz. The data traffic can be symmetrical and asymmetrical. In FDD mode, frequency bands 1920 MHz$-$1980 MHz and 2110 MHz$-$2170 MHz are allocated for uplink and downlink respectively. The QPSK is the modulation that is employed for data representation and spreading. The WCDMA signal has a frame length of 10 ms. In the WCDMA system, power control is used at a rate of $1,500$ times/sec and it is dependent on the signal-to-interference ratio. The peak transmission power of the WCDMA base station is 33 dBm. The typical transmission power from a base station is 20 to 40 W. The maximum transmission power of a mobile unit is 21 dBm. The receiver sensitivities are -121 dBm and -117 dBm for the base station and the mobile unit respectively.

Chapter 3

Basic Fiber Based Radio Access Mechanism

3.1 Air Interface

3.1.1 Path Loss

With large-scale propagation model, the RF power loss in air is expressed as a function of distance between the MS and the base station. The expression for a received signal power is given as follows [4]:

$$P_r = S_{sh} P_t \left(\frac{\lambda}{4\pi r} \right)^{\gamma} \tag{3.1}$$

where, P_r is the received signal power, P_t is the transmitted signal power, S_{sh} is the parameter that reflects the shadowing effect, λ is the wavelength of the transmitted signal, r is the distance from the MS to the base station, and γ is the path loss exponent.

The expression is modified to express the 90% confidence coverage radius (R_{90}) as a function of the received RF power loss in (3.2). This expression

gives the statistical signal attenuation for a distance between the MS and the base station. The distance is said to be 90% confidence coverage radius which means the attenuation at that distance does not exceed the calculated value for 90% of the time. The modified expression is given as follows:

$$L_{wl}(R_{90}) = \frac{1}{S_{sh}} \left(\frac{4\pi R_{90}}{\lambda \, 10^{\left(\frac{-0.13\eta}{\gamma}\right)}} \right)^{\gamma} \tag{3.2}$$

where, R_{90} is the 90% confidence coverage radius. The term $10^{\left(\frac{-0.13\eta}{\gamma}\right)}$ comes from the relationship between the 90% confidence coverage radius R_{90} and the average coverage radius r [16], where η is the standard deviation of the channel loss.

3.1.2 Multipath Fading

Multipath fading occurs when two or more delayed version of the transmitted signal creates interference due to reflection and scattering. The effect is significant because over a small travel distance or time interval the signal strength can change rapidly. At the receiver where the received signal is the summation of the delayed version of the signal, time dispersion or inter symbol interference (ISI) is created. The ISI reduces the useful data rate that can be transmitted. In addition, whenever surrounding objects or the MS are moving at a fast pace, the received signal would appear to have random frequency modulation. This effect is known as Doppler shift.

Due to the random nature of the wireless channel, a statistical model of the channel can be obtained with an ensemble of many measurements taken from a local area. A baseband equivalent of the multipath fading channel is given

in [17] as follows:

$$h_b(t,\tau) = \sum_{i=1}^{L} a_i(t) \exp\big(-j\theta_i(t)\big)\, \delta\big(t-\tau_i(t)\big) \tag{3.3}$$

where, L is the number of resolvable signal paths, $a_i(t)$ is the amplitude, $\theta_i(t)$ is phase shift, and $\tau_i(t)$ is the time delay of individual path. It can be seen from the fading channel expression that the amplitude is time variant, so does angle and time delay.

In the context of this thesis, both WLAN and WCDMA systems are designed to provide coverage for pico- and micro-cell with cell radius from 100 m to 2 km. A macro-cell would typically have a coverage radius of 5–6 km. In smaller cell structures, it is expected that the mobility within the cell is low which means the Doppler spread profile of the channel is quite relaxed. The assumption for such a wireless channel is a frequency selective and a slow fading. With slow fading, the channel can be assumed to remain invariant for at least few symbol periods. The impulse response of the fading channel (3.3) can be rewritten as follows:

$$h_b(\tau) = \sum_{i=1}^{L} a_i \exp\big(-j\theta_i\big)\, \delta\big(t-\tau_i\big) \tag{3.4}$$

A frequency selective channel is related to the delay spread profile of the channel and the transmitted bandwidth. When a transmitted bandwidth is much greater than the coherent bandwidth of the channel, the signal is said to experience frequency selective fading. It has been reported in [18] that for the 2 GHz spectrum the delay spread in urban propagation environment have an average of 1.1 μs for 90% of time and a maximum delay spread of 11 μs. These delay spread parameters translate to a coherent bandwidth in kHz range. The bandwidth of the two systems is in the MHz range. It has

been mentioned that frequency selective channel causes ISI due to multipath components. A RAKE correlator exploits the correlation of signal in different paths to resolve multipath components. In [19], a RAKE correlator is modeled by a tapped delay line with statistically independent time-variant tap weights. For L multipath components, the tap weights can resolve L delayed version of the signal. Assuming RAKE correlator is employed in the WLAN and WCDMA systems, the fading channel can be rewritten as follows:

$$h_b(\tau) = a \exp\left(-j\theta\right) \delta\left(t-\tau\right) \tag{3.5}$$

where, the signal envelop (a) has a Rayleigh distribution, the signal phase shift (θ) is uniformly distributed over $\{\pi, -\pi\}$, and the delay (τ) is uniformly distributed over a symbol period T_{sym}. The PDF of Rayleigh distribution is defined as follows [20]:

$$p(a) = \begin{cases} \frac{a}{\sigma_a^2} \exp\left(-\frac{a^2}{2\sigma_a^2}\right) & \text{for } 0 \leq a \leq \infty \\ 0 & \text{for } a < 0 \end{cases} \tag{3.6}$$

where, a is the Rayleigh distributed random variable of signal amplitude and σ_a^2 is the time-average power of the signal. In some radio environments, there is line of sight (LOS) between the transmitter and receiver. The LOS component of the signal does not undergo fading and the signal envelop is said to have a Rician distribution. The PDF of Rician distribution is given in [20] as follows:

$$p(a) = \begin{cases} \frac{a}{\sigma_a^2} \exp\left(-\frac{a^2+A_{\text{LOS}}^2}{2\sigma_a^2}\right) \mathrm{I_o}\left(-\frac{aA_{\text{LOS}}}{\sigma_a^2}\right) & \text{for } A_{\text{LOS}} \geq 0,\ a \geq 0 \\ 0 & \text{for } a < 0 \end{cases} \tag{3.7}$$

where, A_{LOS} is the peak amplitude of LOS component and $\mathrm{I_o}(\cdot)$ is the modified Bessel function of the first kind and zero-order.

3.2 The Radio over Fiber Link

The ROF link is a fiber-optic system that used to transmit RF signals between the base station and the central base station. In the ROF link, a laser diode is used to convert the RF signals to the optical signals that propagate through fiber-optic cables. The fiber-optic cable can be a single mode fiber or a multimode fiber. The single mode fiber can support much longer transmission distance compares to the multimode fiber. At the end of the ROF link, an optical receiver that consists of a photodiode converts the optical signals back to the RF signals. The major impairments of the ROF link that limit the signal quality are the nonlinear distortion and various noise mechanisms. These impairments limit the optical power can be transmitted through a fiber, thus affect the data rate and the distance that signals can propagate.

3.2.1 Intermodulation Product Distortion

The intermodulation product distortion is one of the nonlinearity that comes from the laser diode. The laser diode can be modeled accurately as a third order polynomial without memory as described in [21] and [22]. Using the polynomial model, the optical power of the laser diode that reaches the optical receiver (photodiode) can be expressed as:

$$P(t) = P_o[1 + s(t) + a_2 s^2(t) + a_3 s^3(t)] \tag{3.8}$$

where, $s(t)$ is the input signal, P_o is mean optical power that reaches the photodiode, a_2 and a_3 are the constants that describe the second and third order laser nonlinearity respectively. The laser model above neglects the optical noise. In addition, the fiber attenuation is embedded in the mean optical power (P_o) that received at the photodiode. The optical noise and fiber atten-

uation are described in details in the subsequent sections. A photodiode that located at the end of the fiber produces a photocurrent that is proportional to the received optical power. The photocurrent can be expressed as:

$$i(t) = I_{\mathrm{D}}[1 + s(t) + a_2 s^2(t) + a_3 s^3(t)] \tag{3.9}$$

and

$$I_{\mathrm{D}} = \Re P_o \tag{3.10}$$

where, I_{D} is the average photocurrent.

The second order intermodulation product creates DC and double frequency interference components. The third order intermodulation product creates in-band and triple frequency interference components. The total power of the intermodulation product distortion depends on the quality of the laser diode. A better laser diode has small nonlinearity constants a_2 and a_3.

3.2.2 Clipping Distortion

Another nonlinear distortion from the laser diode is the clipping distortion that is caused by an input signal that goes below the threshold current of the laser diode. Saleh [23] calculated the clipping distortion power assuming the power spectrum for this distortion is uniform throughout the entire spectrum. Mazo [24] derived a more accurate expression for the power spectrum of the clipping distortion.

The clipping distortion is defined this way: $g(t)$ is a zero-mean Gaussian process representing the summation of all the signals input to a laser; the distortion process is the negative portion of $g(t) + I_{\mathrm{B}}$, where I_{B} is laser bias current. Mazo's analysis is to find the spectrum of the distortion process. His

result is a spectrum that is a few decibels more accurate than Saleh's analysis. In his work, he assumed the occurrence of the clipping as a random Poisson process, and the time between each clipping is Rayleigh distributed. The last assumption is the clipped signals have a parabolic shape. This parabolic shape is used to calculate the power of the clipped signal.

The derivation for the power spectrum of the clipping distortion is discussed here. This discussion begins with parameters that describe the distortion process. The expected rate of clipping occurrence for an input signal modulates a laser diode while assuming the signal is flat over the frequency band $[f_a, f_b]$ is given as follows:

$$v = \sqrt{\frac{f_b^3 - f_a^3}{3(f_b - f_a)}} \exp(-\rho) \tag{3.11}$$

with

$$\rho = \frac{I_{\mathrm{B}}^2}{2\sigma_g^2} \tag{3.12}$$

where, ρ is the ratio of the square of the laser bias current (I_{B}) over two times the power of the input signal (σ_g^2). Another parameter that describes the clipping process is the expected time between each clipping event, which is given as:

$$\overline{\kappa} = \frac{1}{2} \frac{\mathrm{erfc}(\sqrt{\rho})}{v} \tag{3.13}$$

where, erfc($\cdot$) is the complementary error function and it is defined as:

$$\mathrm{erfc}(\chi) = \frac{2}{\sqrt{\pi}} \int_{\chi}^{\infty} e^{-u^2}\, du \tag{3.14}$$

Mazo used the following normalized value to describe the power spectrum of

the clipping distortion. The time between each clipping event (κ) is normalized to $\varpi = \frac{\kappa}{\overline{\kappa}}$ and the normalized frequency is $x = 2\pi\overline{\kappa}f = \overline{\kappa}\omega$. The normalized spectrum of the clipping distortion is given as:

$$y(x) = \frac{1}{2}\frac{\pi}{x^4}\int_0^{\infty} \varpi^3 \left(\frac{\sin\frac{x\varpi}{2}}{\frac{x\varpi}{2}} - \cos\frac{x\varpi}{2}\right)^2 \exp\left(-\frac{\pi}{4}\varpi^2\right) d\varpi \tag{3.15}$$

The integral for the normalized spectrum is very difficult to evaluate, so Mozo had given a simpler version of the spectrum.

$$y(x) = \frac{2}{\pi^2 x^3}\left[\sqrt{\pi}\,F\left(\frac{x}{\sqrt{\pi}}\right) - x + \frac{2x^2}{\sqrt{\pi}}\,F\left(\frac{x}{\sqrt{\pi}}\right)\right] \tag{3.16}$$

with

$$F(\chi) = e^{-\chi^2}\int_0^{\chi} e^{u^2}\,du \tag{3.17}$$

The spectrum of the clipping distortion is given as follows:

$$S(\omega) = \frac{\overline{\kappa}}{2L_{\text{op}}}\left(\frac{\pi}{\rho}\right)^{\frac{3}{2}} \sigma_g^2 \exp(-\rho)\, y(\overline{\kappa}\omega) \tag{3.18}$$

where, L_{op} is total RF power loss in the ROF link. The cumulative RMS optical modulation index (μ) is the weighted sum of individual optical modulation indices. In the FDM system, μ is equivalent to the square of total RF power that modulates the laser, which gives $\mu^2 = \sigma_g^2$. Using optical parameters (μ and I_{B}) and the relationship, $\rho = I_{\text{B}}^2/(2\mu^2)$, the spectrum of the clipping distortion is rewritten as follows:

$$S(\omega) = \sqrt{2}\mu^5 \frac{\overline{\kappa}\pi^{\frac{3}{2}}}{L_{\text{op}} I_{\text{B}}^3} \exp\left(-\frac{I_{\text{B}}^2}{2\mu^2}\right) y(\overline{\kappa}\omega) \tag{3.19}$$

Generally, the lowest frequency channels of the multiplexed signals have about

1 dB more in-band distortion power than those of the highest frequency. A normalized plot of the spectrum of the clipping distortion is given in Figure 3.1. The figure shows that the clipping distortion is dependent on μ. The clipping distortion is exponentially increased with μ because of the exponent of μ is five.

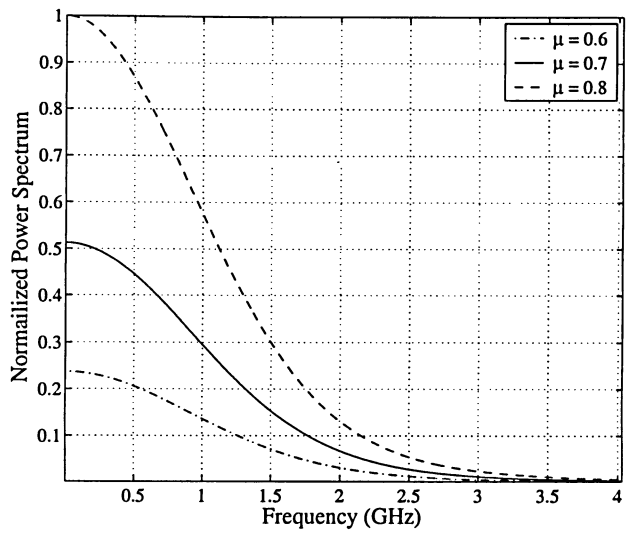

Figure 3.1: This figure illustrates the power spectrum of the clipping distortion of the SCM architecture. Different values of cumulative RMS optical modulation index (μ) are used to generate this plot.

3.2.3 Relative Intensity Noise

The relative intensity noise (RIN) arises from the random nature of stimulated emission of a laser diode that results in fluctuation of the light intensity. It is widely accepted that the power of this noise is proportional to the square of the average received photocurrent, $I_{\mathrm{D}} = \Re P_o$, and the RIN parameter. In [25], the RIN power is given as:

$$\langle i^2_{\mathrm{RIN}} \rangle = \mathrm{RIN}\, I^2_{\mathrm{D}}\, B \tag{3.20}$$

where, RIN is the RIN parameter and B is the bandwidth of the modulated signal. The RIN parameter is defined as the ratio between the mean-square intensity fluctuation of a laser diode output optical power $\langle \Delta P^2(t) \rangle$ to the square of the mean optical power (P_o).

$$\text{RIN} = \frac{\langle \Delta P^2(t) \rangle}{P_o^2} \tag{3.21}$$

It is measured in dB/Hz. This parameter depends on the temperature and the threshold current [26], but for commercial optical transmitter packages, these two factors are optimized. Therefore, the RIN parameter can simply be read off from a data sheet. Now, if we substitute the RIN parameter with the ratio, the square of the mean optical power is cancelled and the power of the RIN expression becomes:

$$\sigma_{\text{RIN}}^2 = \langle \Delta P^2(t) \rangle \, \Re^2 B \tag{3.22}$$

The RIN also increases with the light reflection back to the laser diode [25]. However, this reflection effect can be easily reduced by inserting an optical isolator in the optical transmitter.

The expressions (3.20) and (3.22) are also known as the intrinsic RIN which is accurate for a small optical modulation index ($m < 0.3$). However, for a large optical modulation index ($m > 0.3$), there is a sudden jump in RIN level. This additional RIN mechanism was investigated by Way in [27], and it is labeled as the dynamic RIN. From experimental studies, it is clear that the dynamic RIN increases with the RF power of modulating signals to a laser diode. In [7], Fernando had derived an expression for the dynamic RIN that is independent of device parameters, and the expression agreed with Way's observation. He derived the expression with the following assumption. First,

the optical power reaches the photodiode is given as:

$$P(t) = [1 + m\, s(t)][P_o + \Delta P(t)] \tag{3.23}$$

where, m is the optical modulation index, $s(t)$ is the modulated signal, and $\Delta P(t)$ is the intensity fluctuation of a laser diode output optical power that reaches the photodiode. Then, the output photocurrent is assumed to go through an ideal bandpass filter with impulse response $h(t)$. The RIN power term is among the variance of the current, $\langle I_h^2(t)\rangle$, after the bandpass filter; and it is expressed as:

$$\langle I_h^2(t)\rangle = I_{\mathrm{D}}^2\, m^2 \langle\, s^2(t)\rangle + \langle i_{\mathrm{sh}}^2\rangle + \langle i_{\mathrm{RIN}}^2\rangle \tag{3.24}$$

By removing the contribution of the modulated signal power and the shot noise, the RIN power is given as:

$$\langle i_{\mathrm{RIN}}^2\rangle = \mathrm{E}\left[\left\{\Re \int_{-\infty}^{\infty} [1 + m\, s(\tau)]\, \Delta P(\tau)\, h(t-\tau)\, d\tau\right\}^2\right] \tag{3.25}$$

From the above expression, we can see that the RIN power is independent of the average optical power P_o and convolution is performed to determine the current output from the bandpass filter. After evaluating the expectation, the final RIN power expression is given as:

$$\langle i_{\mathrm{RIN}}^2\rangle = \mathrm{RIN}\, I_{\mathrm{D}}^2\, B\, (1 + \mu^2) \tag{3.26}$$

where, μ is the cumulative RMS optical modulation index; and μ^2 is proportional to the RF power of the modulated signal. Using the earlier assumptions, the index μ is $\sqrt{m^2\langle s^2(t)\rangle}$.

3.2.4 Shot Noise

The shot or quantum noise arises from the random nature of the photons emitted from a laser diode and collected at a photodiode. The noise power of the shot noise is proportional to the average received photocurrent $I_{\mathrm{D}} = \Re P_o$ and the bandwidth B of the modulated signal; it is given as [25]:

$$\langle i_{\mathrm{sh}}^2 \rangle = 2\, q\, I_{\mathrm{D}}\, B \tag{3.27}$$

where, q is the electron charge. The average received photocurrent (I_{D}) is given in (3.10).

3.2.5 Thermal Noise

The mean square value of the thermal noise $\langle i_{\mathrm{th}}^2 \rangle$ is given by:

$$\langle i_{\mathrm{th}}^2 \rangle = \frac{4\, k_{\mathrm{B}}\, K}{R_{\mathrm{L}}} \tag{3.28}$$

where, k_{B} is Boltzmann's constant, K is the absolute temperature, and R_{L} is the receiver resistance.

3.2.6 Power Loss in Optical Fiber

In the ROF link, radio signal experiences power loss due to optical and electrical conversions, fiber attenuation, connector losses, and impedance mismatching. The total RF power loss in signals accounting the losses just mentioned is given as:

$$\begin{aligned} L_{\mathrm{op,dB}} &= 10 \log_{10}\left(\frac{Z_{in}}{G_m^2}\right) + 10 \log_{10}\left(\frac{\Re^2}{Z_{out}}\right) + 2(n_c\, l_c + \eta_f\, d) \\ L_{\mathrm{op}} &= 10^{(L_{op,dB}/10)} \end{aligned} \tag{3.29}$$

In the above expression, the first term accounts for RF power loss due to electrical-to-optical conversion, where G_m is the modulation gain of a laser in mW/mA and Z_{in} is the impedance of the laser in Ohms. The second term accounts for RF power loss due to optical-to-electrical conversion, where $\Re$ is the responsivity of a photodetector in mA/mW and Z_{out} is the impedance of the optical receiver in Ohms. The third term is the connectors loss of n_c connects each has loss of l_c. The last term is the fiber attenuation, where η_f is loss per distance and d is the fiber length.

Chapter 4

Sub-Carrier Multiplexed Architecture

The SCM architecture analyzed in this section employs an ROF link that transmits WCDMA and WLAN IEEE 802.11b signals simultaneously and provides WCDMA and WLAN services to MSs. Figure 1.1 illustrates the basic architecture of a microcellular system that employs SCM ROF links. A central base station with centralized processing capability is linked to multiple remote RAPs through ROF links. A RAP serves as an extended antenna from the central base station and provides wireless services to many mobile units.

Each RAP provides services to large coverage area through WCDMA system, and high-speed small area coverage to strategic locations through WLAN system. The RAP consists of simple devices and its main function is to convert received electrical signals to optical signals and vice versa. The simple RAP allows cost effective deployment of the fiber-wireless architecture with large number of RAPs. To study the performance of the SCM architecture, this section is divided into three portions: uplink analysis, downlink analysis and throughput efficiency of the WLAN. In the analysis section, the SNR, the signal to interference and noise ratio (SINR), the signal to distortion and

noise ratio (SDNR), and the signal to distortion interference and noise ratio (SDINR) are derived at various points of the architecture (see Figure 4.1). In the last portion, the throughput efficiency of the WLAN IEEE 802.11b system is investigated.

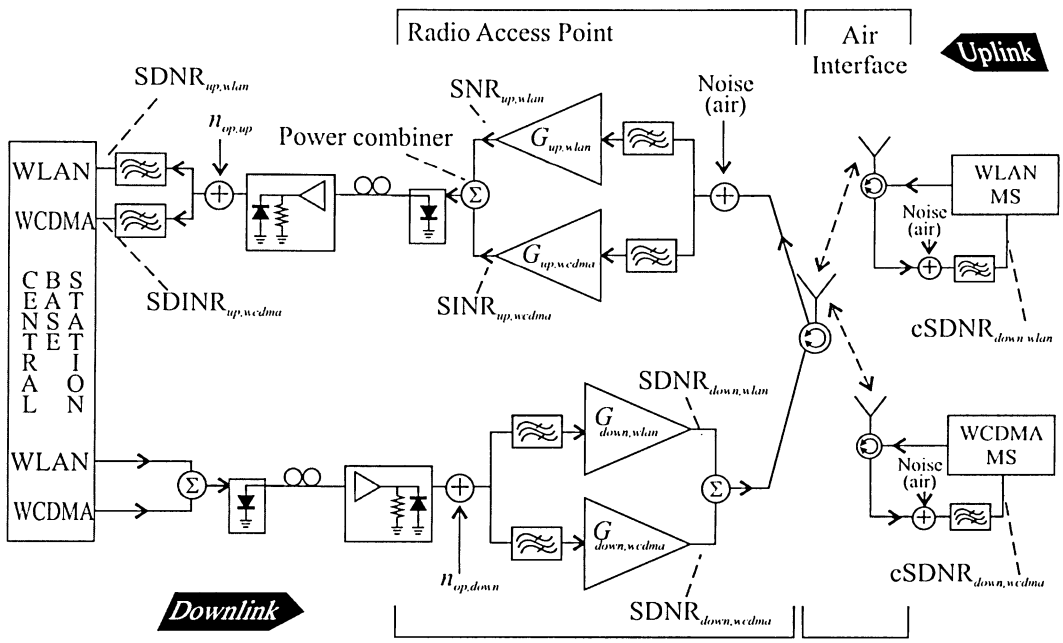

Figure 4.1: SCM architecture

4.1 Uplink Analysis

The SCM architecture supports both WCDMA and WLAN systems. In the uplink of the architecture, wideband spread spectrum signals are transmitted from multiple MSs and then they are received at the RAP. Let a subscript i be the ith MS signal of the WCDMA system for $i = 1, 2, \cdots, n$ where n is the total number of MS that is active in the system. Let a subscript β be an indication for the MS signal that is belonged to the WLAN system. The modulation technique for the signals is direct sequence spread spectrum (DSSS) which has been described in section 2.2. Using $P_{s,i}$ as the symbol

power of the ith WCDMA signal, the WCDMA signal that is received at the RAP is given as:

$$\begin{aligned} s_{\text{wcdma}}(t) &= \sum_{i=1}^{n} \sqrt{2P_{s,i}}\, d_i(t)\, c_i(t) \cos(\omega_\alpha t) \\ &= \sum_{i=1}^{n} A_i\, d_i(t)\, c_i(t) \cos(\omega_\alpha t) \end{aligned} \tag{4.1}$$

where, A_i is the signal amplitude which is Rayleigh distributed and $A_i = \sqrt{2P_{s,i}}$, $d_i(t)$ is the data sequence, $c_i(t)$ is the coded waveform and ω_α is the carrier frequency. Similarly, IEEE 802.11 standard also employs DSSS modulation, so its signal has the same form as the WCDMA signal (4.1).

$$\begin{aligned} s_{\text{wlan}}(t) &= \sqrt{2P_{s,\text{wlan}}}\, d_\beta(t)\, c_\beta(t) \cos(\omega_\beta\, t) \\ &= B_\beta\, d_\beta(t)\, c_\beta(t) \cos(\omega_\beta\, t) \end{aligned} \tag{4.2}$$

where, $P_{s,\text{wlan}}$ is the received symbol power, and B_β is the Rayleigh distributed random variable of signal amplitude and $B_\beta = \sqrt{2P_{s,\text{wlan}}}$, $d_\beta(t)$ is the data sequence, $c_\beta(t)$ is the coded waveform and ω_β is the carrier frequency. Expression (4.2) illustrates the nature of the WLAN system that there is only one MS can access the radio medium at a time therefore no summation. The WLAN system employs the CSMA/CA for medium access control that makes stations sense for idle in medium before transmission, thus only one station transmits at a time. The WLAN system uses the 2.4 GHz band, while the WCDMA system uses the 1.9 GHz band. The WLAN system occupies a larger bandwidth of 22 MHz in comparison to just 5 MHz bandwidth of the WCDMA system. At the RAP, the received signal that consists of both WCDMA and

WLAN signals is given as:

$$\begin{aligned} s_{\mathrm{RAP}}(t) =& s_{\mathrm{wcdma}}(t-\tau_i) + s_{\mathrm{wlan}}(t-\tau_\beta) + n_{\mathrm{up,wl}}(t) \\ =& \sum_{i=1}^{n} A_i\, d_i(t-\tau_i)\, c_i(t-\tau_i) \cos(\omega_\alpha t - \phi_i) \\ &+ B_\beta\, d_\beta(t-\tau_\beta)\, c_\beta(t-\tau_\beta) \cos(\omega_\beta t - \phi_\beta) + n_{\mathrm{up,wl}}(t) \end{aligned} \tag{4.3}$$

where τ_i and τ_β are the time delays, $\phi_i = \omega_\alpha \tau_i$ and $\phi_\beta = \omega_\beta \tau_\beta$ are the phase of signals which are related to the time delays, and $n_{\mathrm{up,wl}}(t)$ is the additive white Gaussian noise in air with a power spectrum density (PSD) $\Phi_{\mathrm{up,wl}}(\omega) = N_{\mathrm{up,wl}}/2$. Due to different cell coverage requirements among the two systems, the WCDMA signal is expected to experience Rayleigh fading in air and the WLAN signal experiences Rician fading in air. These fadings are essentially the same except Rician fading has a LOS component. In the analysis, both systems are assumed to be in a harsh wireless environment where it has no LOS path. The fading in the wireless environment is described with greater detail in section 3.1.2. The effect of path loss in the wireless environment is embedded in the signal amplitudes. The path loss has been discussed in section 3.1.1. The delays τ_i and τ_β are the combination of an access time to the system and propagation delay. The propagation delay has a shorter duration than the access time. The phase is assumed to have an uniform distribution over $[\pi, -\pi]$. The MSs access to the WCDMA system asynchronously which results in different access time for each MS.

At the RAP, the signals have already experienced fading, path loss and additive noise in the air interface. These signals go through two bandpass filters that suppresses out of band noise. Then, separate amplifiers boost the signals to compensate attenuation in air. Finally, a power combiner is used to combine the signal. The added signal then directly modulates the laser.

The quality of the signals is either indicated by the SNR or the SINR. The

ratios are evaluated before the power combiner as indicated in Figure 4.1. The difference between the ratios SINR and SNR is that SINR includes the effect of multiple access interference. The following information is used to evaluate the ratios: i) the received power of ith WCDMA and WLAN signals are $P_{s,i}$ and $P_{s,wlan}$ respectively, ii) each amplifier is assumed to have a noise figure of F, and iii) the bandpass filters have bandwidth of B_{wcdma} and B_{wlan} for WCDMA and WLAN signals respectively. The SINR for the desired WCDMA signal where $i = r$ can be written as follows:

$$\text{SINR}_{\text{up,wcdma}} = \frac{P_{s,r}}{N_{\text{up,wl}}\, B_{\text{wcdma}}\, F + \sum_{\substack{i=1 \\ i \neq r}}^{n} P_{s,i}} \tag{4.4}$$

Similarly, the SNR for the WLAN signal can be written as follows:

$$\text{SNR}_{\text{up,wlan}} = \frac{P_{s,wlan}}{N_{\text{up,wl}}\, B_{\text{wlan}}\, F} \tag{4.5}$$

The term $\sum_{\substack{i=1 \\ i \neq r}}^{n} P_{s,i}$ in expression (4.4) is the power of the interference due to multiple access in the WCDMA system. That power increases with the number of active users in the system. When power control is not employed, multiple access interference can greatly degrade the quality of the weak signals. This is known as near-far effect. To avoid the near-far effect, power control is implemented to make the power $P_{s,i}$ received at the RAP equal. On the contrary, the WLAN system does not have such interference because only one user transmits at a time for a successful transmission.

The actual signal that modulates the laser expressed in the time domain

can be written as follows:

$$\begin{aligned} s_{\text{laser}}(t) =& \sqrt{G_{\text{up,wcdma}}}\,[s_{\text{wcdma}}(t-\tau_i) + n_{\text{up,wcdma}}(t)] \\ &+ \sqrt{G_{\text{up,wlan}}}\,[s_{\text{wlan}}(t-\tau_\beta) + n_{\text{up,wlan}}(t)] \end{aligned} \tag{4.6}$$

Both signal and noise are amplified by the power amplifiers with gain of $G_{\text{up,wcdma}}$ and $G_{\text{up,wlan}}$. Then, the bandpass filters at the RAP filter out of band noise. Assuming bandpass filters are ideal, the PSD of the two noise processes $n_{\text{up,wcdma}}(t)$ and $n_{\text{up,wlan}}(t)$ can be expressed as follows:

$$\Phi_{\text{up,wcdma}}(\omega) = \frac{N_{\text{up,wl}}\,F}{2}\left[\text{rect}\left(\frac{\omega-\omega_\alpha}{\omega_{\text{wcdma}}}\right) + \text{rect}\left(\frac{\omega+\omega_\alpha}{\omega_{\text{wcdma}}}\right)\right] \tag{4.7}$$

$$\Phi_{\text{up,wlan}}(\omega) = \frac{N_{\text{up,wl}}\,F}{2}\left[\text{rect}\left(\frac{\omega-\omega_\beta}{\omega_{\text{wlan}}}\right) + \text{rect}\left(\frac{\omega+\omega_\beta}{\omega_{\text{wlan}}}\right)\right] \tag{4.8}$$

Also, the RF power of the noise can be expressed as follows:

$$\langle n^2_{\text{up,wcdma}}\rangle = N_{\text{up,wl}}\,F\,B_{\text{wcdma}} \tag{4.9}$$

$$\langle n^2_{\text{up,wlan}}\rangle = N_{\text{up,wl}}\,F\,B_{\text{wlan}} \tag{4.10}$$

In the ROF link, the RF power of a modulated signal is indicated by its optical modulation index. The power is proportional to the square of the optical modulation index. The optical modulation index of a WCDMA signal, $m_{\text{wcdma},i}$, is defined as the signal amplitude that modulates the laser. Similarly, the optical modulation index of a WLAN signal, m_{wlan}, is also defined as the signal amplitude that modulates the laser.

$$m_{\text{wcdma},i} = A_i\sqrt{G_{\text{up,wcdma}}} \tag{4.11}$$

$$m_{\text{wlan}} = B_\beta\sqrt{G_{\text{up,wlan}}} \tag{4.12}$$

The two optical modulation indices are also Rayleigh distributed. The reasons

are: first A_i and B_β are Rayleigh distributed, second the power amplifiers have fixed gains $G_{\text{up,wcdma}}$ and $G_{\text{up,wlan}}$. Another optical modulation index, which is known as the cumulative RMS optical modulation index, is defined as the square root of the total RF power that modulates the laser. For SCM architecture, the cumulative RMS optical modulation index μ is given as:

$$\mu = \sqrt{G_{\text{up,wcdma}} \sum_{i=1}^{n} \frac{A_i^2}{2} + G_{\text{up,wlan}} \left(\frac{B_\beta^2}{2} \right)} = \sqrt{\sum_{i=1}^{n} \frac{m_{\text{wcdma},i}^2}{2} + \frac{m_{\text{wlan}}^2}{2}} \quad (4.13)$$

This RMS optical modulation index is a random process that is dependent on the square of the Rayleigh distributed random variables $m_{\text{wcdma},i}$ and m_{wlan} that are expressed in the latter part of the expression (4.13). By substitute the optical modulation indices in (4.6), the signal that modulates the laser can be rewritten as follows:

$$\begin{aligned} s_{\text{laser}}(t) = & \sum_{i=1}^{n} m_{\text{wcdma},i}\, d_i(t-\tau_i)\, c_i(t-\tau_i) \cos(\omega_\alpha t - \phi_i) \\ & + m_{\text{wlan}}\, d_\beta(t-\tau_\beta)\, c_\beta(t-\tau_\beta) \cos(\omega_\beta t - \phi_\beta) + n_{\text{up,air}}(t) \end{aligned} \quad (4.14)$$

and the total noise from the air interface,

$$n_{\text{up,air}}(t) = \sqrt{G_{\text{up,wcdma}}}\, n_{\text{up,wcdma}}(t) + \sqrt{G_{\text{up,wlan}}}\, n_{\text{up,wlan}}(t) \quad (4.15)$$

Knowing the optical modulation indices, we can determine the required RF amplifier power gain. The gains are first calculated with a pre-selected optical modulation index that has been optimized for the performance in the ROF link, it can then be worked out from the following two expressions. For the WCDMA system, the RF gain of the amplifier is expressed as:

$$G_{\text{up,wcdma}} = \frac{\overline{m_{\text{wcdma},i}^2}}{\overline{A_i^2}} \quad (4.16)$$

and for the WLAN system the gain is expressed as:

$$G_{\text{up,wlan}} = \frac{\overline{m_{\text{wlan}}^2}}{\overline{B_\beta^2}} \tag{4.17}$$

where $\overline{A_i}$ and $\overline{B_\beta}$ are the average values for signal amplitude. The gain of the amplifiers is fixed in the SCM architecture.

The quality impairment in the ROF link is due to optical noise and nonlinear distortion. The time domain noise term in the ROF link is written as $n_{\text{op}}(t)$ and it is assumed to be an additive white Gaussian noise process. The noise is categorized into shot noise, thermal noise, and relative intensity noise [7]. The relative intensity noise originates from the laser and it is depended on both the square of the photocurrent and the cumulative RMS optical modulation index μ [7]. However, the shot noise and the thermal noise are independent of the modulation index μ. These three noise mechanisms are described in section 3.2.3 through section 3.2.5. Using expressions (3.27), (3.28), and (3.20), the total optical noise can be quantified in terms of electrical power. The general power expression is given as follows:

$$\langle n_{\text{op}}^2 \rangle = \text{RIN}\, I_{\text{D}}^2\, B\,(1+\mu^2) + 2qI_{\text{D}}B + \frac{4\,k_{\text{B}}\,K}{R_{\text{L}}} \tag{4.18}$$

The ROF link noise power for the WCDMA system is $\langle n_{\text{op,wcdma}}^2 \rangle$ when $B = B_{\text{wcdma}}$; noise power for the WLAN system is $\langle n_{\text{op,wlan}}^2 \rangle$ when $B = B_{\text{wlan}}$.

In the ROF link, there are two main nonlinear distortions: clipping and intermodulation product distortions. The clipping distortion is dependent on the optical modulation index μ [4]. This can be observed from the clipping distortion power spectrum (3.19) that is discussed in section 3.2.2. The exponent on the optical modulation index μ is five in (3.19). This means that the clipping distortion is significant for large μ. The clipping distortion power is

obtained from the integration of the power spectrum, expression (3.19), over the signal bandwidth. If the clipping power spectrum is $S(\omega)$, then the power in the WCDMA band can be expressed as:

$$\langle n^2_{\text{cl,wcdma}} \rangle = \int_{\omega_a}^{\omega_b} S(\omega) \approx S(\omega_\alpha)\, B_{\text{wcdma}} \tag{4.19}$$

where ω_α and B_{wcdma} are the carrier frequency and bandwidth of the WCDMA signal. The approximation for the distortion power is valid because the power spectrum around the carrier frequency is relatively flat over the bandwidth of the WCDMA system. This can be seen from Figure 3.1. Similarly, the clipping distortion power in the WLAN band can be approximated as:

$$\langle n^2_{\text{cl,wlan}} \rangle \approx S(\omega_\beta)\, B_{\text{wlan}} \tag{4.20}$$

Another distortion in the ROF link is the intermodulation product. Section 3.2.1 examines how the laser diode can be modeled by a third order polynomial. When the model is applied, the photocurrent output can be expressed as (3.9). In that expression, the square of the modulated signal creates second order intermodulation product terms, while the cube of the modulated signal creates third order intermodulation product terms. However, for signals within one octave of the bandwidth, only the third order intermodulation product terms would fall in the signals spectrum. In the SCM architecture, the second order intermodulation product distortion can be ignored because both WCDMA and WLAN systems are using the 2 GHz band which mean their signals are within one octave of bandwidth. Applying the model, the

photocurrent is expressed as follows:

$$\begin{aligned} i_{\mathrm{D}}(t) &= \frac{1}{\sqrt{L_{\mathrm{op}}}}\left[s_{\mathrm{laser}}(t) + a_3\, s^3_{\mathrm{laser}}(t)\right] + n_{\mathrm{op}}(t) + n_{\mathrm{cl}}(t) \\ &\approx \frac{s_{\mathrm{laser}}(t)}{\sqrt{L_{\mathrm{op}}}} + \frac{a_3}{\sqrt{L_{\mathrm{op}}}}\left[s_{\mathrm{laser}}(t) - n_{\mathrm{up,air}}(t)\right]^3 + n_{\mathrm{op}}(t) + n_{\mathrm{cl}}(t) \end{aligned} \tag{4.21}$$

where L_{op} is the total RF power loss in the ROF link that is defined in expression (3.29), s_{laser} is the input signal to the laser that is defined in (4.14), $n_{\mathrm{op}}(t)$ is the noise in the link, and $n_{\mathrm{cl}}(t)$ is the distortion due to clipping effect which $n_{\mathrm{cl}}(t) = n_{\mathrm{cl,wcdma}}(t) + n_{\mathrm{cl,wlan}}(t)$. The total RF power loss in the ROF link is dependent on the distance of its link. The DC component of the photocurrent is omitted because it will be removed by the bandpass filter. The second order term is also omitted in the expression because the second order intermodulation product is outside of the signal band. The noise induced from the air interface is part of the signal, s_{laser}, that modulated the laser. According to the cube term of the laser model, the noise from the air interface $n_{\mathrm{up,air}}(t)$ is also cubed. In reality, the noise is quite small, and it is much smaller when it is cubed. Therefore, the cubic term is left out in the analysis and the approximate expression is written to reflect the change.

When expression (4.21) is expanded, the desired, distorted, interfering, and noise signals can be easily grouped. That has been done in appendix A.1. Again, only the WCDMA system has multiple access interference because the system bandwidth is shared among n users. In the appendix, the signals are grouped first according to the code word then to the frequency. The signals are separated into the two systems which take the effect of the photocurrent passed through a bandpass filter into account. The WCDMA and WLAN

signals after the bandpass filters are given as follows:

$$i_{\mathrm{D,wcdma}}(t) = D_{\mathrm{wcdma}}(t) + \sum_{i=1}^{7} Z_i(t) + \sqrt{\frac{G_{\mathrm{up,wcdma}}}{L_{\mathrm{op}}}}\, n_{\mathrm{up,wcdma}}(t) + n_{\mathrm{op,wcdma}}(t) + n_{\mathrm{cl,wcdma}}(t) \tag{4.22}$$

$$i_{\mathrm{D,wlan}}(t) = D_{\mathrm{wlan}}(t) + \sum_{i=1}^{3} M_i(t) + \sqrt{\frac{G_{\mathrm{up,wlan}}}{L_{\mathrm{op}}}}\, n_{\mathrm{up,wlan}}(t) + n_{\mathrm{op,wlan}}(t) + n_{\mathrm{cl,wlan}}(t) \tag{4.23}$$

where $i_{\mathrm{D,wcdma}}(t)$ is the WCDMA signal and $i_{\mathrm{D,wlan}}(t)$ is the WLAN signal. For the WCDMA system, the expression for the desired signal $D_{\mathrm{wcdma}}(t)$ is given in (A.31), and (A.32) through (A.38) are the interfering and distorted signals $\sum_{i=1}^{7} Z_i(t)$. For the WLAN system, the expression for the desired signal $D_{\mathrm{wlan}}(t)$ is given in (A.44), and (A.45) through (A.47) are the distorted signals $\sum_{i=1}^{3} M_i(t)$. From the desired expressions (A.31) and (A.44), it can be observed that the third order intermodulation product distortion produces some desired terms among the distorted one. The multiple access interference in the WCDMA system can be identified from expression (A.32).

In order to evaluate the cumulative SDINR and the cumulative SDNR as it has shown in the uplink portion of Figure 4.1, the RF power of the desired, interfering, and distorted signals are derived next. The power is obtained by taking the mean square of the desired, interfering, and distorted signals. The interfering and distorted signals are independent because the signals have different frequency, thus power is obtained separately for each signal. For the

WCDMA system, the power expressions are given as follows:

$$\langle D^2_{\text{wcdma}} \rangle = \frac{1}{2}\left\{ \frac{m_{\text{wcdma},r}}{\sqrt{L_{\text{op}}}} + \frac{1}{4}\frac{a_3}{\sqrt{L_{\text{op}}}}\left[m^3_{\text{wcdma},r} + 6\, m_{\text{wcdma},r}\left(\sum_{\substack{i=1 \\ i\neq r}}^{n} m^2_{\text{wcdma},i} + m^2_{\text{wlan}} \right) \right] \right\}^2 \tag{4.24}$$

$$\begin{aligned} \langle Z^2_1 \rangle = \frac{1}{2\,L_{\text{op}}} \sum_{\substack{i=1 \\ i\neq r}}^{n} m^2_{\text{wcdma},i} \Bigg\{ \Bigg[1 + \frac{3}{2}\, a_3 \Big(\frac{1}{2}\, m^2_{\text{wcdma},i} + m^2_{\text{wcdma},r} \\ + m^2_{\text{wlan}} + \sum_{\substack{j=1 \\ j\neq r,i}}^{n} m^2_{\text{wcdma},j} \Big) \Bigg]^2 \\ + \frac{9}{16}\, a_3^2\, m^4_{\text{wcdma},r} + \frac{9}{16}\, a_3^2\, m^4_{\text{wlan}} + \frac{9}{16}\, a_3^2 \sum_{\substack{j=1 \\ j\neq r,i}}^{n} m^4_{\text{wcdma},j} \Bigg\} \end{aligned} \tag{4.25}$$

$$\langle Z^2_2 \rangle = \frac{9}{32}\, \frac{a_3^2\, m^2_{\text{wcdma},r}}{L_{\text{op}}} \left[\sum_{\substack{i=1 \\ i\neq r}}^{n} m^4_{\text{wcdma},i} + m^4_{\text{wlan}} \right] \tag{4.26}$$

$$\langle Z^2_3 \rangle = \frac{9}{32}\, \frac{a_3^2\, m^2_{\text{wlan}}}{L_{\text{op}}} \sum_{i=1}^{n} m^4_{\text{wcdma},i} \tag{4.27}$$

$$\langle Z^2_4 \rangle = \frac{27}{32}\, \frac{a_3^2\, m^2_{\text{wcdma},r}}{L_{\text{op}}} \sum_{\substack{j=1 \\ j\neq r}}^{n} \sum_{\substack{k=1 \\ k\neq r,j}}^{n} m^2_{\text{wcdma},j}\, m^2_{\text{wcdma},k} \tag{4.28}$$

$$\langle Z^2_5 \rangle = \frac{9}{16}\, \frac{a_3^2\, m^2_{\text{wcdma},r}\, m^2_{\text{wlan}}}{L_{\text{op}}} \sum_{\substack{k=1 \\ k\neq r}}^{n} m^2_{\text{wcdma},k} \tag{4.29}$$

$$\langle Z^2_6 \rangle = \frac{3}{32}\, \frac{a_3^2}{L_{\text{op}}} \sum_{\substack{i=1 \\ i\neq r}}^{n} \sum_{\substack{j=1 \\ j\neq r,i}}^{n} \sum_{\substack{k=1 \\ k\neq r,i,j}}^{n} m^2_{\text{wcdma},i}\, m^2_{\text{wcdma},j}\, m^2_{\text{wcdma},k} \tag{4.30}$$

$$\langle Z^2_7 \rangle = \frac{9}{32}\, \frac{a_3^2\, m^2_{\text{wlan}}}{L_{\text{op}}} \sum_{\substack{j=1 \\ j\neq r}}^{n} \sum_{\substack{k=1 \\ k\neq r,j}}^{n} m^2_{\text{wcdma},j}\, m^2_{\text{wcdma},k} \tag{4.31}$$

And, for the WLAN system, the power expressions are given as follows:

$$\langle D_{\text{wlan}}^2 \rangle = \frac{1}{2}\left[\frac{m_{\text{wlan}}}{\sqrt{L_{\text{op}}}} + \frac{3}{4}\frac{a_3}{\sqrt{L_{\text{op}}}}\left(m_{\text{wlan}}^3 + 2\,m_{\text{wlan}}\sum_{i=1}^{n} m_{\text{wcdma},i}^2\right)\right]^2 \tag{4.32}$$

$$\langle M_1^2 \rangle = \frac{9}{32}\frac{a_3^2\, m_{\text{wlan}}^2}{L_{\text{op}}}\sum_{i=1}^{n} m_{\text{wcdma},i}^4 \tag{4.33}$$

$$\langle M_2^2 \rangle = \frac{9}{32}\frac{a_3^2\, m_{\text{wlan}}^4}{L_{\text{op}}}\sum_{i=1}^{n} m_{\text{wcdma},i}^2 \tag{4.34}$$

$$\langle M_3^2 \rangle = \frac{27}{32}\frac{a_3^2\, m_{\text{wlan}}^2}{L_{\text{op}}}\sum_{j=1}^{n}\sum_{\substack{k=1 \\ k\neq j}}^{n} m_{\text{wcdma},j}^2\, m_{\text{wcdma},k}^2 \tag{4.35}$$

Finally, the cumulative SDINR of a WCDMA signal is given as:

$$\text{SDINR}_{up,wcdma} = \frac{\langle D_{\text{wcdma}}^2 \rangle}{\frac{G_{\text{up,wcdma}}}{L_{\text{op}}}\langle n_{\text{up,wcdma}}^2 \rangle + \langle n_{\text{op,wcdma}}^2 \rangle + \langle n_{\text{cl,wcdma}}^2 \rangle + \sum_{i=1}^{7}\langle Z_i^2 \rangle} \tag{4.36}$$

Similarly, the cumulative SDNR of a WLAN signal is given as:

$$\text{SDNR}_{up,wlan} = \frac{\langle D_{\text{wlan}}^2 \rangle}{\frac{G_{\text{up,wlan}}}{L_{\text{op}}}\langle n_{\text{up,wlan}}^2 \rangle + \langle n_{\text{op,wlan}}^2 \rangle + \langle n_{\text{cl,wlan}}^2 \rangle + \sum_{i=1}^{3}\langle M_i^2 \rangle} \tag{4.37}$$

where the noise power from air $\langle n_{\text{up,wcdma}}^2 \rangle$ and $\langle n_{\text{up,wlan}}^2 \rangle$ are given in (4.9) and (4.10) respectively, clipping distortion power $\langle n_{\text{cl,wcdma}}^2 \rangle$ and $\langle n_{\text{cl,wlan}}^2 \rangle$ are defined in (4.19) and (4.20) respectively, $\langle n_{\text{op,wcdma}}^2 \rangle$ is the optical noise power for the WCDMA system when $B = B_{\text{wcdma}}$ in (4.18), and $\langle n_{\text{op,wlan}}^2 \rangle$ is the optical noise power for the WLAN system when $B = B_{\text{wlan}}$ in (4.18).

4.2 Downlink Analysis

In the downlink, the signals of both WCDMA and WLAN systems are transmitted from the central base station which is also illustrated in Figure 4.1 (see downlink portion). The signals first go through the ROF link and then the air interface. Let a subscript β denotes the signals that belong to the WLAN system. Let a subscript i be the ith signal of the WCDMA system for $i = 1, 2, \ldots, n$ where n is the total number of users active in the system. Two optical modulation indices are defined for the ROF link to indicate the signal strength. They are $m_{\text{wcdma,i}}$ for the WCDMA signal and m_{wlan} for the WLAN signal. The signals of the two systems are electrically combined to directly modulate a laser. The combined signal that modulates the laser can be expressed in terms of optical modulation indices as follows:

$$\begin{aligned} s_{\text{laser}} = & \sum_{i=1}^{n} m_{\text{wcdma,i}}\, d_i(t-\tau)\, c_i(t-\tau) \cos(\omega_\alpha t - \phi) \\ & + m_{\text{wlan}}\, d_\beta(t-\tau_\beta)\, c_\beta(t-\tau_\beta) \cos(\omega_\beta t - \phi_\beta) \end{aligned} \tag{4.38}$$

where $d_i(t-\tau)$ and $d_\beta(t-\tau_\beta)$ are data sequences, $c_i(t-\tau)$ and $c_\beta(t-\tau_\beta)$ are coded waveforms, τ and τ_β are delays, ϕ and ϕ_β are phases of the corresponding delay, and ω_α and ω_β are carrier frequencies of the systems. The WCDMA system is assumed to have n DSSS signals transmit synchronously. That implies that the signals have the same delay. Therefore, the multiple access interference with the WCDMA system is much less severe. Moreover, it is expected that the effect of intermodulation product distortion is slightly different from the uplink because of the synchronous transmission. The signals that modulate the laser are assumed noiseless. Moreover, the optical modulation indices are considered constant because the optical channel experiences no

fading. The RF power that modulates the laser diode is expressed as follows:

$$\langle s^2_{\text{laser}} \rangle = \frac{1}{T_{sym}} \int_{T_{sym}} s^2_{\text{laser}}(t)\, dt = \sum_{i=1}^{n} \frac{m^2_{\text{wcdma},i}}{2} + \frac{m^2_{\text{wlan}}}{2} \tag{4.39}$$

where T_{sym} is the symbol period. The cumulative RMS optical modulation index can be determined from the power expression above:

$$\mu = \sqrt{\sum_{i=1}^{n} \frac{m^2_{\text{wcdma},i}}{2} + \frac{m^2_{\text{wlan}}}{2}} \tag{4.40}$$

The signal that propagates through a fiber from the central base station to the RAP experiences signal attenuation, optical noise, clipping distortion, and nonlinear distortion. These effects on the signal can be seen from the photocurrent output. At the end of the ROF link, the photocurrent output can be expressed as:

$$i_{\text{D}}(t) = \frac{s_{\text{laser}}(t)}{\sqrt{L_{\text{op}}}} + \frac{a_3}{\sqrt{L_{\text{op}}}} s^3_{\text{laser}}(t) + n_{\text{op}}(t) + n_{\text{cl}}(t) \tag{4.41}$$

where L_{op} is the total RF power loss in the ROF link that is defined in expression (3.29), $s_{\text{laser}}(t)$ is the signal that modulates the laser diode that is defined in (4.38), a_3 is the constant that describes the third order laser nonlinearity, $n_{\text{op}}(t)$ is the noise in the link, and $n_{\text{cl}}(t)$ is the distortion due to clipping effect where, $n_{\text{cl}}(t) = n_{\text{cl,wcdma}}(t) + n_{\text{cl,wlan}}(t)$. The above expression is derived applying a third order polynomial model for lasers, while neglecting the contribution from the second order nonlinearity and the DC term. The total power loss in the ROF link is dependent on the length of the ROF link.

The effect of the intermodulation distortion can be easily separated from the photocurrent expression when the expression is expanded. This is done in appendix A.2. The expressions that are given in the appendix had the distor-

tion terms separated from the desired signal. The effect of the photocurrent past thought the bandpass filters had also taken into account. Using the expressions the first set of SDNR ratios can be evaluated (See Figure 4.1). The WCDMA and WLAN signals after the bandpass filters are given as follows:

$$i_{\mathrm{D,wcdma}}(t) = D_{\mathrm{wcdma}}(t) + \sum_{i=1}^{7} Z_i(t) + n_{\mathrm{op,wcdma}}(t) + n_{\mathrm{cl,wcdma}}(t) \tag{4.42}$$

$$i_{\mathrm{D,wlan}}(t) = D_{\mathrm{wlan}}(t) + \sum_{i=1}^{3} M_i(t) + n_{\mathrm{op,wlan}}(t) + n_{\mathrm{cl,wlan}}(t) \tag{4.43}$$

where $i_{\mathrm{D,wcdma}}(t)$ is the WCDMA signal and $i_{\mathrm{D,wlan}}(t)$ is the WLAN signal. For the WCDMA system, the expression for the desired signal $D_{\mathrm{wcdma}}(t)$ is given in (A.60), and (A.61) through (A.67) are the interfering and distorted signals $\sum_{i=1}^{7} Z_i(t)$. For the WLAN system, the expression for the desired signal $D_{\mathrm{wlan}}(t)$ is given in (A.73), and (A.74) through (A.76) are the distorted signals $\sum_{i=1}^{3} M_i(t)$. From the desired expressions (A.60) and (A.73), it can be observed that the third order intermodulation product distortion produce some desired terms among the distorted one.

In order to evaluate the SDNR for the two systems, the RF power of the desired and distorted signals are derived. The power is obtained by taking the mean square of the desired and distorted signals. For the WCDMA system,

the power expressions are given as follows:

$$\langle D^2_{\text{wcdma}} \rangle = \frac{1}{2\,L_{\text{op}}}\, m^2_{\text{wcdma},r} \left[1 + \frac{3}{4}\, a_3 \Big(m^2_{\text{wcdma},r} + 3 \sum_{\substack{i=1 \\ i \neq r}}^{n} m^2_{\text{wcdma},i} + 2\, m^2_{\text{wlan}} \Big) \right]^2 \tag{4.44}$$

$$\langle Z^2_1 \rangle = \frac{9}{32}\, \frac{a_3^2}{L_{\text{op}}} \sum_{\substack{i=1 \\ i \neq r}}^{n} m^2_{\text{wcdma},i}\, m^4_{\text{wlan}} \tag{4.45}$$

$$\langle Z^2_2 \rangle = \frac{9}{32}\, \frac{a_3^2}{L_{\text{op}}}\, m^2_{\text{wcdma},r}\, m^4_{\text{wlan}} \tag{4.46}$$

$$\langle Z^2_3 \rangle = \frac{9}{32}\, \frac{a_3^2}{L_{\text{op}}}\, m^2_{\text{wlan}} \sum_{i=1}^{n} m^4_{\text{wcdma},i} \tag{4.47}$$

$$\langle Z^2_4 \rangle \approx 0 \tag{4.48}$$

$$\langle Z^2_5 \rangle = \frac{9}{8}\, \frac{a_3^2}{L_{\text{op}}}\, m^2_{\text{wcdma},r}\, m^2_{\text{wlan}} \sum_{\substack{k=1 \\ k \neq r}}^{n} m^2_{\text{wcdma},k} \tag{4.49}$$

$$\langle Z^2_6 \rangle \approx 0 \tag{4.50}$$

$$\langle Z^2_7 \rangle = \frac{9}{32}\, \frac{a_3^2}{L_{\text{op}}}\, m^2_{\text{wlan}} \sum_{\substack{j=1 \\ j \neq r}}^{n} \sum_{\substack{k=1 \\ k \neq r,j}}^{n} m^2_{\text{wcdma},j}\, m^2_{\text{wcdma},k} \tag{4.51}$$

And, for the WLAN system, the power expressions are given as follows:

$$\langle D^2_{\text{wlan}} \rangle = \frac{m^2_{\text{wlan}}}{2\,L_{\text{op}}} \left[1 + \frac{3}{4}\, a_3 \Big(m^2_{\text{wlan}} + 2 \sum_{i=1}^{n} m^2_{\text{wcdma},i} \Big) \right]^2 \tag{4.52}$$

$$\langle M^2_1 \rangle = \frac{9}{32}\, \frac{a_3^2}{L_{\text{op}}}\, m^2_{\text{wlan}} \sum_{i=1}^{n} m^4_{\text{wcdma},i} \tag{4.53}$$

$$\langle M^2_2 \rangle = \frac{9}{32}\, \frac{a_3^2}{L_{\text{op}}}\, m^4_{\text{wlan}} \sum_{i=1}^{n} m^2_{\text{wcdma},i} \tag{4.54}$$

$$\langle M^2_3 \rangle = \frac{9}{32}\, \frac{a_3^2}{L_{\text{op}}}\, m^2_{\text{wlan}} \sum_{j=1}^{n} \sum_{\substack{k=1 \\ k \neq j}}^{n} m^2_{\text{wcdma},j}\, m^2_{\text{wcdma},k} \tag{4.55}$$

In the above expressions, some terms that have low correlation with the desired

signal are removed. In the WCDMA system, the terms with low correlation have the same frequency, data waveform and coded waveform as $\cos(\omega_\alpha t - \phi)\, d_i(t-\tau)\, c_i(t-\tau)$ in expression (A.61). For the fact that those terms are synchronized with the desired signal, when correlation detection is used those terms will become very small thus can be neglected. Using this rational, expressions (4.45), (4.48), (4.50) and (4.55) have been modified.

The SDNR of a WCDMA signal is given as:

$$\mathrm{SDNR}_{down,wcdma} = \frac{\langle D^2_{\mathrm{wcdma}} \rangle}{\langle n^2_{\mathrm{op,wcdma}} \rangle F + \langle n^2_{\mathrm{cl,wcdma}} \rangle + \sum_{i=1}^{7} \langle Z_i^2 \rangle} \tag{4.56}$$

Similarly, the SDNR of a WLAN signal is given as:

$$\mathrm{SDNR}_{down,wlan} = \frac{\langle D^2_{\mathrm{wlan}} \rangle}{\langle n^2_{\mathrm{op,wlan}} \rangle F + \langle n^2_{\mathrm{cl,wlan}} \rangle + \sum_{i=1}^{3} \langle M_i^2 \rangle} \tag{4.57}$$

where clipping distortion power $\langle n^2_{\mathrm{cl,wcdma}} \rangle$ and $\langle n^2_{\mathrm{cl,wlan}} \rangle$ are defined in (4.19) and (4.20) respectively, $\langle n^2_{\mathrm{op,wcdma}} \rangle$ is the optical noise power for the WCDMA system when $B = B_{\mathrm{wcdma}}$ in (4.18), $\langle n^2_{\mathrm{op,wlan}} \rangle$ is the optical noise power for the WLAN system when $B = B_{\mathrm{wlan}}$ in (4.18), and F is the noise figure of the amplifier.

According to the downlink, the signal that reaches the RAP is then transmitted through air and received by users within the cell. The signal that propagates through air experiences path loss, fading and additive noise. The impairments are similar to that discussed in the uplink.

The path loss in air that described in section 3.1.1 is modeled as a large-scale propagation model. The model provides the average signal attenuation with a given distance away from the RAP. The distance is said to be 90%

confidence coverage radius which means the attenuation at that distance does not exceed the calculated value for 90% of the time. In addition, the multipath fading also causes loss in signal power, but over a small distance or short time. However, the effect of fading is limited with the assumption of a slow fading and frequency selective channel. A slow fading channel means that the channel characteristic does not change over several data symbols. A frequency selective channel refers to a transmitted bandwidth is much greater than the coherent bandwidth. The effect can cause ISI due to different delay for individual propagation path. However, when a RAKE correlator that exploits the correlation of signal in different paths to resolve multipath components is employed, the effect of ISI can be reduced.

With the multipath component resolved using a RAKE correlator, the wireless channel is sufficiently described by the large-scale propagation model. The expression for the path loss described by the large-scale propagation model is given as in (3.2). All noise that induced in the air interface is assumed to be additive white Gaussian noise with a PSD of $\Phi_{down,wl}(\omega) = N_{down,wl}/2$. The cumulative SDNR that accounts for all the impairments in the downlink is evaluated at the MS. Although it might be expected that there is interference from multiple access in the WCDMA system, the access to the system is synchronous in the downlink that WCDMA code words keep signal between users orthogonal. This is the reason that SDNR is evaluated instead of SDINR. The

cumulative SDNR for a WCDMA signal is given as follows:

$$\begin{aligned}\mathrm{cSDNR}_{down,wcdma} &= \frac{\frac{\langle D^2_{\mathrm{wcdma}}\rangle}{L_{wl}(R_{90})}}{\frac{\langle n^2_{\mathrm{op,wcdma}}\rangle F + \langle n^2_{\mathrm{cl,wcdma}}\rangle + \sum_{i=1}^{7}\langle Z_i^2\rangle}{L_{wl}(R_{90})} + N_{down,wl}\,B_{wcdma}} \\ &= \left(\frac{1}{\mathrm{SDNR}_{down,wcdma}} + \frac{1}{\mathrm{SNR}_{air,wcdma}}\right)^{-1}\end{aligned} \tag{4.58}$$

Similarly, the cumulative SDNR of a WLAN signal is given as:

$$\begin{aligned}\mathrm{cSDNR}_{down,wlan} &= \frac{\frac{\langle D^2_{\mathrm{wlan}}\rangle}{L_{wl}(R_{90})}}{\frac{\langle n^2_{\mathrm{op,wlan}}\rangle F + \langle n^2_{\mathrm{cl,wlan}}\rangle + \sum_{i=1}^{3}\langle M_i^2\rangle}{L_{wl}(R_{90})} + N_{down,wl}\,B_{wlan}} \\ &= \left(\frac{1}{\mathrm{SDNR}_{down,wlan}} + \frac{1}{\mathrm{SNR}_{air,wlan}}\right)^{-1}\end{aligned} \tag{4.59}$$

where $L_{wl}(R_{90})$ is the path loss in the air interface, $\mathrm{SNR}_{air,wcdma}$ is the SNR for the WCDMA signal that only accounts for noise induced in the air interface, and $\mathrm{SNR}_{air,wlan}$ is the SNR for the WLAN signal that only accounts for noise induced in the air interface. The two SNR ratios are given as follow:

$$\mathrm{SNR}_{air,wcdma} = \frac{\langle D^2_{\mathrm{wcdma}}\rangle}{L_{wl}(R_{90})\,N_{down,wl}\,B_{wcdma}} \tag{4.60}$$

$$\mathrm{SNR}_{air,wlan} = \frac{\langle D^2_{\mathrm{wlan}}\rangle}{L_{wl}(R_{90})\,N_{down,wl}\,B_{wlan}} \tag{4.61}$$

4.3 Throughput And Packet Delay For IEEE 802.11b

In the SCM architecture, the physical layer has an additional ROF link. This additional ROF link distance increases the propagation time of the signals, so the timing expression for a slot time should be modified to adjust for the change. To modify the expression, a propagation time through the ROF link is introduced. The propagation time in terms of the fiber core index of refraction n_f and the distance of the ROF link d is as follows:

$$\text{aRofPropagationTime} = \frac{c}{n_f} d \tag{4.62}$$

where c is the speed of light. The new expression for a slot time is given as follows:

$$\text{aSlotTime} = \text{aCCATime} + \text{aRxTxTurnaroundTime} + \delta + \text{aMACProcessingDelay} \tag{4.63}$$

and

$$\delta = \text{aAirPropagationTime} + \text{aRofPropagationTime} \tag{4.64}$$

where, δ is the total propagation time including the air and ROF link propagation times. Expression (2.2) for the DIFS time depends on the duration of a slot time. For the SCM architecture, the DIFS time increases with the slot time. Since the slot time and the DIFS time are dependent on the fiber length, different fiber length would result in different values for the DIFS time and the slot time. Therefore, it is possible to assign a set of DIFS time and

slot time values for a range of ROF link distances.

The WLAN signal in the SCM architecture travels the additional distance through the ROF link. This leads to 25 μs and 50 μs increase in the propagation delay for a 5 km and a 10 km ROF links respectively. This increase does not affect the accuracy of the saturated throughput (2.3) and the average packet delay (2.7) expressions. However, the duration for a DIFS and slot time should be determined from the modified slot time expression (4.63) for the SCM architecture. With the increase in the DIFS time and the slot time, we can expect a roll back in the saturated throughput and an increase in the average packet delay. Figure 4.2 illustrates the saturated throughput for a normal WLAN system and a WLAN system in the SCM architecture with extra 10 km of fiber that signals propagates. It is generated using the saturated throughput model developed by Chatzimisios et al. [12]. It can be observed that even with 10 km ROF link, the throughput only slightly reduces.

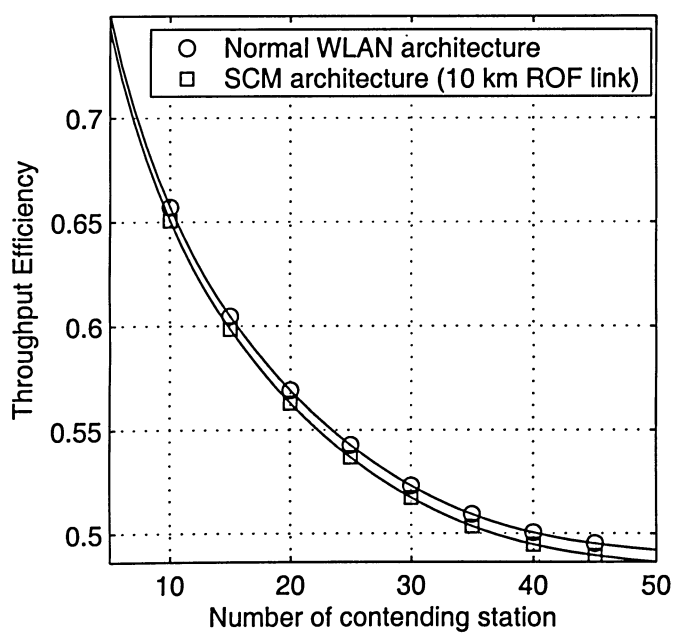

Figure 4.2: This figure illustrates the saturated throughput of the WLAN system in the normal environment and in the SCM architecture environment.

Chapter 5

Numerical Results and Discussions

5.1 Uplink Simulation Parameters

For the uplink, the numerical results generated are the cumulative SDINR and cumulative SDNR ratios versus various system parameters. Figures 5.1–5.6 are the results generated for the uplink. In the uplink, the signal first goes through the air interface then through the ROF link. The cumulative SDINR and SDNR are evaluated at the end of the ROF link where the central base station is located. The ratios include cumulative impairments from the air interface and the ROF link including the additive noise in both interfaces and the nonlinear distortion from the ROF link.

The following assumptions are considered for generating the results: i) all WCDMA signals at the RAP have equal power assuming perfect power control; ii) all signals are assumed to experience the same noise spectrum in the air interface, however the noise powers are different as discussed earlier; and iii) an optical modulation index ratio T is introduced to indicate the relative power distribution among signals. The layout of the plots is to put the result of a WCDMA signal right after the result of a WLAN signal. This is easy for immediate comparison between the quality of the WCDMA and WLAN

systems.

The cumulative SDINR of a WCDMA signal is referred to expression (4.36). The cumulative SDNR of a WLAN signal is referred to expression (4.37). The major system parameters used in the plots are: the cumulative RMS optical modulation index μ (4.13), the optical modulation index ratio $T = m_{\text{wlan}}/m_{\text{wcdma},i}$, the length of the ROF link, and the SNR of the WLAN signal at the RAP ($\text{SNR}_{\text{up,wlan}}$). The rest of the parameters and constants are listed in the table 5.1. Notice that the cumulative RMS optical modulation index μ has the same expression for both uplink and downlink, but it is a random variable in the uplink while it is deterministic in the downlink and thus should not treat them as they are equal. In the uplink, signal strength received from the air interface has random power.

n	Number of active MSs in WCDMA system	64
$G_{\text{up,wcdma}}$	RF power gain for WCDMA signal	20 dB
$G_{\text{up,wlan}}$	RF power gain for WLAN signal	20 dB
F	RAP/Receiver amplifier noise factor	1 dB
B_{wcdma}	Bandwidth of WCDMA	5 MHz
B_{wlan}	Bandwidth of WLAN	22 MHz
P_o	Laser mean optical power	1 mW
G_m	Laser modulation gain	0.12 A/W
$\Re$	Photo diode responsivity	0.75 W/A
n_c	Number of optical connectors	2
l_c	Optical connector loss	1 dB
α	Fiber attenuation	0.5 dB/km
RIN	Relative intensity noise parameter	-155 dB/Hz
K	Optical receiver temperature	275 K
R_L	Receiver load resistance	50 Ω
a_3	Third-order nonlinearity parameter	1/3

Table 5.1: Parameters for numerical results

5.2 Downlink Simulation Parameters

For the downlink, the numerical results generated are the cumulative SDNR for a WCDMA and a WLAN signal versus various system parameters. Figures 5.7–5.15 are the results generated for the downlink. In the downlink, the signal first goes through the ROF link then through the air interface. The cumulative SDNR is evaluated at the MS. The ratio includes the cumulative impairments from the air interface and the ROF link including the additive noise in both interfaces and the nonlinear distortion from the ROF link.

The results are generated assuming the most demanding scenario. The scenario is when all WCDMA MSs are located at the edge of the cell and are demanding for a certain guaranteed SNR. The SNR, however, depends on the distance between the MS to the base station for a fixed noise spectrum. Moreover, the RF power transmitted through the ROF link is limited because when RF power is too high the nonlinear distortion would be excessive.

The following assumptions are taken for generating the results: i) all WCDMA signals have equal power; ii) all signals are assumed to experience the same noise spectrum in the air interface; and iii) an optical modulation index ratio T is introduced to indicate the relative power distribution among WCDMA and WLAN signals.

The cumulative SDNR of a WCDMA signal is referred to expression (4.58). The cumulative SDNR of a WLAN signal is referred to expression (4.59). The major system parameters used in the plots are: i) the cumulative RMS optical modulation index μ (4.40), ii) the optical modulation index ratio $T = m_{\text{wlan}}/m_{\text{wcdma},i}$, iii) the length of the ROF link, iv) the distance between a WCDMA MS and the RAP, and v) the distance between a WLAN MS and the RAP. The rest of the parameters and constants are listed in the table 5.1.

5.3 Discussions

In Figure 5.1(a), the cumulative SDINR of a WCDMA signal versus the cumulative RMS optical modulation index μ is plotted. The value of the ratio is negative because multiple access interference accounts for a large amount of interfering power. When μ is larger than 0.3, the effect of the nonlinear distortion becomes significant, therefore the SDINR ratio is dropping. On the other end for small μ, less than 10^{-4}, only the optical noise comes into effect. Generally, the optical noise relatively increases with the length of the ROF link because actually the signal gets attenuated in the fiber. However, for the useful range of the index μ (0.01−0.2) the SDINR does not change with fiber length. This is because the optical noise is relatively too small in this scenario.

Similar characteristics can be observed from Figure 5.1(b) which illustrated the cumulative SDNR of a WLAN signal versus the index μ. The nonlinear distortion comes into effect for large μ, and the optical noise comes into effect for very small μ. For small μ, longer ROF has lower SDNR ratio because of the effect of optical noise. However, Figure 5.1(b) is the same as the WCDMA case in Figure 5.1(a) that the optical noise has no effect in the useful range of μ. Therefore, there is no difference in the SDNR for different fiber lengths. A conclusion can be drawn that in the useful range of μ the quality of the signal is not affected by the length of the ROF link and this applies to both WCDMA and WLAN signals. In addition, the cumulative SDINR and SDNR ratios remain very much constant for the useful range. That means μ can appropriately selected within this useful range without sacrificing the SDNR performance while other conditions hold. Recall that the square of the cumulative RMS optical modulation index is equivalent to the total RF power that modulates the laser.

Figures 5.2(a) and 5.2(b) illustrate the effect of optical modulation index

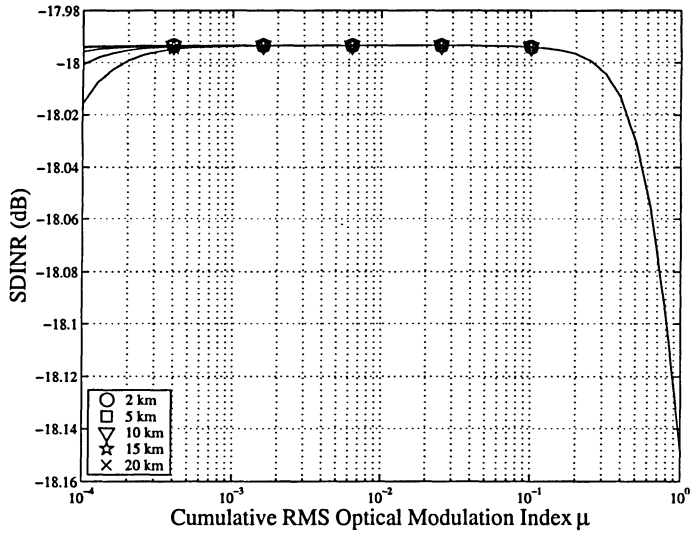

(a) The cumulative SDINR of a WCDMA signal versus the cumulative RMS optical modulation index μ is plotted.

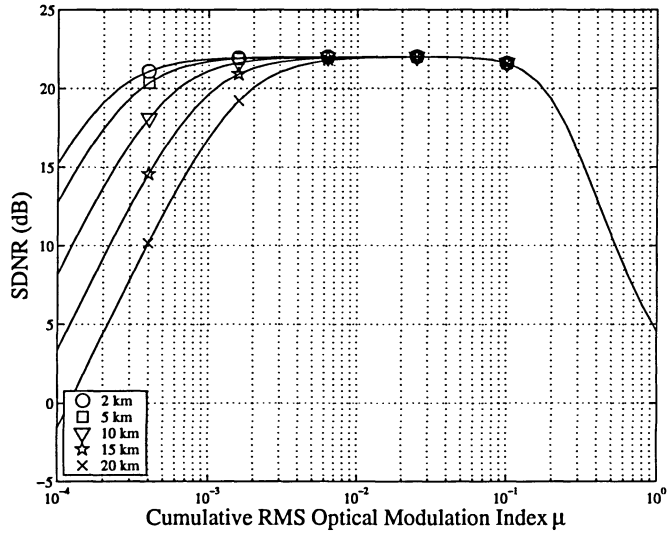

(b) The cumulative SDNR of a WLAN signal versus the cumulative RMS optical modulation index μ is plotted.

Figure 5.1: The two figures are the uplink results. The figures have five curves corresponding to various lengths of a ROF link. The other parameters are: the optical modulation index ratio T is 1 which means the WCDMA and WLAN systems have equal RF power, and the $\mathrm{SNR}_{\mathrm{up,wlan}}$ is 40dB.

ratio T by generating five curves corresponding to various values of T. T is the ratio between the optical modulation index of the WLAN signal to the WCDMA signal, $T = m_{\text{wlan}}/m_{\text{wcdma,i}}$. The power distribution among signals of the two systems is indicated by the optical modulation index ratio T. $T > 1$ means WLAN has more power and vice versa. With the assumption of perfect power control, the optical modulation index of all WCDMA signals would have the same value. In this way, the ratio can be seen as an indication for the relative power distribution between the two systems. Figure 5.2(a) that illustrates the cumulative SDINR of a WCDMA signal is similar to Figure 5.1(a). In both graphs the SDINR ratio rolls off for μ larger than 0.2.

The interesting difference between the two graphs in the useful range of μ is that the quality of a WCDMA signal does not dependent on the ratio T, whereas the quality of a WLAN signal changes according to the ratio T. The WCDMA signal does note dependent on T is because the effect of T is small on a single WCDMA signal. When T is large meaning more power distributed to the WLAN system a better cumulative SDNR is resulted and for T is small the cumulative SDNR ratio becomes smaller. The results from the two figures imply that more power should be allocated to the WLAN system. In other words, there is an increase in the quality for the WLAN system when more power is allocated to WLAN, while the quality for the WCDMA system stays very much the same irrespective of the power ratio.

The cumulative SDINR of a WCDMA signal versus the $SNR_{\text{up,wlan}}$ is plotted in Figure 5.3(a). The $SNR_{\text{up,wlan}}$ is the SNR for a WLAN signal at the RAP. It is used as a reference for the signal quality that enters the ROF link from air. The signal quality is impaired by the noise in the air interface, hence the $SNR_{\text{up,wlan}}$ is really reflected the amount of noise collected from the air interface. Moreover, it has been assumed that both systems experience the same noise spectrum, but different noise power due to different system

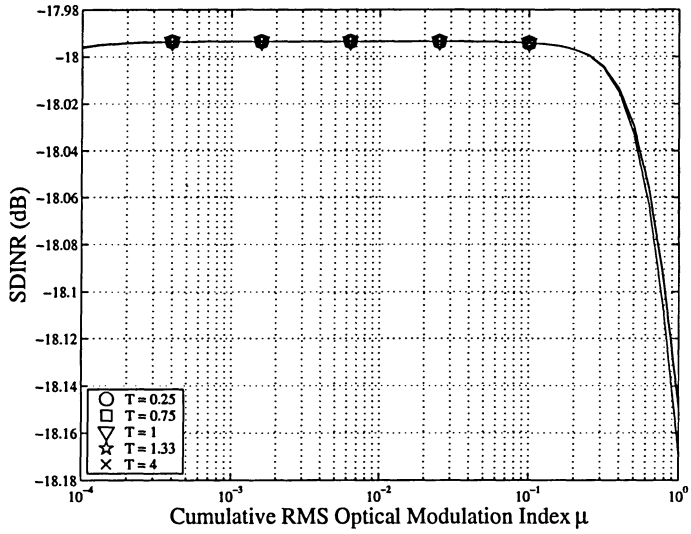

(a) The cumulative SDINR of a WCDMA signal versus the cumulative RMS optical modulation index μ is plotted.

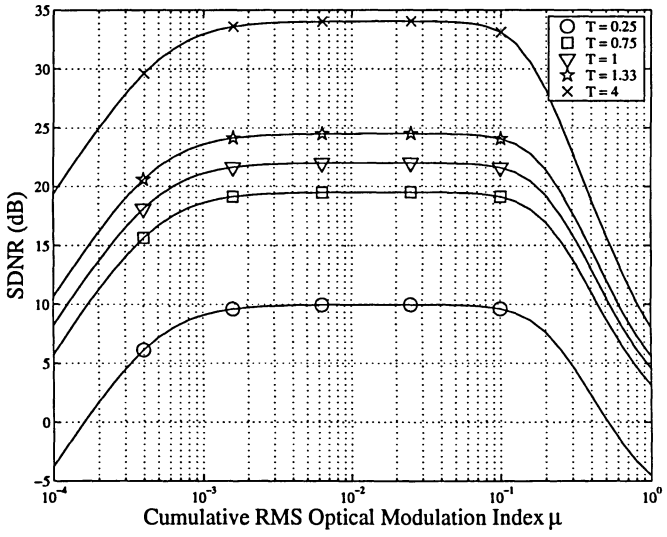

(b) The cumulative SDNR of a WLAN signal versus the cumulative RMS optical modulation index μ is plotted.

Figure 5.2: The two figures are the uplink results. The figures have five curves corresponding to various optical modulation index ratios $T = m_{\text{wlan}}/m_{\text{wcdma}}$. The other fixed parameters are: 5 km ROF link, and 40dB for the $\text{SNR}_{\text{up,wlan}}$.

bandwidths. The SNR is given in expression (4.5). In the figures, it can be observed that the cumulative SDINR does not improve beyond 20 dB of SNR at the RAP. This is a big contrast to the cumulative SDNR of a WLAN case in Figure 5.3(b) where the cumulative SDNR improves up to about 40 dB of SNR at the RAP. For the WCDMA system, it implies that the signal that input to the ROF link should have an SNR of at least 20 dB to give good cumulative SDINR. However, the WLAN system has a stronger dependency on the SNR at the RAP. Figure 5.3(b) shows that when the SNR increases up to 40 dB, the cumulative SDNR increases with the SNR. It seems that the quality of the two systems is independent of the length of the ROF link. However, this independency is because of the value of μ (=0.5). This can be crossed reference with figures 5.1(a) and 5.1(b) for μ is 0.5.

Figures 5.4(a) and 5.4(b) show three curves generated for three different values of μ. In these two figures, the similar trend of dependency on the SNR at the RAP is observed. The WLAN system has stronger dependency on the SNR compared to the WCDMA system. Furthermore, the SNR reduces as the cumulative optical modulation index μ increases. Figure 5.4(a) shows that the cumulative SDINR does not improve when SNR larger 20 dB for small μ (0.01 and 0.1), and then for a larger μ of 0.8 the SDINR saturates beyond 10 dB of SNR. Figure 5.4(b) also illustrates the same trend. This can be explained that large μ causes more nonlinear distortion in the ROF that limits the overall performance of the systems.

In Figure 5.5, it illustrates two plots which are the cumulative SDINR and the cumulative SDNR versus the optical modulation index ratio T. Recall, the ratio T is used to indicate the relative power distribution between the WCDMA and WLAN systems. Large T means more power is allocated to the WLAN system and vice versa. Figure 5.5(a) shows that the performance of the WCDMA decreases as the ratio T increase beyond 10. The cumulative SDNR

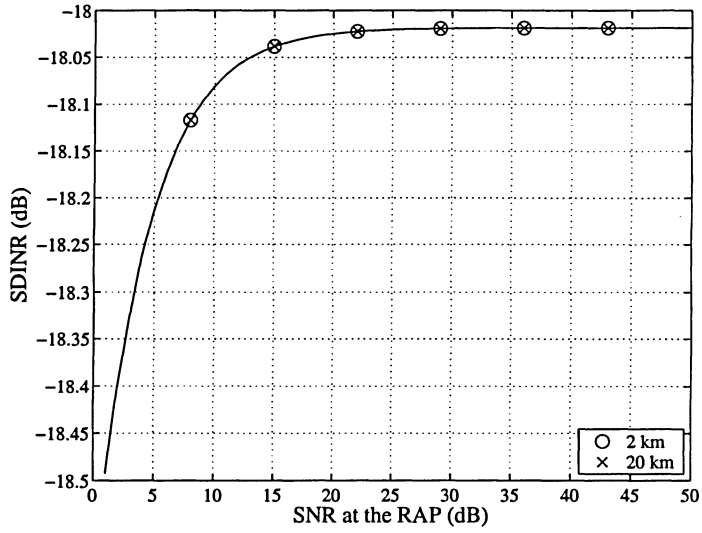

(a) The cumulative SDINR of a WCDMA signal versus the $SNR_{up,wlan}$ of WLAN at the RAP is plotted.

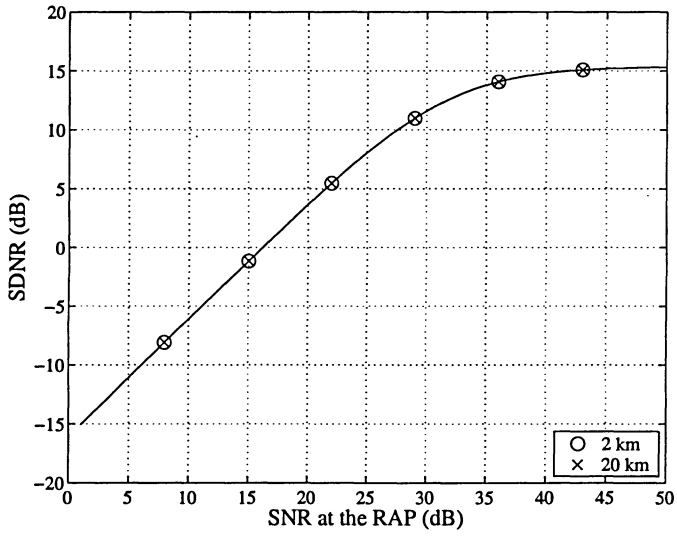

(b) The cumulative SDNR of a WLAN signal versus the $SNR_{up,wlan}$ of WLAN at the RAP is plotted.

Figure 5.3: The figures are the uplink results. The figures have two curves corresponding to 2 and 20 km of ROF link. The $SNR_{up,wlan}$ is an indication to the signal quality that input to the ROF link. The other parameters are: the optical modulation index ratios T is 1 which means the WCDMA and WLAN systems have equal RF power, and the cumulative RMS optical modulation index μ is 0.5.

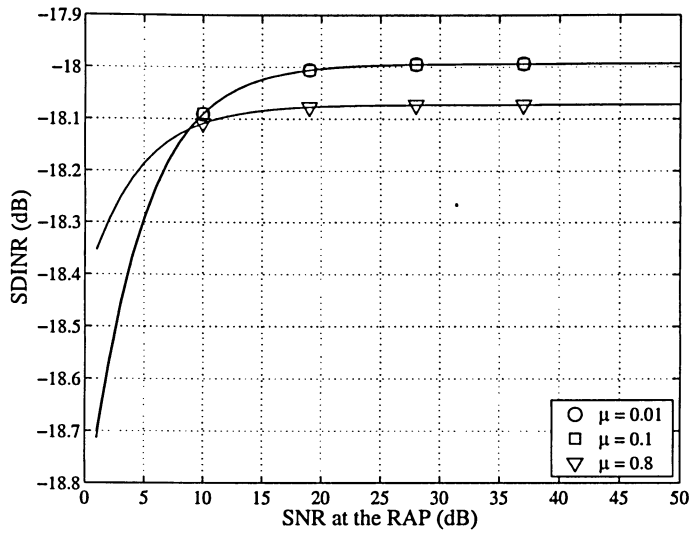

(a) The cumulative SDINR of a WCDMA signal versus the $SNR_{up,wlan}$ of WLAN at the RAP is plotted.

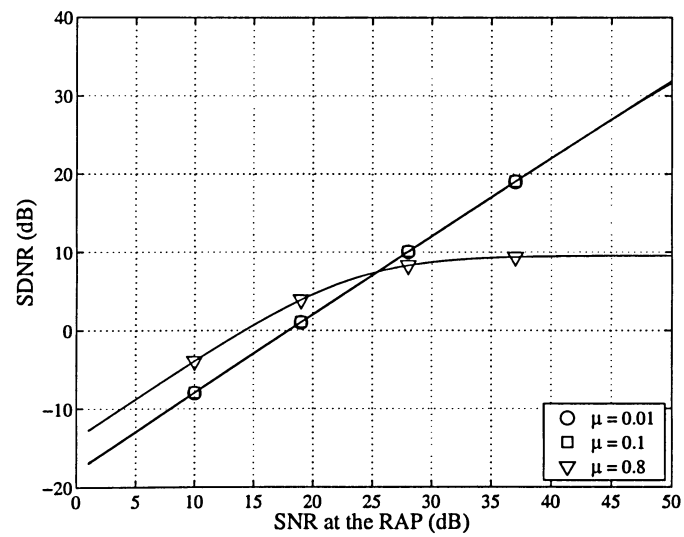

(b) The cumulative SDNR of a WLAN signal versus the $SNR_{up,wlan}$ of WLAN at the RAP is plotted.

Figure 5.4: The figures are the uplink results. The figures have three curves corresponding to various cumulative RMS optical modulation indices of 0.01, 0.1, and 0.8. The $SNR_{up,wlan}$ is an indication to the signal quality that input to the ROF link. The other parameters are: the optical modulation index ratios T is 1 which means equal power distribution between the WCDMA and WLAN systems, and the length of the ROF link is 10 km.

ratio is constant for most of the range of T plot in the figure which means T has little effect for WCDMA system. That is because there are many users in the WCDMA system where combine distortion from users is proportional to the increase in individual signal power of a user. Figure 5.5(b) shows that the performance of the WLAN increases with the ratio T for the entire range of T in the figure. It shows T has more effect in the WLAN system than the WCDMA system. It has been mentioned that for μ of 0.5 there is no effect from using a longer ROF link or a shorter ROF link.

Figure 5.6 shows three curves generated for three different values of μ. The similar characteristics from the previous figure can be observed in this figure that T has more effect in the WLAN system than the WCDMA system. When μ is small (0.01 and 0.1), the SDINR of the WCDMA signal is independent of the ratio T. This is illustrated in Figure 5.6(a). As expected that large μ results in lower performance, the cumulative SDNR curves for μ of 0.8 is lower than then the rest (See figures 5.6(a) and 5.6(b)).

From here onward, the discussion is on the results for the downlink. The downlink performance of the SCM architecture in relation to the cumulative RMS optical modulation index μ is illustrated in Figure 5.7. Figure 5.7(a) illustrates the cumulative SDNR of a WCDMA signal versus μ and the Figure 5.7(b) illustrates the cumulative SDNR of a WLAN signal versus μ. An optimal μ that gives the maximum cumulative SDNR can be observed from the two figures for each fiber length. This contrasts to the uplink (refer to figures 5.1 and 5.2): first, the maximum of the cumulative SDNR is observed for a specific μ; second, the cumulative SDNR is dependent on the fiber length in the useful range of μ. The downward shift of the cumulative SDNR curves as fiber length getting longer is the effect of the optical noise. In the WCDMA case, the peak cumulative SDNR for a 5 km ROF link can be achieved by selecting μ to be 0.1. Similar, μ of 0.1 also results in peak cumulative SDNR

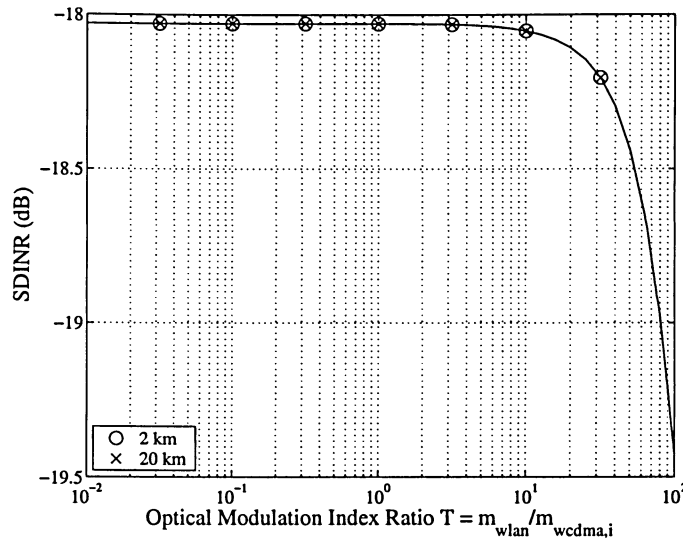

(a) The cumulative SDINR of a WCDMA signal versus the optical modulation index ratios T is plotted.

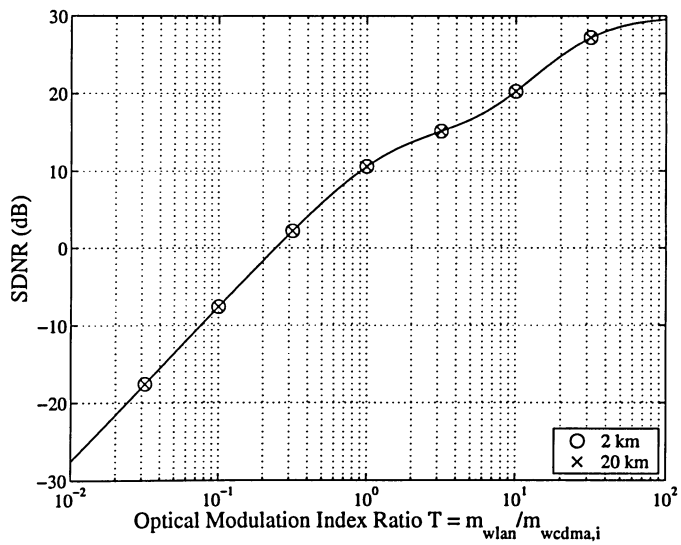

(b) The cumulative SDNR of a WLAN signal versus the optical modulation index ratios T is plotted.

Figure 5.5: The figures are the uplink results. The figures have two curves corresponding to 2 and 10 km of the ROF link. The optical modulation index ratios T is used to indicate the power distribution between the WCDMA and WLAN systems. The other parameters are: the $SNR_{up,wlan}$ is 40dB, and the cumulative RMS optical modulation index μ is 0.5.

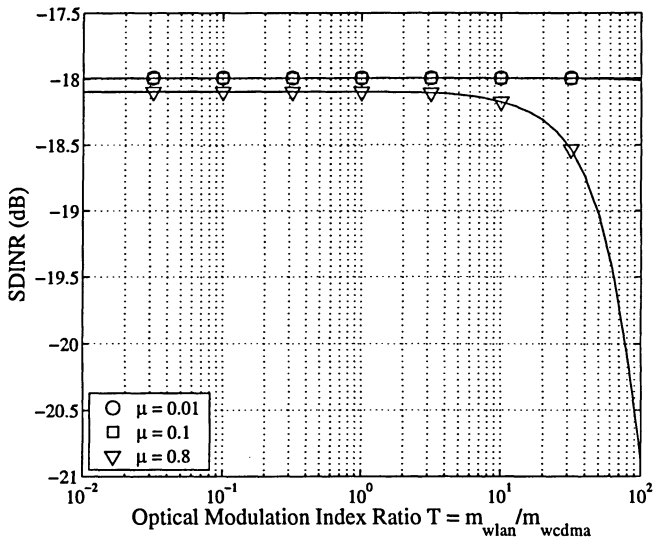

(a) The cumulative SDINR of a WCDMA signal versus the optical modulation index ratios T is plotted.

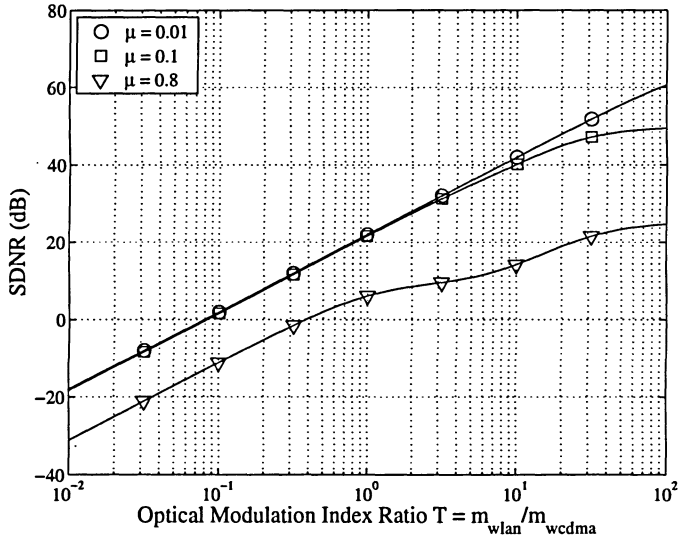

(b) The cumulative SDNR of a WLAN signal versus the optical modulation index ratios T is plotted.

Figure 5.6: The figures are the uplink results. The figures have three curves corresponding to cumulative RMS optical modulation indices of 0.01, 0.1 and 0.8. The optical modulation index ratios T is used to indicate the power distribution between the WCDMA and WLAN systems. The other parameters are: the $SNR_{up,wlan}$ is 40dB, and the length of the ROF link is 10 km.

for the WLAN case. A useful range of μ is from 0.01 to 0.2. The optical noise is the dominant effect in this range.

The performance of the WCDMA and WLAN signals in terms of the cumulative SDNR versus the index μ is illustrated in Figures 5.8(a) and 5.8(b). The results are generated with different optical modulation index ratios T. Recall that the ratio T indicates the relative power distribution between the systems. For the entire range of the index μ, it can be observed that the performance of the WLAN system improves with more power is being allocated(T is large); see Figure 5.8(b). However, there is no improvement in performance for the WCDMA system even if more power is allocated (T is small). The same trend is observed from the uplink that suggests more power can be allocated to the WLAN system without sacrificing the performance of the WCDMA system.

Figures 5.9(a) and 5.9(b) illustrate the relationship between the system performance in terms of the cumulative SDNR and the distance between a MS and the RAP. The two figures which describe the WCDMA and the WLAN systems presented very similar results. For small index μ (= 0.01 and 0.1), the cumulative SDNR improves inversely with the distance. While at large index μ, the performance is almost independent of the distance between a MS and the RAP. The independence is due the nonlinear distortion is much larger than the noise in the air interface. The optimal μ for a 5 km ROF link is 0.1 as mentioned earlier. As expected both figures show that μ of 0.1 gives the best system performance compare to the rest of the μ values. Furthermore, figures 5.10 and 5.11 illustrate the performance trends when μ is small and large respectively. When μ is small, the performance deteriorates with the distance. When μ is large, the performance is independent of the distance.

Figures 5.12(a) and 5.12(b) illustrate the relationship between the system performance and the distance between a MS and the RAP in a different way. Each figure has five curves with various lengths of the ROF link with an op-

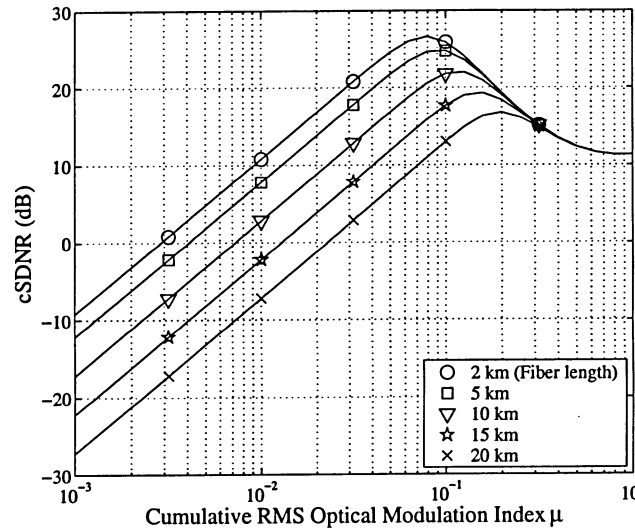

(a) The cumulative SDNR of a WCDMA signal versus the cumulative optical modulation index μ is plotted.

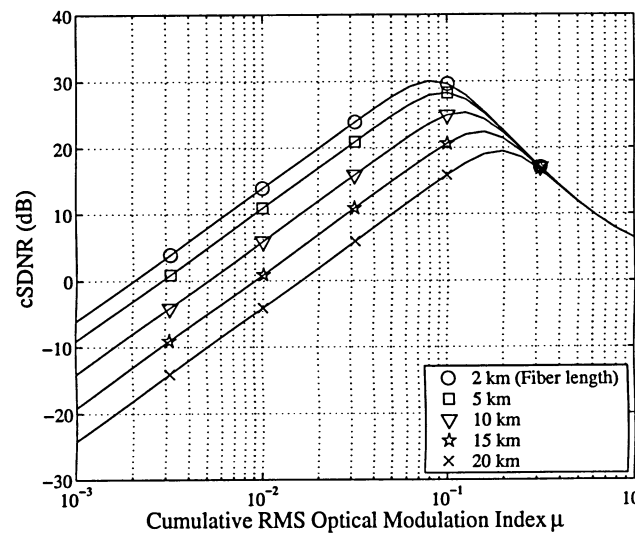

(b) The cumulative SDNR of a WLAN signal versus the cumulative optical modulation index μ is plotted.

Figure 5.7: The figures are the downlink results. The figures each has five curves corresponding to various lengths of the ROF link. The other parameters are: the optical modulation index ratio T is 1 which means the WCDMA and WLAN signals have the same RF power, the distance from a WCDMA MS to the RAP is 1500 m, and the distance from a WLAN MS to the RAP is 500 m.

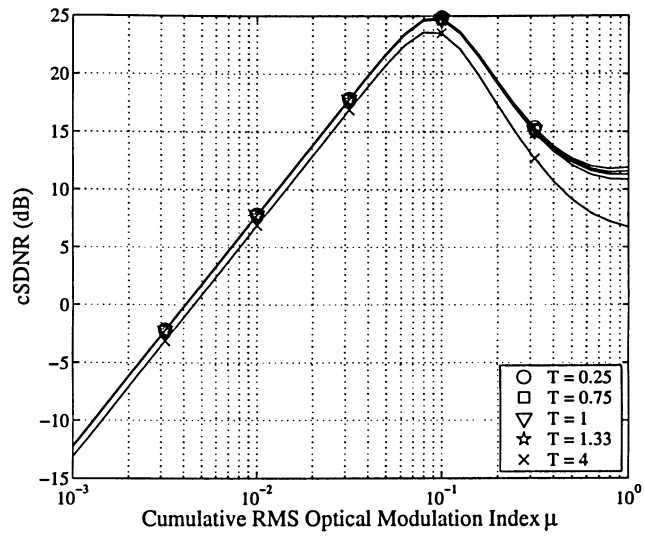

(a) The cumulative SDNR of a WCDMA signal versus the cumulative optical modulation index μ is plotted.

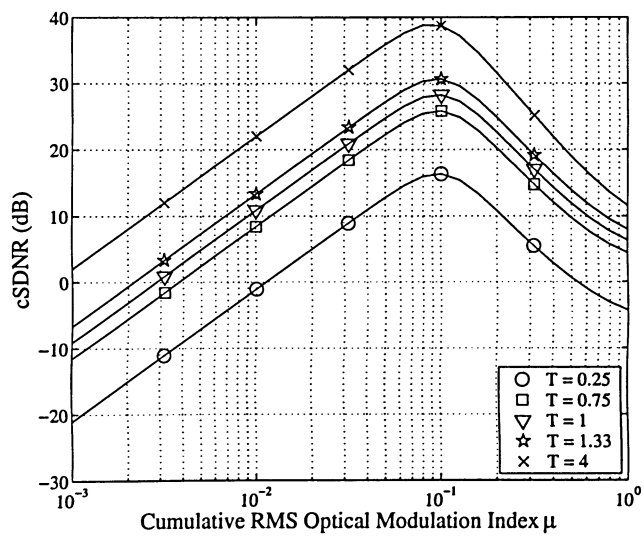

(b) The cumulative SDNR of a WLAN signal versus the cumulative optical modulation index μ is plotted.

Figure 5.8: The figures are the downlink results. The figures each has five curves corresponding to various optical modulation index ratios. The other parameters are: the length of the ROF link is 5 km, the distance from a WCDMA MS to the RAP is 1500 m, the distance from a WLAN MS to the RAP is 500 m, and the optical modulation index ratio T is 1 which means the WCDMA and WLAN signals have the same RF power.

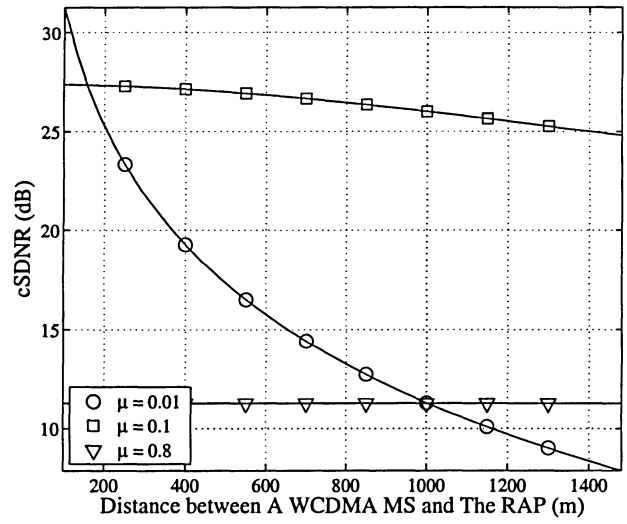

(a) The cumulative SDNR of a WCDMA signal versus the distance between a WCDMA MS and the RAP is plotted.

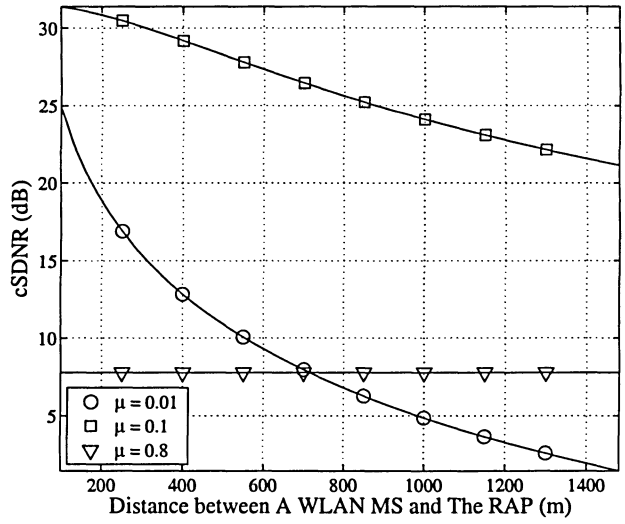

(b) The cumulative SDNR of a WLAN signal versus the distance between a WLAN MS and the RAP is plotted.

Figure 5.9: The figures are the downlink results. The figures each has three curves corresponding to cumulative optical modulation indices of 0.01, 0.1, and 0.8. The other parameters are: the length of the ROF link is 5 km, and the optical modulation index ratio T is 1 which means the WCDMA and WLAN signals have the same RF power.

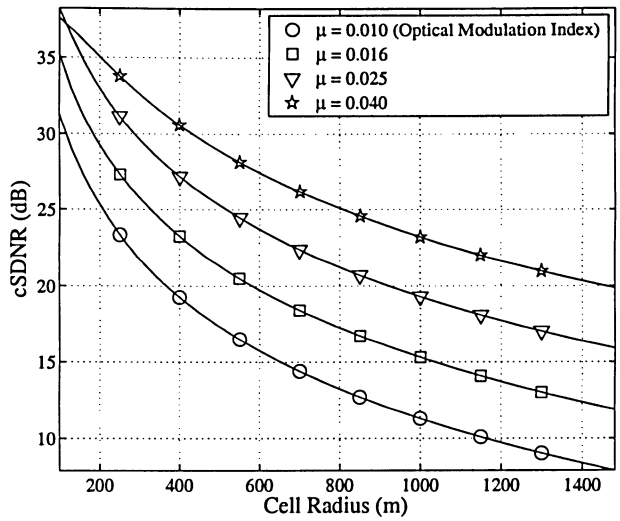

(a) The cumulative SDNR of a WCDMA signal versus the distance between a WCDMA MS and the RAP is plotted.

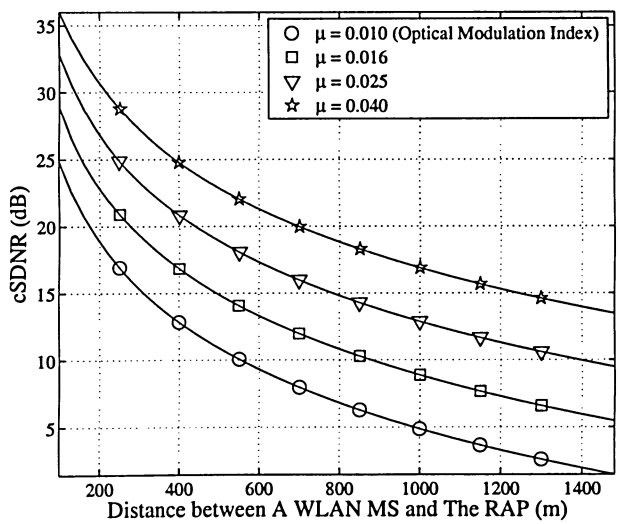

(b) The cumulative SDNR of a WLAN signal versus the distance between a WLAN MS and the RAP is plotted.

Figure 5.10: These figures illustrate the effect when μ is small. The four curves correspond to cumulative optical modulation indices of 0.010, 0.016, 0.025, and 0.040. The other parameters are: the length of the ROF link is 5 km, and the optical modulation index ratio T is 1.

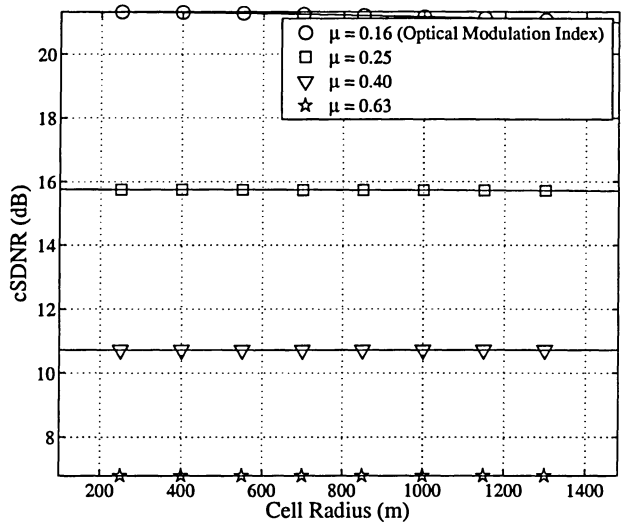

(a) The cumulative SDNR of a WCDMA signal versus the distance between a WCDMA MS and the RAP is plotted.

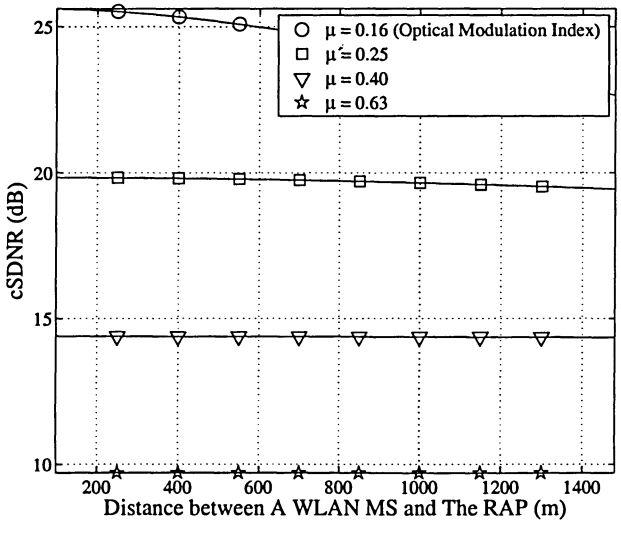

(b) The cumulative SDNR of a WLAN signal versus the distance between a WLAN MS and the RAP is plotted.

Figure 5.11: These figures illustrate the effect when μ is small. The four curves correspond to cumulative optical modulation indices of 0.16, 0.25, 0.40, and 0.63. The other parameters are: the length of the ROF link is 5 km, and the optical modulation index ratio T is 1.

timal μ of 0.1 used. The two figures show almost identical results. First, a downward trend in the performance versus the distance is observed for small μ of 0.01 and 0.1. This means that the optical noise is dominant. Second, the performance is remain the same for large μ (=0.8). This is because the non-linear distortion is larger than the optical noise from the ROF link. However, when the ROF is operated at the optimal μ (=0.1), the cumulative SDNR is better than the rest even for a 20 km ROF link.

Figure 5.13 illustrates the system performance in terms of the cumulative SDNR versus the length of the ROF link. The two plots give the same trends. Using the previous results, it can be concluded that longer ROF link decreases the system performance and larger distance between a MS and the RAP also decreases the system performance. In the WCDMA system, when the distance between a MS and the RAP is less than 1000 m, the performance decreases by no more than 1.5 dB even if the fiber is 20 km long (see Figure 5.13(a)). In the WLAN system, when the distance between a MS and the RAP is less than 300 m, the performance also decreases by no more than 1.5 dB even if the fiber is 20 km long (see Figure 5.13(b)).

Figure 5.14 illustrate the system performance in terms of the cumulative SDNR versus the various values of μ. Recall the ratio T is defined as $m_{\text{wlan}}/m_{\text{wcdma},i}$. For the WCDMA system (see Figure 5.14(a)), a downward trend versus the ratio T is observed and it is obvious because the less power is being allocated to the WCDMA system for larger T. Figure 5.14(b) illustrate the reverse trend which is true when the ratio T gets larger meaning more power is being allocated to the WLAN system. For large index μ, the curve behaves differently than with small μ. The nonlinear effect is the cause of such a different pattern. The two plots in Figure 5.15 also demonstrate the same trends as the previous results. For small T, the WCDMA system performance is constant (depending on the fiber length), then it starts to deteriorate. However, in the WLAN case,

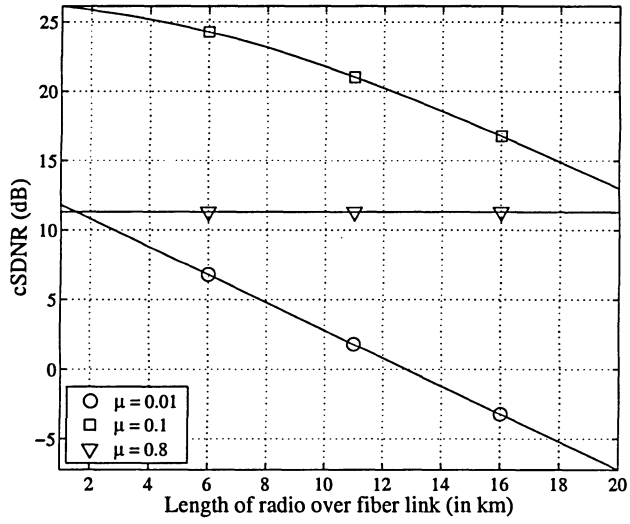

(a) The cumulative SDNR of a WCDMA signal versus the length of the ROF link.

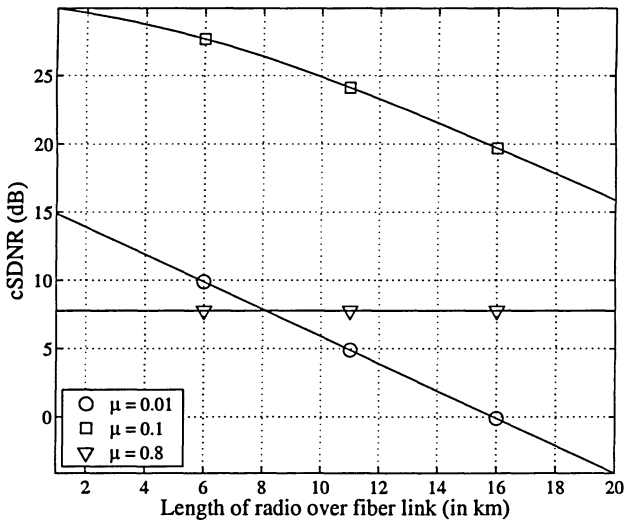

(b) The cumulative SDNR of a WLAN signal versus the distance between a WLAN MS and the RAP is plotted.

Figure 5.12: The figures are the downlink results. The figures each has three curves corresponding to cumulative optical modulation indices of 0.01, 0.1, and 0.8. The other parameters are: the optical modulation index ratio T is 1 which means the WCDMA and WLAN signals have the same RF power, the distance from a WCDMA MS to the RAP is 1500 m, and the distance from a WLAN MS to the RAP is 500 m.

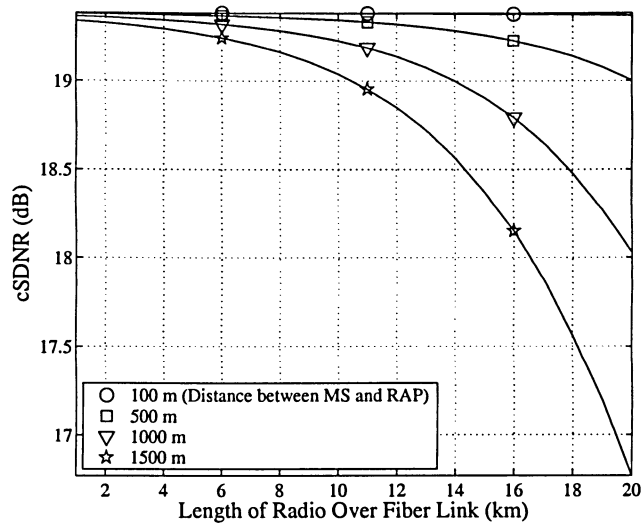

(a) The cumulative SDNR of a WCDMA signal versus the length of the ROF link is plotted.

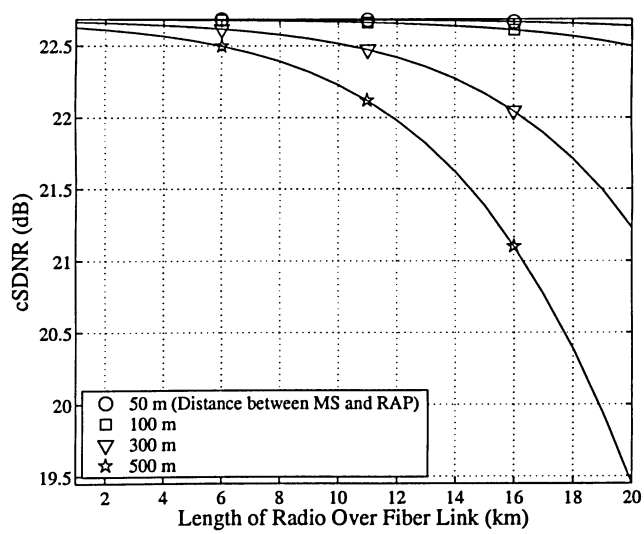

(b) The cumulative SDNR of a WLAN signal versus the length of the ROF link is plotted.

Figure 5.13: The figures are the downlink results. The figures each has four curves corresponding to various distance between the MS and the RAP. The other parameters are: the cumulative optical modulation index is 0.1, and the optical modulation index ratio T is 1 which means the WCDMA and WLAN signals have the same RF power.

the performance almost linearly increases with T. Therefore, selecting T just above one seems to give a good solution for both systems.

5.4 Conclusion and Future Work

In this thesis, the SCM architecture that jointly supports the WLAN system and the WCDMA cellular mobile system are investigated. The IEEE 802.11 WLAN and the third generation WCDMA mobile communication systems are first studied. Then, the fiber based radio access scheme for the air interface and the ROF link characteristics are investigated. In the air interface, the signals experience path loss and multipath fading. In the ROF link, the signals experience optical noise, nonlinear impairments and power loss. The noise are the RIN, shot noise, and thermal noise. The nonlinear impairments are the intermodulation product distortion and clipping distortion. Finally, the uplink and downlink analysis that accounts for the cumulative effects for all the impairments are carried out.

In the numerical results, the performance of both systems in the SCM architecture is illustrated graphically. The results are generated assuming that the WCDMA system has 64 active users and the WLAN system is operating with one user active at a time according to collision detection protocol. The results illustrates that this architecture can jointly support the two systems. The system performance is limited by the nonlinear distortion of ROF link when the cumulative RMS optical modulation index μ is large. Large μ means large RF power modulates the laser. When μ is larger than the optimal range, excessive nonlinear distortion deteriorates the system performance. In the uplink, the system should operate μ in the range of 0.01 to 0.1. In this range of μ, the system performance is not strongly dependent on the fiber length as shown by up to 20 km of fiber length (which typically the highest length with practical

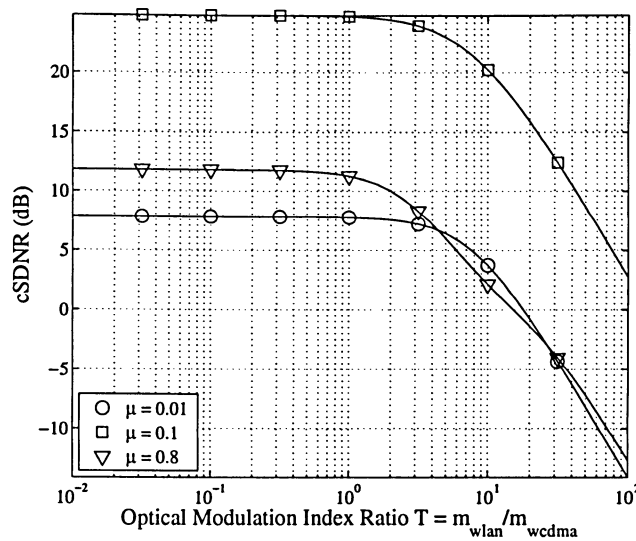

(a) The cumulative SDNR of a WCDMA signal versus the optical modulation index ratio T is plotted.

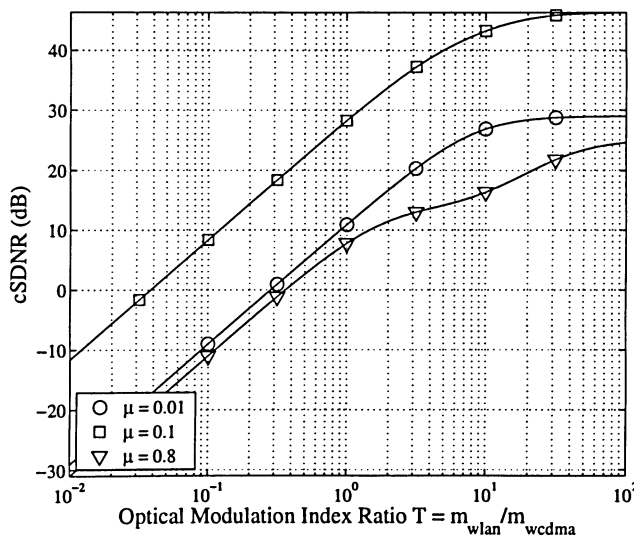

(b) The cumulative SDNR of a WLAN signal versus the optical modulation index ratio T is plotted.

Figure 5.14: The figures are the downlink results. The figures each has three curves corresponding to cumulative optical modulation indices of 0.01, 0.1, and 0.8. The other parameters are: the length of the ROF link is 5 km, the distance from a WCDMA MS to the RAP is 1500 m, and the distance from a WLAN MS to the RAP is 500 m.

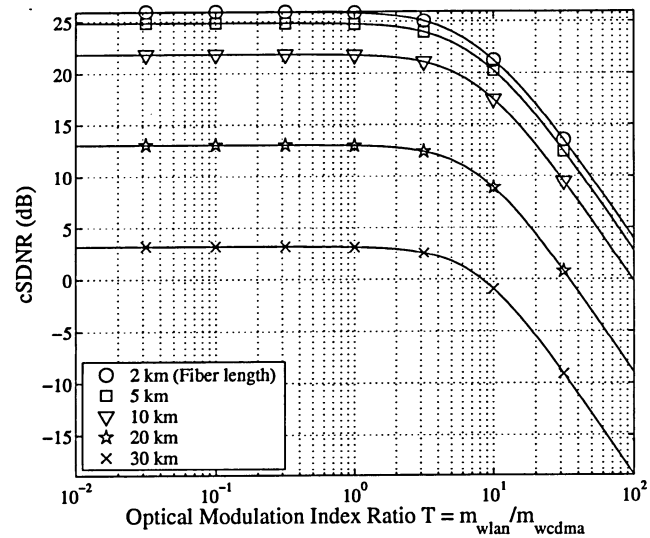

(a) The cumulative SDNR of a WCDMA signal versus the optical modulation index ratio T is plotted.

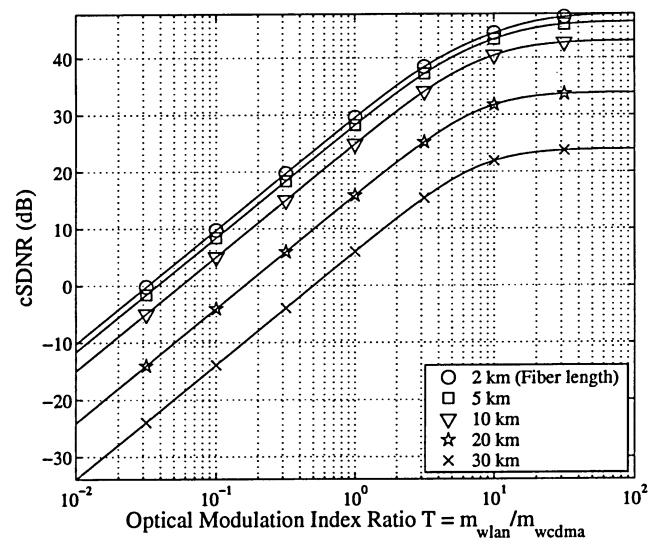

(b) The cumulative SDNR of a WLAN signal versus the optical modulation index ratio T is plotted.

Figure 5.15: The figures are the downlink results. The figures each has five curves corresponding to various length of the ROF link. The other parameters are: the cumulative optical modulation index μ is 0.1, the distance from a WCDMA MS to the RAP is 1500 m, and the distance from a WLAN MS to the RAP is 500 m.

ROF links), no large drop in performance is observed. This is because, the contribution of the SNR of the ROF link noise (which will relatively decrease with the fiber length) is not significant in this scenario.

However, for the downlink, the results have shown that the length of the ROF link does matter. The optical noise is the dominant source of impairments in this case. In the downlink, a 5 km ROF link should operate with $0.02 < \mu < 0.2$ for good performance.

The ratio T is used to indicate the relative power distribution between the WCDMA and WLAN systems. The results for both the uplink and the downlink have suggested that relatively more power should be allocated to the WLAN to improve the performance of both systems. The performance of the WCDMA system stays almost the same even if more power is allocated to WLAN ($T < 1$). However, the performance of WLAN system almost increases linearly with T. There is an upper limit to the power that can be allocated to the WLAN system. That is, the WLAN system must comply with the maximum power specified for the ISM band. The results also show that the WCDMA system can afford a larger cell size than the WLAN system. Both these observations probably attribute to the inherent advantage of code division multiple access that requires less power to maintain a certain system performance.

For possible future work, alternative architectures that also simultaneously support 3G WCDMA and WLAN IEEE 802.11 standards should be investigated. A possible architecture is to transmit baseband digital WLAN and passband WCDMA signals. The architecture can use mostly off the shelf components cost saving is possible. The WLAN signals are in the baseband digital format from the core network, which will make it easy to transmit. The effectiveness of such architecture requires similar analysis that is done for the SCM architecture in this thesis.

References

[1] L. M. Correia, and R. Prasad, "An overview of wireless broadband communications," *Communications Magazine, IEEE*, vol. 35, no. 1, pp. 28 – 33, January 1997.

[2] A. Doufexi, E. Tameh, A. Nix, S. Armour, and A. Molina, "Hotspot wireless LANs to enhance the performance of 3G and beyond cellular networks," *Communications Magazine, IEEE*, vol. 41, no. 7, pp. 58 – 65, July 2003.

[3] U. Varshney , "The status and future of 802.11-based WLANs," *Computer, IEEE*, vol. 36, no. 6, pp. 102 – 105, June 2003.

[4] O. K. Tonguz and H. Jung, "Personal communications access networks using subcarrier multiplexed optical links," *Lightwave Technology, Jounal of*, vol. 14, no. 6, pp. 1400 – 1409, June 1996.

[5] X. N. Fernando and A. Anpalagan, "On the design of optical fiber based wireless access systesm," in *International Conference on Communication, Proceedings of*, Paris, France, June 2004, vol. WC17-7, pp. 3550 – 3555.

[6] S. D. Walker, M. Li, A. C. Boucouvalas, D. G. Cunningham, and A. N. Coles, "Design techniques for subcarrier multiplexed broadcast optical networks," *Selected Areas in Communications, IEEE Journal on*, vol. 8, no. 7, pp. 1276 – 1284, Sept. 1990.

[7] X. N. Fernando, "An improved expression for dynamic relative intensity noise in radio over fiber applications," Under review to be published in IEEE Transactions on Communications, 2004.

[8] H. Kim and Y. C. Chung, "Passive optical network for CDMA-based microcellular communication systems," *Journal of Lightwave Technology*, vol. 19, no. 3, pp. 301 – 311, March 2001.

[9] J. C. Fan, C. L. Lu and L. G. Kazovsky, "Dynamic range requirements for microcellular personal communication systems using analog fiber-optic links," *Microwave Theory and Techniques, IEEE Transations on*, vol. 45, no. 8, pp. 1390 – 1397, Aug. 1997.

[10] ANSI/IEEE Std 802.11, *Part11: Wireless Medium Access Control (*MAC*) and Physical Layer (*PHY *Specifications*, (r2003) edition, 1999.

[11] G. Bianchi, "IEEE 802.11–saturation throughput analysis," *IEEE Communications Letters*, vol. 2, no. 12, pp. 318–320, December 1998.

[12] P. Chatzimisios, A. C. Boucouvalas and V. Vitsas, "Influence of channel BER on IEEE 802.11 DCF," *Electronics Letters*, vol. 39, no. 23, pp. 1687 – 1689, Nov. 2003.

[13] IEEE Std 802.11b, *Part11: Wireless Medium Access Control (*MAC*) and Physical Layer (*PHY *Specifications: Higher-Speed Physical Layer extension in the 2.4* GHz *Band*, (r2003) edition, September 1999.

[14] B. Walke, P. Seidenberg, and M.P. Althoff, *UMTS : the fundamentals*, Chichester, West Sussex, England ; Hoboken, NJ, USA : Wiley, 2003.

[15] Vijay K. Garg, *Wireless network evolution : 2G to 3G*, Upper Saddle River, NJ : Prentice Hall, 2002.

[16] W. C. Y. Lee, *Mobile communications Engineering*, New York: McGraw Hill, 1982.

[17] T. K. Fong, M. Tabara, D. J. M. Sabido, IX and L. G. Kazovsky, "Dynamic range of externally modulated analog optical links: optical amplification versus coherent detection," *Photonics Technology Letters, IEEE*, vol. 6, no. 2, pp. 270 – 272, Feb. 1994.

[18] P. Papazian, "Basic transmission loss and delay spread measurements for frequencies between 430 and 5750 MHz," *IEEE Transactions on Antennas and Propagation*, vol. 53, no. 2, pp. 694 – 701, Feb. 2005.

[19] John G. Proakis, *Digital Communications*, Boston : McGraw-Hill, 4th edition, 2001.

[20] T. S. Rappaport, *Wireless communications : principles and practice*, Upper Saddle River, N.J. : Prentice Hall PTR, 1996.

[21] J. Daly, "Fiber optic intermodulation distortion," *Communications, IEEE Transactions on*, vol. 30, no. 8, pp. 1954 – 1958, Aug. 1982.

[22] K. Stubkjaer and M. Danielsen, "Nonlinearities of GaAlAs lasers–harmonic distortion," *Quantum Electronics, IEEE Journal of*, vol. 16, no. 5, pp. 531 – 537, May 1980.

[23] A. A. M. Saleh, "Fundamental limit on number of channels in subcarrier-multiplexed lightwave CATV system," *Electronics Letters*, vol. 25, no. 12, pp. 776 – 777, June 1989.

[24] J. E. Mazo, "Asymptotic distortion spectrum of clipped, DC-biased, gaussian noise," *Communications, IEEE Transactions on*, vol. 40, no. 8, pp. 1339 – 1344, Aug. 1992.

[25] Gerd Keiser, *Optical Fiber Communications*, Boston, MA : McGraw-Hill, 3rd edition, 2000.

[26] John M. Senior, *Optical Fiber Communications: Principles and Practice*, Prentice Hall, 2nd edition, 1992.

[27] W. I. Way, "Subcarrier multiplexed lightwave system design considerations for subscriber loop applications," *Lightwave Technology, Journal of*, vol. 7, no. 11, pp. 1806 – 1818, Nov. 1989.

Appendix A

Nonlinearity of Radio over Fiber Link

The expansion of photocurrent expressions in the uplink and downlink is derived in this section. The intermodulation distortion terms and desired signals can be easily separated in the expanded expressions. Generally, the photocurrent is expressed in the following form:

$$i_{\mathrm{D}}(t) = C_1 \sum_{i=1}^{M} s_i + C_2 \left[\sum_{i=1}^{M} s_i\right]^2 + C_3 \left[\sum_{i=1}^{M} s_i\right]^3 + n(t) \quad \text{for } i = 1, 2, \ldots, r, \ldots, M \tag{A.1}$$

where C_1, C_2, and C_3 are constants, each s_i represent the modulating signal, the subscript $i = r$ represents the desired signal, and $n(t)$ is the aggregate noise. Expanding the second order term with respect to the desired signal s_r, the following expression is derived:

$$\left[\sum_{i=1}^{M} s_i\right]^2 = \sum_{i=1}^{M} s_i^2 + 2s_r \sum_{\substack{i=1 \\ i\neq r}}^{M} s_i + \sum_{\substack{i=1 \\ i\neq r}}^{M} \sum_{\substack{j=1 \\ j\neq r,i}}^{M} s_j\, s_i \tag{A.2}$$

Similarly, expanding the third order term with respect to the desired signal s_r, the following expression is derived:

$$\left[\sum_{i=1}^{M} s_i\right]^3 = \sum_{i=1}^{M} s_i^3 + 3\,s_r^2 \sum_{\substack{i=1 \\ i\neq r}}^{M} s_i + 3\,s_r \sum_{\substack{i=1 \\ i\neq r}}^{M} s_i^2 + 3 \sum_{\substack{j=1 \\ j\neq r}}^{M} \sum_{\substack{k=1 \\ k\neq r,j}}^{M} s_j^2\, s_k + 3\,s_r \sum_{\substack{j=1 \\ j\neq r}}^{M} \sum_{\substack{k=1 \\ k\neq r,j}}^{M} s_j\, s_k + \sum_{\substack{i=1 \\ i\neq r}}^{M} \sum_{\substack{j=1 \\ j\neq r,i}}^{M} \sum_{\substack{k=1 \\ k\neq r,i,j}}^{M} s_i\, s_j\, s_k \tag{A.3}$$

In the SCM architecture, the term $\sum_{i=1}^{M} s_i$ contains both the WCDMA and WLAN signals. Let α_i represents the ith WCDMA signal where the WCDMA system has n signals. Let β represents the WLAN signal. Mapping s_i to α_i for $i = 1, 2, \ldots, n$ and s_{n+1} to β, then $\sum_{i=1}^{M} s_i$ can be rewritten as follows:

$$\sum_{i=1}^{M} s_i = \sum_{i=1}^{n} \alpha_i + \beta \tag{A.4}$$

The expansion of the third order term has been illustrated in expression (A.3). The expansion results in six expanded terms. When the desired signal is one of the signals in the WCDMA system, then s_r becomes α_r. Substituting expression (A.4) in expression (A.3) and α_r for the desired signal s_r, the six expanded terms can further be expanded as follows:

$$\sum_{i=1}^{M} s_i^3 = \sum_{i=1}^{n} \alpha_i^3 + \beta^3 \tag{A.5}$$

$$3\,s_r^2 \sum_{\substack{i=1 \\ i\neq r}}^{M} s_i = 3\,\alpha_r^2 \left(\sum_{\substack{i=1 \\ i\neq r}}^{n} \alpha_i + \beta \right) = 3\,\alpha_r^2 \sum_{\substack{i=1 \\ i\neq r}}^{n} \alpha_i + 3\,\alpha_r^2\,\beta \tag{A.6}$$

$$3\,s_r \sum_{\substack{i=1 \\ i\neq r}}^{M} s_i^2 = 3\,\alpha_r \left(\sum_{\substack{i=1 \\ i\neq r}}^{n} \alpha_i^2 + \beta^2 \right) = 3\,\alpha_r \sum_{\substack{i=1 \\ i\neq r}}^{n} \alpha_i^2 + 3\,\alpha_r\,\beta^2 \tag{A.7}$$

$$
\begin{aligned}
3\sum_{\substack{j=1\\ j\neq r}}^{M}\sum_{\substack{k=1\\ k\neq r,j}}^{M} s_j^2\, s_k &= 3\sum_{\substack{k=1\\ k\neq r,j}}^{M}\left(\sum_{\substack{j=1\\ j\neq r}}^{n}\alpha_j^2+\beta^2\right)s_k \\
&= 3\sum_{\substack{j=1\\ j\neq r}}^{n}\alpha_j^2\left(\sum_{\substack{k=1\\ k\neq r,j}}^{M} s_k\right)+3\,\beta^2\sum_{\substack{k=1\\ k\neq r,M}}^{M} s_k \\
&= 3\sum_{\substack{j=1\\ j\neq r}}^{n}\alpha_j^2\left(\sum_{\substack{k=1\\ k\neq r,j}}^{n}\alpha_k+\beta\right)+3\,\beta^2\sum_{\substack{k=1\\ k\neq r}}^{n}\alpha_k \\
&= 3\sum_{\substack{j=1\\ j\neq r}}^{n}\sum_{\substack{k=1\\ k\neq r,j}}^{n}\alpha_j^2\,\alpha_k+3\,\beta\sum_{\substack{j=1\\ j\neq r}}^{n}\alpha_j^2+3\,\beta^2\sum_{\substack{k=1\\ k\neq r}}^{n}\alpha_k
\end{aligned}
\tag{A.8}
$$

$$
\begin{aligned}
3\,s_r\sum_{\substack{j=1\\ j\neq r}}^{M}\sum_{\substack{k=1\\ k\neq r,j}}^{M} s_j\, s_k &= 3\,\alpha_r\sum_{\substack{k=1\\ k\neq r,j}}^{M}\left(\sum_{\substack{j=1\\ j\neq r}}^{n}\alpha_j+\beta\right)s_k \\
&= 3\,\alpha_r\sum_{\substack{j=1\\ j\neq r}}^{n}\alpha_j\left(\sum_{\substack{k=1\\ k\neq r,j}}^{M} s_k\right)+3\,\alpha_r\,\beta\sum_{\substack{k=1\\ k\neq r,M}}^{M} s_k \\
&= 3\,\alpha_r\sum_{\substack{j=1\\ j\neq r}}^{n}\alpha_j\left(\sum_{\substack{k=1\\ k\neq r}}^{n}\alpha_k+\beta\right)+3\,\alpha_r\,\beta\sum_{\substack{k=1\\ k\neq r}}^{n}\alpha_k \\
&= 3\,\alpha_r\sum_{\substack{j=1\\ j\neq r}}^{n}\sum_{\substack{k=1\\ k\neq r,j}}^{n}\alpha_j\,\alpha_k+3\,\alpha_r\,\beta\sum_{\substack{j=1\\ j\neq r}}^{n}\alpha_j+3\,\alpha_r\,\beta\sum_{\substack{k=1\\ k\neq r}}^{n}\alpha_k \\
&= 3\,\alpha_r\sum_{\substack{j=1\\ j\neq r}}^{n}\sum_{\substack{k=1\\ k\neq r,j}}^{n}\alpha_j\,\alpha_k+6\,\alpha_r\,\beta\sum_{\substack{k=1\\ k\neq r}}^{n}\alpha_k
\end{aligned}
\tag{A.9}
$$

$$\sum_{\substack{i=1\\ i\neq r}}^{M}\sum_{\substack{j=1\\ j\neq r,i}}^{M}\sum_{\substack{k=1\\ k\neq r,i,j}}^{M} s_i\, s_j\, s_k = \sum_{\substack{j=1\\ j\neq r,i}}^{M}\sum_{\substack{k=1\\ k\neq r,i,j}}^{M}\left(\sum_{\substack{i=1\\ i\neq r}}^{n}\alpha_i\right) s_j\, s_k + \sum_{\substack{j=1\\ j\neq r,M}}^{M}\sum_{\substack{k=1\\ k\neq r,i,j}}^{M}\beta\, s_j\, s_k$$

$$= \sum_{\substack{k=1\\ k\neq r,i,j}}^{M}\left(\sum_{\substack{i=1\\ i\neq r}}^{n}\alpha_i\right)\left(\sum_{\substack{j=1\\ j\neq r,i}}^{n}\alpha_j\right) s_k + \sum_{\substack{k=1\\ k\neq r,i,M}}^{M}\left(\sum_{\substack{i=1\\ i\neq r}}^{n}\alpha_i\right)\beta\, s_k$$

$$+ \sum_{\substack{k=1\\ k\neq r,M,j}}^{M}\beta\left(\sum_{\substack{j=1\\ j\neq r}}^{n}\alpha_j\right) s_k$$

$$= \left(\sum_{\substack{i=1\\ i\neq r}}^{n}\alpha_i\right)\left(\sum_{\substack{j=1\\ j\neq r,i}}^{n}\alpha_j\right)\left(\sum_{\substack{k=1\\ k\neq r,i,j}}^{n}\alpha_k\right) + \left(\sum_{\substack{i=1\\ i\neq r}}^{n}\alpha_i\right)\left(\sum_{\substack{j=1\\ j\neq r,i}}^{n}\alpha_j\right)\beta$$

$$+ \left(\sum_{\substack{i=1\\ i\neq r}}^{n}\alpha_i\right)\beta\left(\sum_{\substack{k=1\\ k\neq r,i}}^{n}\alpha_k\right) + \beta\left(\sum_{\substack{j=1\\ j\neq r}}^{n}\alpha_j\right)\left(\sum_{\substack{k=1\\ k\neq r,j}}^{n}\alpha_k\right)$$

$$= \sum_{\substack{i=1\\ i\neq r}}^{n}\sum_{\substack{j=1\\ j\neq r,i}}^{n}\sum_{\substack{k=1\\ k\neq r,i,j}}^{n}\alpha_i\,\alpha_j\,\alpha_k + 3\,\beta\sum_{\substack{j=1\\ j\neq r}}^{n}\sum_{\substack{k=1\\ k\neq r,j}}^{n}\alpha_j\,\alpha_k \tag{A.10}$$

When the desired signal is the WLAN system, the six expanded terms for the third order nonlinearity would be different. For the WLAN desired signal, s_r becomes β. Substituting expression (A.4) in expression (A.3) and β for the

desired signal s_r, the six expanded terms can be written as follows:

$$\sum_{i=1}^{M} s_i^3 = \beta^3 + \sum_{i=1}^{n} \alpha_i^3 \tag{A.11}$$

$$3s_r^2 \sum_{\substack{i=1 \\ i\neq r}}^{M} s_i = 3\beta^2 \sum_{i=1}^{n} \alpha_i \tag{A.12}$$

$$3\, s_r \sum_{\substack{i=1 \\ i\neq r}}^{M} s_i^2 = 3\beta \sum_{i=1}^{n} \alpha_i^2 \tag{A.13}$$

$$3 \sum_{\substack{j=1 \\ j\neq r}}^{M} \sum_{\substack{k=1 \\ k\neq r,j}}^{M} s_j^2\, s_k = 3 \sum_{j=1}^{n} \sum_{\substack{k=1 \\ k\neq j}}^{n} \alpha_j^2\, \alpha_k \tag{A.14}$$

$$3\, s_r \sum_{\substack{j=1 \\ j\neq r}}^{M} \sum_{\substack{k=1 \\ k\neq r,j}}^{M} s_j\, s_k = 3\beta \sum_{j=1}^{n} \sum_{\substack{k=1 \\ k\neq j}}^{n} \alpha_j\, \alpha_k \tag{A.15}$$

$$\sum_{\substack{i=1 \\ i\neq r}}^{M} \sum_{\substack{j=1 \\ j\neq r,i}}^{M} \sum_{\substack{k=1 \\ k\neq r,i,j}}^{M} s_i\, s_j\, s_k = \sum_{i=1}^{n} \sum_{\substack{j=1 \\ j\neq i}}^{n} \sum_{\substack{k=1 \\ k\neq i,j}}^{n} \alpha_i\, \alpha_j\, \alpha_k \tag{A.16}$$

Up until here, the expansion of the third order terms has used symbolic representation α_i and β for the WCDMA and WLAN signals respectively. The two sections to follow provide the complete derivation that uses the complete form of signals. The uplink and downlink signals in the complete form are different, so derivation is divided into two sections.

A.1 Third Order Nonlinearity for Uplink

In (4.21), the photocurrent of the uplink of SCM architecture is expressed as follow:

$$i_{\mathrm{D}}(t) = \frac{s_{\mathrm{laser}}(t)}{\sqrt{L_{\mathrm{op}}}} + \frac{a_3}{\sqrt{L_{\mathrm{op}}}} \Big[s_{\mathrm{laser}}(t) - n_{\mathrm{up,air}}(t) \Big]^3 + n_{\mathrm{op}}(t) + n_{\mathrm{cl}}(t) \tag{A.17}$$

where $s_{\text{laser}}(t)$ is defined in (4.14). In $s_{\text{laser}}(t)$, it consists of WCDMA and WLAN signals as well as the noise induced from the air interface. Let α_i represents the ith WCDMA signal as the following:

$$\alpha_i = m_{\text{wcdma},i}\, d_i(t-\tau_i)\, c_i(t-\tau_i)\cos(\omega_\alpha t - \phi_i) \qquad \text{for} \quad i = 1, 2, \ldots, n \tag{A.18}$$

Similarly, β represents the WLAN signal as the following:

$$\beta = m_{\text{wlan}}\, d_\beta(t-\tau_\beta)\, c_\beta(t-\tau_\beta)\cos(\omega_\beta t - \phi_\beta) \tag{A.19}$$

Therefore, excluding the noise, there are $M = n + 1$ signals in $s_{\text{laser}}(t)$. Let $s_i = \alpha_i$ and $s_{n+1} = \beta$, then $s_{\text{laser}}(t)$ can be written as the following:

$$\begin{aligned} s_{\text{laser}}(t) &= \sum_{i=1}^{n} \alpha_i + \beta + n_{\text{up,air}}(t) \\ &= \sum_{i=1}^{M} s_i + n_{\text{up,air}}(t) \end{aligned} \tag{A.20}$$

Using $s_{\text{laser}}(t)$ above, the photocurrent (A.17) can be rewritten as the following:

$$i_{\text{D}}(t) = \frac{1}{\sqrt{L_{\text{op}}}} \sum_{i=1}^{M} s_i + \frac{a_3}{\sqrt{L_{\text{op}}}} \left[\sum_{i=1}^{M} s_i \right]^3 + \frac{n_{\text{up,air}}(t)}{\sqrt{L_{\text{op}}}} + n_{\text{op}}(t) + n_{\text{cl}}(t) \tag{A.21}$$

According to the SCM architecture illustrated in Figure 4.1, the photocurrent is passed through bandpass filters that separate the signals in the photocurrent into corresponding systems. To do this mathematically, the cubic term of the photocurrent is required to expand, and then groups the expanded terms according to the WCDMA or WLAN bands that they fall into. Any term that is out of the WCDMA and WLAN bands will be dropped.

The expansion of the third order term has been illustrated in expression (A.3). Also, the expressions (A.5)–(A.10) are especially derived for the WCDMA sys-

tem where the desired signal s_r is α_r. The six expressions (A.5)–(A.10) can be further expanded by substituting expressions (A.18) and (A.19). Moreover, the following relations are used to simplify the expanded expressions:

$$d^3(t-\tau)\,c^3(t-\tau) = d(t-\tau)\,c(t-\tau) \tag{A.22}$$

$$d^2(t-\tau)\,c^2(t-\tau) = 1 \tag{A.23}$$

and omits any term that does not fall in the WCDMA band except intermodulation terms with frequencies of $2\omega_\alpha - \omega_\beta$ and $2\omega_\beta - \omega_\alpha$. The following are the expressions with the substitution:

$$\sum_{i=1}^{M} s_i^3 = \frac{3}{4}\sum_{i=1}^{n} m_{\text{wcdma},i}^3\, d_i(t-\tau_i)\, c_i(t-\tau_i)\cos(\omega_\alpha t - \phi_i) \tag{A.24}$$

$$\begin{aligned} 3\,s_r^2 \sum_{\substack{i=1\\ i\neq r}}^{M} s_i &= \frac{3}{4}\, m_{\text{wcdma},r}^2 \sum_{\substack{i=1\\ i\neq r}}^{n} m_{\text{wcdma},i}\, d_i(t-\tau_i)\, c_i(t-\tau_i) \\ &\quad \cdot \left[\cos(\omega_\alpha t + \phi_i - 2\phi_r) + 2\cos(\omega_\alpha t - \phi_i)\right] \\ &\quad + \frac{3}{4}\, m_{\text{wcdma},r}^2\, m_{\text{wlan}}\, d_\beta(t-\tau_\beta)\, c_\beta(t-\tau_\beta) \\ &\quad \cdot \cos\left((2\omega_\alpha - \omega_\beta)t - 2\phi_r + \phi_\beta\right) \end{aligned} \tag{A.25}$$

$$\begin{aligned} 3\,s_r \sum_{\substack{i=1\\ i\neq r}}^{M} s_i^2 &= \frac{3}{4}\, m_{\text{wcdma},r}\, d_r(t-\tau_r)\, c_r(t-\tau_r) \sum_{\substack{i=1\\ i\neq r}}^{n} m_{\text{wcdma},i}^2 \\ &\quad \cdot \left[\cos(\omega_\alpha t + \phi_r - 2\phi_i) + 2\cos(\omega_\alpha t - \phi_r)\right] \\ &\quad + \frac{3}{4}\, m_{\text{wlan}}^2\, m_{\text{wcdma},r}\, d_r(t-\tau_r)\, c_r(t-\tau_r) \\ &\quad \cdot \left[\cos\left((2\omega_\beta - \omega_\alpha)t - 2\phi_\beta + \phi_r\right) + 2\cos(\omega_\alpha t - \phi_r)\right] \end{aligned} \tag{A.26}$$

$$
\begin{aligned}
3\sum_{\substack{j=1\\ j\neq r}}^{M}\sum_{\substack{k=1\\ k\neq r,j}}^{M} s_j^2\, s_k = {} & \frac{3}{4}\sum_{\substack{j=1\\ j\neq r}}^{n}\sum_{\substack{k=1\\ k\neq r,j}}^{n} m_{\text{wcdma},j}^2\, m_{\text{wcdma},k}\, d_k(t-\tau_k)\, c_k(t-\tau_k) \\
& \cdot \left[\cos(\omega_\alpha t + \phi_k - 2\phi_j) + 2\cos(\omega_\alpha t - \phi_k)\right] \\
& + \frac{3}{4}\, m_{\text{wlan}}\, d_\beta(t-\tau_\beta)\, c_\beta(t-\tau_\beta) \sum_{\substack{j=1\\ j\neq r}}^{n} m_{\text{wcdma},j}^2 \\
& \cdot \cos\left((2\omega_\alpha - \omega_\beta)t - 2\phi_j + \phi_\beta\right) \\
& + \frac{3}{4}\, m_{\text{wlan}}^2 \sum_{\substack{k=1\\ k\neq r}}^{n} m_{\text{wcdma},k}\, d_k(t-\tau_k)\, c_k(t-\tau_k) \\
& \cdot \left[\cos\left((2\omega_\beta - \omega_\alpha)t - 2\phi_\beta + \phi_k\right) + 2\cos(\omega_\alpha t - \phi_k)\right]
\end{aligned}
\tag{A.27}
$$

$$
\begin{aligned}
3\, s_r \sum_{\substack{j=1\\ j\neq r}}^{M}\sum_{\substack{k=1\\ k\neq r,j}}^{M} s_j\, s_k = {} & \frac{3}{4}\, m_{\text{wcdma},r}\, d_r(t-\tau_r)\, c_r(t-\tau_r) \sum_{\substack{j=1\\ j\neq r}}^{n}\sum_{\substack{k=1\\ k\neq r,j}}^{n} m_{\text{wcdma},j} \\
& \cdot m_{\text{wcdma},k}\, d_j(t-\tau_j)\, c_j(t-\tau_j)\, d_k(t-\tau_k)\, c_k(t-\tau_k) \\
& \cdot \left[\cos(\omega_\alpha t - \phi_r - \phi_j + \phi_k) + \cos(\omega_\alpha t - \phi_r + \phi_j - \phi_k)\right. \\
& \quad \left. + \cos(\omega_\alpha t + \phi_r - \phi_j - \phi_k)\right] \\
& + \frac{3}{2}\, m_{\text{wcdma},r}\, m_{\text{wlan}}\, d_r(t-\tau_r)\, c_r(t-\tau_r)\, d_\beta(t-\tau_\beta) \\
& \cdot c_\beta(t-\tau_\beta) \sum_{\substack{k=1\\ k\neq r}}^{n} m_{\text{wcdma},k}\, d_k(t-\tau_k)\, c_k(t-\tau_k) \\
& \cdot \cos\left((2\omega_\alpha - \omega_\beta)t - \phi_r - \phi_k + \phi_\beta\right)
\end{aligned}
\tag{A.28}
$$

$$\sum_{\substack{i=1\\ i\neq r}}^{M}\sum_{\substack{j=1\\ j\neq r,i}}^{M}\sum_{\substack{k=1\\ k\neq r,i,j}}^{M} s_i\, s_j\, s_k = \frac{1}{4}\sum_{\substack{i=1\\ i\neq r}}^{n}\sum_{\substack{j=1\\ j\neq r,i}}^{n}\sum_{\substack{k=1\\ k\neq r,i,j}}^{n} m_{\text{wcdma},i}\, m_{\text{wcdma},j}\, m_{\text{wcdma},k}\, d_i(t-\tau_i)$$
$$\cdot\, c_i(t-\tau_i)\, d_j(t-\tau_j)\, c_j(t-\tau_j)\, d_k(t-\tau_k)\, c_k(t-\tau_k)$$
$$\cdot \big[\cos(\omega_\alpha t-\phi_i-\phi_j+\phi_k)+\cos(\omega_\alpha t-\phi_i+\phi_j-\phi_k)$$
$$+\cos(\omega_\alpha t+\phi_i-\phi_j-\phi_k)\big]$$
$$+\frac{3}{4}\, m_{\text{wlan}}\, d_\beta(t-\tau_\beta)\, c_\beta(t-\tau_\beta)\sum_{\substack{j=1\\ j\neq r}}^{n}\sum_{\substack{k=1\\ k\neq r,j}}^{n} m_{\text{wcdma},j}$$
$$\cdot\, m_{\text{wcdma},k}\, d_j(t-\tau_j)\, c_j(t-\tau_j)\, d_k(t-\tau_k)\, c_k(t-\tau_k)$$
$$\cdot \cos\big((2\omega_\alpha-\omega_\beta)t-\phi_j-\phi_k+\phi_\beta\big) \tag{A.29}$$

The cubic term is now expanded completely and out of band terms are also dropped. Grouping the desired, distorted and interfering signals in the WCDMA band is the last step. The signals are first grouped according to code word and then frequency. They can be expressed as follows:

$$i_{\text{D,wcdma}}(t) = D_{\text{wcdma}}(t)+\sum_{i=1}^{7} Z_i(t)+\sqrt{\frac{G_{\text{up,wcdma}}}{L_{\text{op}}}}\, n_{\text{up,wcdma}}(t)$$
$$+\, n_{\text{op,wcdma}}(t)+n_{\text{cl,wcdma}}(t) \tag{A.30}$$

where $n_{\text{up,wcdma}}(t)$, $n_{\text{op,wcdma}}(t)$ and $n_{\text{cl,wcdma}}(t)$ are respectively the noise in the air interface, the noise in ROF link and the clipping distortion after they passed through a bandpass filter. The desired $D_{\text{wcdma}}(t)$, distorted and interfering signals $Z_i(t)$ are expressed in terms of optical modulation indices. The

expression after the grouping is given as follows:

$$D_{\text{wcdma}}(t) = \left\{ \frac{m_{\text{wcdma},r}}{\sqrt{L_{\text{op}}}} + \frac{1}{4}\frac{a_3}{\sqrt{L_{\text{op}}}}\left[m^3_{\text{wcdma},r} + 6\, m_{\text{wcdma},r}\left(\sum_{\substack{i=1 \\ i\neq r}}^{n} m^2_{\text{wcdma},i} + m^2_{\text{wlan}} \right) \right] \right\} \cdot d_r(t-\tau_r)\, c_r(t-\tau_r) \cos(\omega_\alpha t - \phi_r) \tag{A.31}$$

$$\begin{aligned} Z_1(t) = \frac{1}{\sqrt{L_{\text{op}}}} \sum_{\substack{i=1 \\ i\neq r}}^{n} m_{\text{wcdma},i} \Bigg\{ & \left[1 + \frac{3}{2} a_3 \left(\frac{1}{2} m^2_{\text{wcdma},i} + m^2_{\text{wcdma},r} + m^2_{\text{wlan}} + \sum_{\substack{j=1 \\ j\neq r,i}}^{n} m^2_{\text{wcdma},j} \right) \right] \cos(\omega_\alpha t - \phi_i) \\ & + \frac{3}{4} a_3\, m^2_{\text{wcdma},r} \cos(\omega_\alpha t + \phi_i - 2\,\phi_r) \\ & + \frac{3}{4} a_3\, m^2_{\text{wlan}} \cos\left((2\omega_\beta - \omega_\alpha)t - 2\phi_\beta + \phi_i \right) \\ & + \frac{3}{4} a_3 \sum_{\substack{j=1 \\ j\neq r,i}}^{n} m^2_{\text{wcdma},j} \cos(\omega_\alpha t + \phi_i - 2\phi_j) \Bigg\} \\ & \cdot d_i(t-\tau_i)\, c_i(t-\tau_i) \end{aligned} \tag{A.32}$$

$$Z_2(t) = \frac{3}{4}\frac{a_3\, m_{\text{wcdma},r}}{\sqrt{L_{\text{op}}}}\Bigg[\sum_{\substack{i=1\\ i\neq r}}^{n} m^2_{\text{wcdma},i}\cos(\omega_\alpha t + \phi_r - 2\phi_i) + m^2_{\text{wlan}}\cos\left((2\omega_\beta - \omega_\alpha)t - 2\phi_\beta + \phi_r\right)\Bigg] d_r(t-\tau_r)\, c_r(t-\tau_r) \tag{A.33}$$

$$Z_3(t) = \frac{3}{4}\frac{a_3\, m_{\text{wlan}}}{\sqrt{L_{\text{op}}}}\sum_{i=1}^{n} m^2_{\text{wcdma},i}\cos\left((2\omega_\alpha - \omega_\beta)t + 2\phi_i - \phi_\beta\right) \cdot d_\beta(t-\tau_\beta)\, c_\beta(t-\tau_\beta) \tag{A.34}$$

$$Z_4(t) = \frac{3}{4}\frac{a_3\, m_{\text{wcdma},r}}{\sqrt{L_{\text{op}}}}\sum_{\substack{j=1\\ j\neq r}}^{n}\sum_{\substack{k=1\\ k\neq r,j}}^{n} m_{\text{wcdma},j}\, m_{\text{wcdma},k}\Big[\cos(\omega_\alpha t - \phi_r - \phi_j + \phi_k) + \cos(\omega_\alpha t - \phi_r + \phi_j - \phi_k) + \cos(\omega_\alpha t + \phi_r - \phi_j - \phi_k)\Big] \cdot d_r(t-\tau_r)\, c_r(t-\tau_r)\, d_j(t-\tau_j)\, c_j(t-\tau_j)\, d_k(t-\tau_k)\, c_k(t-\tau_k) \tag{A.35}$$

$$Z_5(t) = \frac{3}{2}\frac{a_3\, m_{\text{wcdma},r}\, m_{\text{wlan}}}{\sqrt{L_{\text{op}}}} \sum_{\substack{k=1 \\ k\neq r}}^{n} m_{\text{wcdma},k} \cos\left((2\omega_\alpha - \omega_\beta)t - \phi_r - \phi_k + \phi_\beta\right)$$
$$\cdot\, d_r(t-\tau_r)\, c_r(t-\tau_r)\, d_\beta(t-\tau_\beta)\, c_\beta(t-\tau_\beta)\, d_k(t-\tau_k)\, c_k(t-\tau_k) \tag{A.36}$$

$$Z_6(t) = \frac{1}{4}\frac{a_3}{\sqrt{L_{\text{op}}}} \sum_{\substack{i=1 \\ i\neq r}}^{n} \sum_{\substack{j=1 \\ j\neq r,i}}^{n} \sum_{\substack{k=1 \\ k\neq r,i,j}}^{n} m_{\text{wcdma},i}\, m_{\text{wcdma},j}\, m_{\text{wcdma},k}$$
$$\cdot \Big[\cos(\omega_\alpha t - \phi_i - \phi_j + \phi_k) + \cos(\omega_\alpha t - \phi_i + \phi_j - \phi_k) + \cos(\omega_\alpha t + \phi_i - \phi_j - \phi_k)\Big] \tag{A.37}$$
$$\cdot\, d_i(t-\tau_i)\, c_i(t-\tau_i)\, d_j(t-\tau_j)\, c_j(t-\tau_j)\, d_k(t-\tau_k)\, c_k(t-\tau_k)$$

$$Z_7(t) = \frac{3}{4}\frac{a_3\, m_{\text{wlan}}}{\sqrt{L_{\text{op}}}} \sum_{\substack{j=1 \\ j\neq r}}^{n} \sum_{\substack{k=1 \\ k\neq r,j}}^{n} m_{\text{wcdma},j}\, m_{\text{wcdma},k}$$
$$\cdot \cos\left((2\omega_\alpha - \omega_\beta)t - \phi_j - \phi_k + \phi_\beta\right)$$
$$\cdot\, d_\beta(t-\tau_\beta)\, c_\beta(t-\tau_\beta)\, d_j(t-\tau_j)\, c_j(t-\tau_j)\, d_k(t-\tau_k)\, c_k(t-\tau_k) \tag{A.38}$$

The same approach is taken for the WLAN system with the desired signal $s_r = \beta$. The already expanded third order terms for the WLAN system are found in (A.11)–(A.16). These six expressions can be further expanded by substituting expressions (A.18) and (A.19). Also, the expression can be simplified further using the relations (A.22) and (A.23). Any term that does not fall in the WLAN band except intermodulation terms with frequencies of $2\omega_\alpha - \omega_\beta$ and $2\omega_\beta - \omega_\alpha$ is dropped. From a quick inspection, (A.14) and (A.16) will never produce any term that is in the WLAN band, so the expressions are

automatically dropped. The following are the modified expressions:

$$\sum_{i=1}^{M} s_i^3 = \frac{3}{4} m_{\text{wlan}}^3 \, d_\beta(t-\tau_\beta) \, c_\beta(t-\tau_\beta) \cos(\omega_\beta t - \phi_\beta) \tag{A.39}$$

$$\begin{aligned} 3\, s_r^2 \sum_{\substack{i=1 \\ i\neq r}}^{M} s_i = \frac{3}{4} m_{\text{wlan}}^2 \sum_{i=1}^{n} m_{\text{wcdma},i} \, d_i(t-\tau_i) \, c_i(t-\tau_i) \\ \cdot \cos\left((2\omega_\beta - \omega_\alpha)t - 2\phi_\beta + \phi_i\right) \end{aligned} \tag{A.40}$$

$$\begin{aligned} 3\, s_r \sum_{\substack{i=1 \\ i\neq r}}^{M} s_i^2 = \frac{3}{4} m_{\text{wlan}} \, d_\beta(t-\tau_\beta) \, c_\beta(t-\tau_\beta) \sum_{i=1}^{n} m_{\text{wcdma},i}^2 \\ \cdot \left[\cos\left((2\omega_\alpha - \omega_\beta)t - 2\phi_i + \phi_\beta\right) + 2\cos(\omega_\beta t - \phi_\beta)\right] \end{aligned} \tag{A.41}$$

$$\begin{aligned} 3\, s_r \sum_{\substack{j=1 \\ j\neq r}}^{M} \sum_{\substack{k=1 \\ k\neq r,j}}^{M} s_j \, s_k = \frac{3}{4} m_{\text{wlan}} \, d_\beta(t-\tau_\beta) \, c_\beta(t-\tau_\beta) \sum_{j=1}^{n} \sum_{\substack{k=1 \\ k\neq j}}^{n} m_{\text{wcdma},j} \, m_{\text{wcdma},k} \\ \cdot d_j(t-\tau_j) \, c_j(t-\tau_j) \, d_k(t-\tau_k) \, c_k(t-\tau_k) \\ \cdot \left[\cos\left((2\omega_\alpha - \omega_\beta)t - \phi_j - \phi_k + \phi_\beta\right)\right. \\ \left. + \cos(\omega_\beta - \phi_\beta + \phi_j - \phi_k) + \cos(\omega_\beta - \phi_\beta - \phi_j + \phi_k)\right] \end{aligned} \tag{A.42}$$

The cubic term is now expanded completely and out of band terms are also dropped. The last step is to group the desired, distorted and interfering signals in the WLAN band. Again, the signals are first grouped according to code word and then frequency. The expression after the grouping is given as follows:

$$\begin{aligned} i_{\text{D,wlan}}(t) = D_{\text{wlan}}(t) + \sum_{i=1}^{3} M_i(t) + \sqrt{\frac{G_{\text{up,wlan}}}{L_{\text{op}}}} \, n_{\text{up,wlan}}(t) \\ + n_{\text{op,wlan}}(t) + n_{\text{cl,wlan}}(t) \end{aligned} \tag{A.43}$$

where $n_{\text{up,wlan}}(t)$, $n_{\text{op,wlan}}(t)$ and $n_{\text{cl,wlan}}(t)$ are respectively the noise in the air

interface, the noise in ROF link and the clipping distortion after they passed through a bandpass filter. The desired $D_{\text{wlan}}(t)$, distorted and interfering signals $M_i(t)$ are expressed in terms of optical modulation indices and they are listed below:

$$D_{\text{wlan}}(t) = \left[\frac{m_{\text{wlan}}}{\sqrt{L_{\text{op}}}} + \frac{3}{4}\frac{a_3}{\sqrt{L_{\text{op}}}}\left(m_{\text{wlan}}^3 + 2\,m_{\text{wlan}}\sum_{i=1}^{n} m_{\text{wcdma},i}^2\right)\right] \cdot \cos(\omega_\beta t - \phi_\beta)\, d_\beta(t-\tau_\beta)\, c_\beta(t-\tau_\beta) \tag{A.44}$$

$$M_1(t) = \frac{3}{4}\frac{a_3\, m_{\text{wlan}}}{\sqrt{L_{\text{op}}}}\sum_{i=1}^{n} m_{\text{wcdma},i}^2 \cos\left((2\omega_\alpha - \omega_\beta)t - 2\phi_i + \phi_\beta\right) \cdot d_\beta(t-\tau_\beta)\, c_\beta(t-\tau_\beta) \tag{A.45}$$

$$M_2(t) = \frac{3}{4}\frac{a_3\, m_{\text{wlan}}^2}{\sqrt{L_{\text{op}}}}\sum_{i=1}^{n} m_{\text{wcdma},i} \cos\left((2\omega_\beta - \omega_\alpha)t - 2\phi_\beta + \phi_i\right) \cdot d_i(t-\tau_i)\, c_i(t-\tau_i) \tag{A.46}$$

$$M_3(t) = \frac{3}{4}\frac{a_3\, m_{\text{wlan}}}{\sqrt{L_{\text{op}}}}\sum_{j=1}^{n}\sum_{\substack{k=1\\k\neq j}}^{n} m_{\text{wcdma},j}\, m_{\text{wcdma},k} \cdot \Big[\cos\left((2\omega_\alpha - \omega_\beta)t - \phi_j - \phi_k + \phi_\beta\right) + \cos(\omega_\beta - \phi_\beta + \phi_j - \phi_k) + \cos(\omega_\beta - \phi_\beta - \phi_j + \phi_k)\Big] \cdot d_\beta(t-\tau_\beta)\, c_\beta(t-\tau_\beta)\, d_j(t-tau_j)\, c_j(t-\tau_j) \cdot d_k(t-\tau_k)\, c_k(t-\tau_k) \tag{A.47}$$

A.2 Third Order Nonlinearity for Downlink

The photocurrent of the downlink is given in (4.41) as follows:

$$i_{\text{D}}(t) = \frac{s_{\text{laser}}(t)}{\sqrt{L_{\text{op}}}} + \frac{a_3}{\sqrt{L_{\text{op}}}}\, s_{\text{laser}}^3(t) + n_{\text{op}}(t) + n_{\text{cl}}(t) \tag{A.48}$$

where $s_{\text{laser}}(t)$ is a different signal from the uplink and is defined in (4.38). Using the representation from the previous section, α_i and β represent the

WCDMA and WLAN signals respectively. Also, s_i is mapped to α_i for $i = 1, 2, \ldots, n$ and $s_{n=1}$ is mapped to β. The signal $s_{\text{laser}}(t)$ can now be rewritten as follows:

$$\begin{aligned} s_{\text{laser}}(t) &= \sum_{i=1}^{n} \alpha_i + \beta \\ &= \sum_{i=1}^{M} s_i \end{aligned} \tag{A.49}$$

By substituting the above expression into the photocurrent expression, the expression matches the general photocurrent expression that is given in (A.1).

$$i_{\text{D}}(t) = \frac{1}{\sqrt{L_{\text{op}}}} \sum_{i=1}^{M} s_i + \frac{a_3}{\sqrt{L_{\text{op}}}} \left[\sum_{i=1}^{M} s_i \right]^3 + n_{\text{op}}(t) + n_{\text{cl}}(t) \tag{A.50}$$

According to the downlink of the SCM architecture illustrated in Figure 4.1, there are bandpass filters that separate the signals in the photocurrent into corresponding systems. This is done mathematically by the expansion of the photocurrent (A.1), and then groups the expanded terms according to the WCDMA or WLAN bands. Any term that is out of the WCDMA and WLAN bands will be dropped. The complete expansion of the photocurrent requires the substitution of the downlink signals which are given as follows:

$$\alpha_i = m_{\text{wcdma,i}}\, d_i(t-\tau)\, c_i(t-\tau) \cos(\omega_\alpha t - \phi) \quad \text{for} \quad i = 1, 2, \ldots, n \tag{A.51}$$

$$\beta = m_{\text{wlan}}\, d_\beta(t-\tau_\beta)\, c_\beta(t-\tau_\beta) \cos(\omega_\beta t - \phi_\beta) \tag{A.52}$$

Recall that the expansion for the third order term using α_i and β has been derived earlier. The expressions (A.5)–(A.10) are especially derived for the WCDMA system where the desired signal s_r is α_r. Now, substitute the downlink signals (A.51) and (A.52) in the six expressions, and use the relations (A.22) and (A.23) to simplify the results. The following are the expressions

with substitution:

$$\sum_{i=1}^{M} s_i^3 = \frac{3}{4} \sum_{i=1}^{n} m_{\text{wcdma},i}^3 \, d_i(t-\tau) \, c_i(t-\tau) \cos(\omega_\alpha t - \phi) \tag{A.53}$$

$$\begin{aligned} 3\, s_r^2 \sum_{\substack{i=1 \\ i \neq r}}^{M} s_i = {} & \frac{9}{4} \, m_{\text{wcdma},r}^2 \sum_{\substack{i=1 \\ i \neq r}}^{n} m_{\text{wcdma},i} \, d_i(t-\tau) \, c_i(t-\tau) \cos(\omega_\alpha t - \phi) \\ & + \frac{3}{4} \, m_{\text{wcdma},r}^2 \, m_{\text{wlan}} \, d_\beta(t-\tau_\beta) \, c_\beta(t-\tau_\beta) \\ & \cdot \cos\left((2\omega_\alpha - \omega_\beta)t - 2\phi + \phi_\beta\right) \end{aligned} \tag{A.54}$$

$$\begin{aligned} 3\, s_r \sum_{\substack{i=1 \\ i \neq r}}^{M} s_i^2 = {} & \frac{9}{4} \, m_{\text{wcdma},r} \, d_r(t-\tau) \, c_r(t-\tau) \sum_{\substack{i=1 \\ i \neq r}}^{n} m_{\text{wcdma},i}^2 \cos(\omega_\alpha t - \phi) \\ & + \frac{3}{4} \, m_{\text{wlan}}^2 \, m_{\text{wcdma},r} \, d_r(t-\tau) \, c_r(t-\tau) \\ & \cdot \left[\cos\left((2\omega_\beta - \omega_\alpha)t - 2\phi_\beta + \phi\right) + 2\cos(\omega_\alpha t - \phi)\right] \end{aligned} \tag{A.55}$$

$$\begin{aligned} 3 \sum_{\substack{j=1 \\ j \neq r}}^{M} \sum_{\substack{k=1 \\ k \neq r,j}}^{M} s_j^2 \, s_k = {} & \frac{9}{4} \sum_{\substack{j=1 \\ j \neq r}}^{n} \sum_{\substack{k=1 \\ k \neq r,j}}^{n} m_{\text{wcdma},j}^2 \, m_{\text{wcdma},k} \, d_k(t-\tau) \, c_k(t-\tau) \\ & \cdot \cos(\omega_\alpha t - \phi) \\ & + \frac{3}{4} \, m_{\text{wlan}} \, d_\beta(t-\tau_\beta) \, c_\beta(t-\tau_\beta) \sum_{\substack{j=1 \\ j \neq r}}^{n} m_{\text{wcdma},j}^2 \\ & \cdot \cos\left((2\omega_\alpha - \omega_\beta)t - 2\phi + \phi_\beta\right) \\ & + \frac{3}{4} \, m_{\text{wlan}}^2 \sum_{\substack{k=1 \\ k \neq r}}^{n} m_{\text{wcdma},k} \, d_k(t-\tau) \, c_k(t-\tau) \\ & \cdot \left[\cos\left((2\omega_\beta - \omega_\alpha)t - 2\phi_\beta + \phi\right) + 2\cos(\omega_\alpha t - \phi)\right] \end{aligned} \tag{A.56}$$

$$
\begin{aligned}
3\,s_r \sum_{\substack{j=1\\ j\neq r}}^{M}\sum_{\substack{k=1\\ k\neq r,j}}^{M} s_j\,s_k =& \frac{9}{4}\,m_{\mathrm{wcdma},r}\,d_r(t-\tau)\,c_r(t-\tau)\sum_{\substack{j=1\\ j\neq r}}^{n}\sum_{\substack{k=1\\ k\neq r,j}}^{n} m_{\mathrm{wcdma},j} \\
&\cdot m_{\mathrm{wcdma},k}\,d_j(t-\tau)\,c_j(t-\tau)\,d_k(t-\tau)\,c_k(t-\tau) \\
&\cdot \cos(\omega_\alpha t-\phi) \\
&+\frac{3}{2}\,m_{\mathrm{wcdma},r}\,m_{\mathrm{wlan}}\,d_r(t-\tau)\,c_r(t-\tau)\,d_\beta(t-\tau_\beta) \\
&\cdot c_\beta(t-\tau_\beta)\sum_{\substack{k=1\\ k\neq r}}^{n} m_{\mathrm{wcdma},k}\,d_k(t-\tau)\,c_k(t-\tau) \\
&\cdot \cos\left((2\omega_\alpha-\omega_\beta)t-2\phi+\phi_\beta\right)
\end{aligned}
\tag{A.57}
$$

$$
\begin{aligned}
\sum_{\substack{i=1\\ i\neq r}}^{M}\sum_{\substack{j=1\\ j\neq r,i}}^{M}\sum_{\substack{k=1\\ k\neq r,i,j}}^{M} s_i\,s_j\,s_k =& \frac{3}{4}\sum_{\substack{i=1\\ i\neq r}}^{n}\sum_{\substack{j=1\\ j\neq r,i}}^{n}\sum_{\substack{k=1\\ k\neq r,i,j}}^{n} m_{\mathrm{wcdma},i}\,m_{\mathrm{wcdma},j}\,m_{\mathrm{wcdma},k}\,d_i(t-\tau) \\
&\cdot c_i(t-\tau)\,d_j(t-\tau)\,c_j(t-\tau)\,d_k(t-\tau)\,c_k(t-\tau) \\
&\cdot \cos(\omega_\alpha t-\phi) \\
&+\frac{3}{4}\,m_{\mathrm{wlan}}\,d_\beta(t-\tau_\beta)\,c_\beta(t-\tau_\beta)\sum_{\substack{j=1\\ j\neq r}}^{n}\sum_{\substack{k=1\\ k\neq r,j}}^{n} m_{\mathrm{wcdma},j} \\
&\cdot m_{\mathrm{wcdma},k}\,d_j(t-\tau)\,c_j(t-\tau)\,d_k(t-\tau)\,c_k(t-\tau) \\
&\cdot \cos\left((2\omega_\alpha-\omega_\beta)t-2\phi+\phi_\beta\right)
\end{aligned}
\tag{A.58}
$$

The cubic term is now expanded completely and out of band terms are also dropped. Grouping the desired, distorted and interfering signals in the WCDMA band is the last step. The signals are first grouped according to code word and then frequency. They can be expressed as follows:

$$
i_{\mathrm{D,wcdma}}(t) = D_{\mathrm{wcdma}}(t) + \sum_{i=1}^{7} Z_i(t) + n_{\mathrm{op,wcdma}}(t) + n_{\mathrm{cl,wcdma}}(t) \tag{A.59}
$$

where $n_{\text{up,wcdma}}(t)$, $n_{\text{op,wcdma}}(t)$ and $n_{\text{cl,wcdma}}(t)$ are respectively the noise in the air interface, the noise in ROF link and the clipping distortion after they passed through a bandpass filter. The desired $D_{\text{wcdma}}(t)$, distorted and interfering signals $Z_i(t)$ are expressed in terms of optical modulation indices. The expression after the grouping is given as follows:

$$\begin{aligned} D_{\text{wcdma}}(t) = & \left[\frac{m_{\text{wcdma},r}}{\sqrt{L_{\text{op}}}} + \frac{3}{4} \frac{a_3\, m_{\text{wcdma},r}}{\sqrt{L_{\text{op}}}} \left(m^2_{\text{wcdma},r} \right.\right. \\ & \left.\left. +3 \sum_{\substack{i=1 \\ i \neq r}}^{n} m^2_{\text{wcdma},i} + 2m^2_{\text{wlan}} \right) \right] \\ & \cdot \cos(\omega_\alpha t - \phi)\, d_r(t-\tau)\, c_r(t-\tau) \end{aligned} \tag{A.60}$$

$$\begin{aligned} Z_1(t) = & \frac{1}{\sqrt{L_{\text{op}}}} \sum_{\substack{i=1 \\ i \neq r}}^{n} m_{\text{wcdma},i} \left\{ \left[1 + \frac{3}{4} a_3 \left(m^2_{\text{wcdma},i} + 3m^2_{\text{wcdma},r} \right.\right.\right. \\ & \left.\left.\left. + 2m^2_{\text{wlan}} + 3 \sum_{\substack{j=1 \\ j \neq r,i}}^{n} m^2_{\text{wcdma},j} \right) \right] \cos(\omega_\alpha t - \phi) \right. \\ & \left. + \frac{3}{4} a_3\, m^2_{\text{wlan}} \cos\left((2\omega_\beta - \omega_\alpha)t - 2\phi_\beta + \phi \right) \right\} \\ & \cdot d_i(t-\tau)\, c_i(t-\tau) \end{aligned} \tag{A.61}$$

$$\begin{aligned} Z_2(t) = & \frac{3}{4} \frac{a_3}{\sqrt{L_{\text{op}}}} m_{\text{wcdma},r}\, m^2_{\text{wlan}} \cos\left((2\omega_\beta - \omega_\alpha)t - 2\phi_\beta + \phi \right) \\ & \cdot d_r(t-\tau)\, c_r(t-\tau) \end{aligned} \tag{A.62}$$

$$\begin{aligned} Z_3(t) = & \frac{3}{4} \frac{a_3\, m_{\text{wlan}}}{\sqrt{L_{\text{op}}}} \sum_{i=1}^{n} m^2_{\text{wcdma},i} \cos\left((2\omega_\alpha - \omega_\beta)t + 2\phi_i - \phi_\beta \right) \\ & \cdot d_\beta(t-\tau_\beta)\, c_\beta(t-\tau_\beta) \end{aligned} \tag{A.63}$$

$$\begin{aligned} Z_4(t) = & \frac{9}{4} \frac{a_3\, m_{\text{wcdma},r}}{\sqrt{L_{\text{op}}}} \sum_{\substack{j=1 \\ j \neq r}}^{n} \sum_{\substack{k=1 \\ k \neq r,j}}^{n} m_{\text{wcdma},j}\, m_{\text{wcdma},k} \cos(\omega_\alpha t - \phi) \\ & \cdot d_r(t-\tau)\, c_r(t-\tau)\, d_j(t-\tau)\, c_j(t-\tau)\, d_k(t-\tau)\, c_k(t-\tau) \end{aligned} \tag{A.64}$$

$$Z_5(t) = \frac{3}{2}\frac{a_3}{\sqrt{L_{\text{op}}}} m_{\text{wcdma},r}\, m_{\text{wlan}} \sum_{\substack{k=1 \\ k\neq r}}^{n} m_{\text{wcdma},k} \cos\left((2\omega_\alpha - \omega_\beta)t - 2\phi + \phi_\beta\right)$$
$$\cdot\, d_r(t-\tau)\, c_r(t-\tau)\, d_\beta(t-\tau_\beta)\, c_\beta(t-\tau_\beta)\, d_k(t-\tau)\, c_k(t-\tau) \tag{A.65}$$

$$Z_6(t) = \frac{3}{4}\frac{a_3}{\sqrt{L_{\text{op}}}} \sum_{\substack{i=1 \\ i\neq r}}^{n} \sum_{\substack{j=1 \\ j\neq r,i}}^{n} \sum_{\substack{k=1 \\ k\neq r,i,j}}^{n} m_{\text{wcdma},i}\, m_{\text{wcdma},j}\, m_{\text{wcdma},k} \cos(\omega_\alpha t - \phi) \tag{A.66}$$
$$\cdot\, d_i(t-\tau)\, c_i(t-\tau)\, d_j(t-\tau)\, c_j(t-\tau)\, d_k(t-\tau)\, c_k(t-\tau)$$

$$Z_7(t) = \frac{3}{4}\frac{a_3\, m_{\text{wlan}}}{\sqrt{L_{\text{op}}}} \sum_{\substack{j=1 \\ j\neq r}}^{n} \sum_{\substack{k=1 \\ k\neq r,j}}^{n} m_{\text{wcdma},j}\, m_{\text{wcdma},k}$$
$$\cdot \cos\left((2\omega_\alpha - \omega_\beta)t - 2\phi + \phi_\beta\right) \tag{A.67}$$
$$\cdot\, d_\beta(t-\tau_\beta)\, c_\beta(t-\tau_\beta)\, d_j(t-\tau)\, c_j(t-\tau)\, d_k(t-\tau)\, c_k(t-\tau)$$

The same approach is taken for the WLAN system with the desired signal $s_r = \beta$. The already expanded third order terms for the WLAN system are found in (A.11)–(A.16). These six expressions can be further expanded by substituting expressions (A.18) and (A.19). Also, the expression can be simplified further using the relations (A.22) and (A.23). Any term that does not fall in the WLAN band except intermodulation terms with frequencies of $2\omega_\alpha - \omega_\beta$ and $2\omega_\beta - \omega_\alpha$ is dropped. From a quick inspection, (A.14) and (A.16) will never produce any term that is in the WLAN band, so the expressions are

automatically dropped. The following are the modified expressions:

$$\sum_{i=1}^{M} s_i^3 = \frac{3}{4} m_{\text{wlan}}^3 \, d_\beta(t-\tau_\beta) \, c_\beta(t-\tau_\beta) \cos(\omega_\beta t - \phi_\beta) \tag{A.68}$$

$$\begin{aligned} 3\, s_r^2 \sum_{\substack{i=1 \\ i\neq r}}^{M} s_i = \frac{3}{4} m_{\text{wlan}}^2 \sum_{i=1}^{n} m_{\text{wcdma},i} \, d_i(t-\tau) \, c_i(t-\tau) \\ \cdot \cos\left((2\omega_\beta - \omega_\alpha)t - 2\phi_\beta + \phi\right) \end{aligned} \tag{A.69}$$

$$\begin{aligned} 3\, s_r \sum_{\substack{i=1 \\ i\neq r}}^{M} s_i^2 = \frac{3}{4} m_{\text{wlan}} \, d_\beta(t-\tau_\beta) \, c_\beta(t-\tau_\beta) \sum_{i=1}^{n} m_{\text{wcdma},i}^2 \\ \cdot \left[\cos\left((2\omega_\alpha - \omega_\beta)t - 2\phi + \phi_\beta\right) + 2\cos(\omega_\beta t - \phi_\beta)\right] \end{aligned} \tag{A.70}$$

$$\begin{aligned} 3\, s_r \sum_{\substack{j=1 \\ j\neq r}}^{M} \sum_{\substack{k=1 \\ k\neq r,j}}^{M} s_j \, s_k = \frac{3}{4} m_{\text{wlan}} \, d_\beta(t-\tau_\beta) \, c_\beta(t-\tau_\beta) \sum_{j=1}^{n} \sum_{\substack{k=1 \\ k\neq j}}^{n} m_{\text{wcdma},j} \, m_{\text{wcdma},k} \\ \cdot \, d_j(t-\tau) \, c_j(t-\tau) \, d_k(t-\tau) \, c_k(t-\tau) \\ \cdot \left[\cos\left((2\omega_\alpha - \omega_\beta)t - 2\phi + \phi_\beta\right) + 2\cos(\omega_\beta t - \phi_\beta)\right] \end{aligned} \tag{A.71}$$

The cubic term is now expanded completely and out of band terms are also dropped. The last step is to group the desired, distorted and interfering signals in the WLAN band. Again, the signals are first grouped according to code word and then frequency. The expression after the grouping is given as follows:

$$i_{\text{D,wlan}}(t) = D_{\text{wlan}}(t) + \sum_{i=1}^{3} M_i(t) + n_{\text{op,wlan}}(t) + n_{\text{cl,wlan}}(t) \tag{A.72}$$

where $n_{\text{op,wlan}}(t)$ and $n_{\text{cl,wlan}}(t)$ are respectively the noise in ROF link and the clipping distortion after they passed through a bandpass filter. The desired $D_{\text{wlan}}(t)$, distorted and interfering signals $M_i(t)$ are expressed in terms

of optical modulation indices and they are listed below:

$$D_{\text{wlan}}(t) = \left[\frac{m_{\text{wlan}}}{\sqrt{L_{\text{op}}}} + \frac{3}{4}\frac{a_3}{\sqrt{L_{\text{op}}}}\left(m_{\text{wlan}}^3 + 2\,m_{\text{wlan}}\sum_{i=1}^{n} m_{\text{wcdma},i}^2\right)\right] \cdot \cos(\omega_\beta t - \phi_\beta)\, d_\beta(t-\tau_\beta)\, c_\beta(t-\tau_\beta) \tag{A.73}$$

$$M_1(t) = \frac{3}{4}\frac{a_3\, m_{\text{wlan}}}{\sqrt{L_{\text{op}}}}\sum_{i=1}^{n} m_{\text{wcdma},i}^2 \cos\left((2\omega_\alpha - \omega_\beta)t - 2\phi + \phi_\beta\right) \cdot d_\beta(t-\tau_\beta)\, c_\beta(t-\tau_\beta) \tag{A.74}$$

$$M_2(t) = \frac{3}{4}\frac{a_3\, m_{\text{wlan}}^2}{\sqrt{L_{\text{op}}}}\sum_{i=1}^{n} m_{\text{wcdma},i} \cos\left((2\omega_\beta - \omega_\alpha)t - 2\phi_\beta + \phi\right) \cdot d_i(t-\tau)\, c_i(t-\tau) \tag{A.75}$$

$$M_3(t) = \frac{3}{4}\frac{a_3\, m_{\text{wlan}}}{\sqrt{L_{\text{op}}}}\sum_{j=1}^{n}\sum_{\substack{k=1\\k\neq j}}^{n} m_{\text{wcdma},j}\, m_{\text{wcdma},k} \cdot \left[\cos\left((2\omega_\alpha - \omega_\beta)t - 2\phi + \phi_\beta\right) + 2\cos(\omega_\beta - \phi_\beta)\right] \cdot d_\beta(t-\tau_\beta)\, c_\beta(t-\tau_\beta)\, d_j(t-\tau)\, c_j(t-\tau) \cdot d_k(t-\tau)\, c_k(t-\tau) \tag{A.76}$$